Pattern Recognition and Tomographic Reconstruction with Terahertz Signals for Applications in Biomedical Engineering

by

Xiaoxia (Sunny) Yin

Bachelor of Engineering (Industrial Electronics),
Dalian University, 1996

Thesis submitted for the degree of

Doctor of Philosophy

in

Electrical and Electronic Engineering
University of Adelaide

2008

Appendix A

Oblique Projection Operation

THIS appendix introduces an oblique projection operation, which underpins the subspace system identification algorithms discussed in Chapter 7. In addition, a few figures are drawn to illustrate parts of the subspace identification procedures.

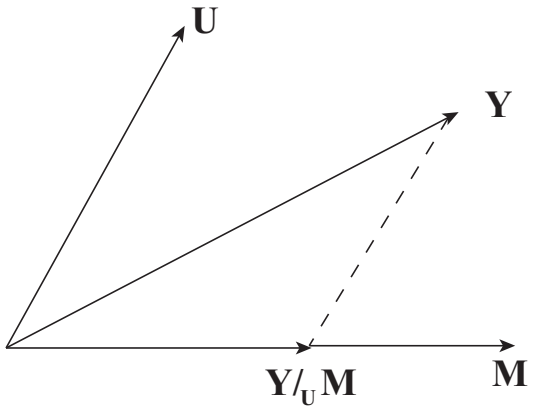

Figure A.1. Schematic of oblique projection. Oblique projection of **Y** onto **M** along the direction of **U**.

An oblique projection operation is illustrated in Fig. A.1. In this case, there are three rows spaces involved: $\mathbf{Y}, \mathbf{U}$ and $\mathbf{M}$. The notation $\mathbf{Y}/_{\mathbf{U}}\mathbf{M}$ is used to denote the oblique projection of $\mathbf{Y}$ onto $\mathbf{M}$ along the direction of $\mathbf{U}$. The vector space $\mathbf{Y}$ in the oblique projection should lie in the span of $\{\mathbf{U}, \mathbf{M}\}$, otherwise it should be first projected orthogonally onto that span before the oblique projection operation is carried out. The oblique projection is defined by two properties, which are obvious from Fig. A.1:

$$\mathbf{U}/_{\mathbf{U}}\mathbf{M} = 0 \tag{A.1}$$

$$\mathbf{M}/_{\mathbf{U}}\mathbf{M} = \mathbf{M}. \tag{A.2}$$

Any transformation that satisfies Eq. (A.1) and Eq. (A.2) can be adopted as an oblique projection operator. The following formula satisfies the conditions for the projection operator:

$$\mathbf{M}/_{\mathbf{U}}\mathbf{M} = (Y/U^{\perp})(M/U^{\perp})^{*}M \tag{A.3}$$

where $*$ denotes the Moore-Penrose pseudo-inverse, $\perp$ indicates an orthogonal projection.

In fact, Eq. (A.1) follows from the fact that $(U/U^{\perp})$ is zero by definition, whereas Eq. (A.3) is satisfied because $(M/U^{\perp})(M/U^{\perp})^{*}$ equals the identity matrix.

Oblique projection vectors are also drawn in Fig. A.2(a) to represent the row spaces of the involved matrices in Eq. (7.20), Section 7.5.1. The row space $\mathbf{Y}_f$ is seen to be the sum

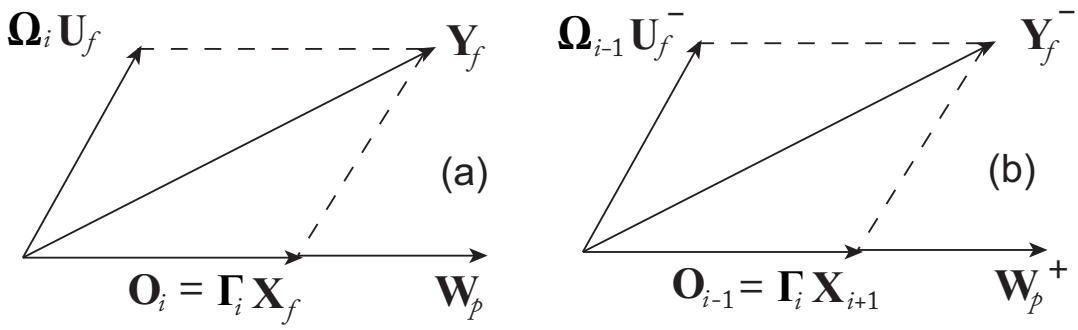

Figure A.2. The projections regarding state-space sequences. Determination of (a) the future state sequence X_f and (b) the shifted state sequence X_{i+1}. After Galvão *et al.* (2005).

of $\mathbf{\Gamma}_i \mathbf{X}_f$ and $\mathbf{\Omega}_i \mathbf{U}_f$. In this projection operation, the direction of $\mathbf{\Omega}_i \mathbf{U}_f$ is known, since $\mathbf{U}_f$, consisting of input data, is known, and $\mathbf{\Omega}_i$, albeit unknown, $\mathbf{\Omega}_i \mathbf{U}_f$ can be realised via the performance of rescalings and rotations of the rows of $\mathbf{U}_f$ in the hyperplane in which they lie. As a consequence, the oblique projection of $\mathbf{Y}_f$ along $\mathbf{U}_f$ or along $\mathbf{\Omega}_i \mathbf{U}_f$ is the same. The direction of $\mathbf{W}_p$ is also known, composed of input and output data. Moreover, if the system is observable, it is easy to see that $\mathbf{X}_f$ lies in the $\mathbf{W}_p$ space, because $\mathbf{x}[i]$ can be estimated according to the input $u[k]$ and output $y[k]$ data up to the instant $k = i - 1$. As a result, we can obtain the direction with respect to the oblique projection of $\mathbf{Y}_f$. Owing to the availability of known deterministic input data, the identification allows to be carried out by performing an oblique projection.

The augmented matrix $\bar{A}$ has a column zeros, which results in an eigenvalue at $z = 0$. In fact, an eigenvalue at the origin corresponds to the z^{-1} delay factor, which introduces a pole at $z = 0$ in the transfer function $\bar{G}_d(z)$.

Fig. A.2(b) illustrates the projection procedure regarding the shifted state sequence, which is represented in Eq. (7.28), Section 7.5.1. It is similar to the reasoning related to Fig. A.2(a). The $\mathbf{O}_{i-1}$ is the oblique projection of $\mathbf{Y}_f^-$ (with omitting of the first row of the matrix) along $H_{i-1}U_f^-$ direction. It must be performed on the row space of the expanded matrix of input-output data $\mathbf{W}_p^+$, which is obtained from $\mathbf{W}_p$ by adding one row at the bottom.

Appendix B

Back Projection Algorithms

THIS Appendix provides further details about back projection algorithms. This is a specific supplement made for Chapter 10 in respect of computed tomography reconstruction.

B.1 Theory

The back projection is represented via parallel beam projections. Recalling the formula for the inverse Fourier transform, the object function, $f(x,y)$, can be expressed as

$$f(x,y) = \int_{-\infty}^{\infty}\int_{-\infty}^{\infty} F(u,v)e^{j2\pi(ux+vy)}\mathrm{d}u\mathrm{d}v. \tag{B.1}$$

Exchanging the rectangular coordinate system in the frequency domain, (u,v), for a polar coordinate system, (w,θ), by making the substitutions

$$u = w\cos\theta \tag{B.2}$$

$$v = w\sin\theta \tag{B.3}$$

and changing the differentials by using

$$\mathrm{d}u\mathrm{d}v = w\mathrm{d}w\mathrm{d}\theta, \tag{B.4}$$

we can write the inverse Fourier transform of a polar function as

$$f(x,y) = \int_{0}^{2\pi}\int_{0}^{\infty} F(w,\theta)e^{j2\pi w(x\cos\theta+y\sin\theta)}w\mathrm{d}w\mathrm{d}\theta. \tag{B.5}$$

This integral can be split into two by considering θ from 0° to 180° and then from 180° to 360°,

$$\begin{aligned} f(x,y) \;=\; & \int_{0}^{\pi}\int_{0}^{\infty} F(w,\theta)e^{j2\pi w(x\cos\theta+y\sin\theta)}w\mathrm{d}w\mathrm{d}\theta \\ & + \int_{0}^{\pi}\int_{0}^{\infty} F(w,\theta)e^{j2\pi w[x\cos(\theta+180^\circ)+y\sin(\theta+180^\circ)]}w\mathrm{d}w\mathrm{d}\theta \end{aligned} \tag{B.6}$$

and then using the property

$$F(w,\theta+180^\circ) = F(-w,\theta) \tag{B.7}$$

the above expression for $f(x,y)$ may be written as

$$f(x,y) = \int_{0}^{\pi}\left[\int_{-\infty}^{\infty} F(w,\theta)|w|e^{j2\pi wt}\mathrm{d}w\right]\mathrm{d}\theta. \tag{B.8}$$

Here, we have simplified the expression by setting

$$t = x\cos\theta + y\sin\theta. \tag{B.9}$$

If we substitute the Fourier transform of the projection at angle θ, $s_\theta(w)$, for the two-dimensioinal Fourier transform $F(w,\theta)$, we get

$$f(x,y) = \int_{0}^{\pi}\left[\int_{-\infty}^{\infty} s_\theta(w)|w|e^{j2\pi wt}\mathrm{d}w\right]\mathrm{d}\theta. \tag{B.10}$$

This integral in Eq. (B.10) may be expressed as

$$f(x,y) = \int_0^{\pi} Q_\theta(x\cos\theta + y\sin\theta)\mathrm{d}\theta \tag{B.11}$$

where

$$Q_\theta = \int_{-\infty}^{\infty} S_\theta(w)|w|e^{j2\pi wt}\mathrm{d}w. \tag{B.12}$$

Eq. (B.11) represents a filtering operation, where the frequency response of the filter is given by $|w|$; therefore $Q_\theta(w)$ is called a 'filtered projection'. The resulting projections for different angles θ are then back projected to form the estimate of $f(x,y)$.

We relabel $S_\theta(w)$ to $S(\theta,\beta)$, t to ξ, then we rewrite Eq. (B.11) to yield,

$$I(x,y) = \int_0^{\pi}\left[\int_{-\infty}^{\infty} S(\theta,\beta)|\beta|\exp[i2\pi\beta\xi]\mathrm{d}\beta\right]\mathrm{d}\theta \tag{B.13}$$

where, Eq. (B.13) is the same as Eq. (10.2) that we use in Section 10.2 for THz reconstruction.

Appendix C

Error Analysis Regarding Wavelet Based Local Reconstruction

THIS Appendix provides further details about error analysis with respect to wavelet based local reconstruction. This is a specific supplement made for Chapter 12 to validate local CT via wavelet transforms.

C.1 Methodology

Radon transform error is not negligible because of the nonlocal property of the derivative Hilbert transform (the impulse response of the filter $|\beta|$). In this case, even a small local ROI can be reconstructed by considering some data outside the region of interest for a negligible reconstruction error. In terms of the amount of nonlocal data applied in the reconstruction, an upper bound of the reconstruction error can be calculated. The comparison is made between the wavelet based reconstruction and the traditional reconstruction algorithm for the local tomography image recovery.

In the current algorithm, the region of interest (ROI) and the region of exposure (ROE), are assumed to be centered at the center of an image. The support of a completed image is a disk of radius R pixels centered at the origin. Disks of radius r_i pixels and r_e pixels centered at the origin are used to denote the ROI and ROE, respectively. Consider the Eq. (C.5), the traditional filtered back projection algorithm, which is shifted to the time domain scheme.

$$I_r(x,y) = \int_0^{\pi} s(\theta,\xi) h_\theta(x\cos\theta + y\sin\theta)\mathrm{d}\theta. \tag{C.1}$$

The reconstructed function $I_r(x,y)$ is an approximation of the function $I(x,y)$ if h_θ is the angle dependent impulse response of the ramp filter, $\theta \in [0, 2\pi)$, and is an approximation of the wavelet and scaling coefficients if wavelet and scaling filters are substituted for $|\beta|$.

The discrete version is expressed as follows:

$$I_r(x,y) = \frac{\pi}{k}\sum_{k=1}^{k}\frac{1}{R}\sum_{n=-R}^{R} s_{\theta_k}(n) h_{\theta_k}(m-n) \tag{C.2}$$

where $m = (x\cos\theta + y\sin\theta) \in$ ROE, K is the number of the measured projection angles, s_{θ_k} indicates the projection at kth angle and $\theta_k = k(\pi/k)$. The completed image based on global data consists of two parts: the ROE and its complement $\overline{\text{ROE}}$,

$$I_r(x,y) = \frac{\pi}{k}\sum_{k=1}^{k}\frac{1}{R}\sum_{|n|\le r_e} s_{\theta_k}(n) h_{\theta_k}(m-n) + \frac{\pi}{k}\sum_{k=1}^{k}\frac{1}{R}\sum_{|n|> r_e} s_{\theta_k}(n) h_{\theta_k}(m-n). \tag{C.3}$$

Therefore the magnitude of error regarding the ROE can be calculated as follows:

$$|\epsilon(x,y)| = \left|\frac{\pi}{k}\sum_{k=1}^{k}\frac{1}{R}\sum_{|n|> r_e} s_{\theta_k}(n) h_{\theta_k}(m-n)\right|. \tag{C.4}$$

The Cauchy-Schwartz inequality is used to achieve an upper bound of the error calculation,

$$\begin{aligned} |\epsilon(x,y)| &= \left| \frac{\pi}{k} \sum_{k=1}^{k} \frac{1}{R} \sum_{|n|>r_e} s_{\theta_k}(n) h_{\theta_k}(m-n) \right| \\ &\leq \frac{\pi}{k} \sum_{k=1}^{k} \frac{1}{R} \sum_{|n|>r_e} |s_{\theta_k}(n) h_{\theta_k}(m-n)| \\ &\leq \frac{\pi}{k} \sum_{k=1}^{k} \frac{1}{R} \left(\sum_{|n|>r_e} |s_{\theta_k}(n)|^2 \right)^{1/2} \left(\sum_{|n|>r_e} |h_{\theta_k}(m-n)|^2 \right)^{1/2}. \end{aligned} \tag{C.5}$$

There exists such an approximation that $|s_{\theta_k}| \leq 2 \max |I(x,y)|$.

$$|\epsilon(x,y)| = \frac{2\sqrt{2}\pi}{k} \max |I(x,y)| \frac{\sqrt{R-r_e}}{R} \cdot \sum_{k=1}^{K} \left(\sum_{|n|>r_e} |h_{\theta_k}(m-n)|^2 \right)^{1/2}. \tag{C.6}$$

The relative error is defined as:

$$\begin{aligned} |\epsilon_{\text{rel}}(x,y)| &= |\epsilon(x,y)| / \max |I(x,y)| \\ &= \frac{2\sqrt{2}\pi}{k} \frac{\sqrt{R-r_e}}{R} \cdot \sum_{k=1}^{K} \left(\sum_{|n|>r_e} |h_{\theta_k}(m-n)|^2 \right)^{1/2}. \end{aligned} \tag{C.7}$$

It is observed that after applying wavelet based ramp filter, the reconstructed intensity of an terahertz image is much higher than traditional ramp filtered based reconstruction. Thus in the calculation of relative error, normalisation of the reconstructed local images is important for comparison between the global and local reconstruction. A normalisation scaling factor is calculated via dividing maximum intensity of global reconstruction, denoted by $I(x,y)$ by maximum intensity of local reconstruction, denoted by $I_{\text{local}}(x,y)$. The function is as follows:

$$N_{I_{g,l}} = \max |I(x,y)| / \max |I_{\text{local}}(x,y)|. \tag{C.8}$$

Combine Eq. (C.7) and Eq. (C.8), and then we achieve a relative error calculation equation in terahertz image reconstruction,

$$|\epsilon_{\text{rel}}(x,y)| = N_{I_{g,l}} \cdot \frac{2\sqrt{2}\pi}{k} \frac{\sqrt{R-r_e}}{R} \cdot \sum_{k=1}^{K} \left(\sum_{|n|>r_e} |h_{\theta_k}(m-n)|^2 \right)^{1/2}. \tag{C.9}$$

The ROI can be viewed as a point is its worst case. The function above can be described as:

$$|\epsilon_{\text{rel}}(x,y)| = N_{I_{g,l}} \frac{2\sqrt{2}\pi}{k} \frac{\sqrt{R-r_e}}{R} \cdot \sum_{k=1}^{K} \left(\sum_{|n|>r_e-r_i} |h_{\theta_k}(n)|^2 \right)^{1/2}. \tag{C.10}$$

The truncated filter is defined as:

$$h_{\theta_k}^T(n) \begin{cases} h_{\theta_k}(n) & \text{if } |n| < r_e - r_i, \\ 0 & \text{otherwise .} \end{cases} \tag{C.11}$$

Hence,

$$|\epsilon_{\text{rel}}| = N_{I_{g,l}} \cdot \frac{2\sqrt{2}\pi}{k} \frac{\sqrt{R - r_e}}{R} \cdot \sum_{k=1}^{K} \left(\sum_{|n|=-R}^{R} |h_{\theta_k}(n) - h_{\theta_k}^T(n)|^2 \right)^{1/2} \tag{C.12}$$

The inner sum can be described in the frequency domain

$$\begin{aligned} |\epsilon_{\text{rel}}(x,y)| &= N_{I_{g,l}} \cdot \frac{2\sqrt{2}\pi}{k} \frac{\sqrt{R - r_e}}{R} \\ &\cdot \sum_{k=1}^{K} \left(\sum_{|n|=-R}^{R} |\{[H_{\theta_k}(l) - H_{\theta_k}^T(l)] \exp[i2\pi\beta\xi]\}|^2 \right)^{1/2} \end{aligned} \tag{C.13}$$

where H_{θ_k} and $H_{\theta_k}^T$ are the Fourier transform of h_{θ_k} and $h_{\theta_k}^T$, respectively. To calculation of upper bound for the error in standard filtered back projection algorithm, h_{θ_k} in Eq. (C.9) is replaced by the ramp filter $|\beta|$. The upper bound of the relative error in the reconstructed image of wavelet and scaling coefficients can be obtained by replacing H_{θ_k} in Eq. (C.9) with in Eq. (C.14) and via multiplication by a normalization factor,

$$\begin{cases} H_\theta^C = |\beta| \Phi_{2^j}(\beta\cos\theta, \beta\sin\theta) = |\beta| \Phi_{2^j}(\beta\cos\theta) \Phi_{2^j}(\beta\sin\theta) \\ H_\theta^{D^H} = |\beta| \Psi_{2^j}^h(\beta\cos\theta, \beta\sin\theta) = |\beta| \Phi_{2^j}(\beta\cos\theta) \Psi_{2^j}(\beta\sin\theta) \\ H_\theta^{D^V} = |\beta| \Phi_{2^j}^V(\beta\cos\theta, \beta\sin\theta) = |\beta| \Psi_{2^j}(\beta\cos\theta) \Phi_{2^j}(\beta\sin\theta) \\ H_\theta^{D^D} = |\beta| \Psi_{2^j}^d(\beta\cos\theta, \beta\sin\theta) = |\beta| \Psi_{2^j}(\beta\cos\theta) \Psi_{2^j}(\beta\sin\theta) \end{cases} \tag{C.14}$$

where H_θ^C and $H_\theta^{D^i}, (i = H, V, D)$ are called scaling and wavelet ramp filters.

The relative error in the reconstruction image from approximate reconstruction coefficients is as follows:

$$\begin{aligned} |\epsilon_{\text{rel}}(x,y)| &= N_{I_{g,l_C}} \cdot \frac{2\sqrt{2}\pi}{k} \frac{\sqrt{R - r_e}}{R} \\ &\cdot \sum_{k=1}^{K} \left(\sum_{|n|=-R}^{R} |\{[H_{\theta_k}^C(l) - H^{C^T}{}_{\theta_k}(l)] \exp[i2\pi\beta\xi]\}|^2 \right)^{1/2} \end{aligned} \tag{C.15}$$

where $N_{I_{g,l_C}}$ is the normalised scale factor of an image in relation to approximate reconstruction coefficients, which is calculated via dividing maximum intensity of global reconstruction, denoted by $\{I(x,y)\}$, by maximum intensity of local reconstruction regarding approximate wavelet coefficients, denoted by $\{I^C_{\text{local}}(x,y)\}$. The normalised scale factor is as follows:

$$N_{I_{g,l_C}} = \max|I(x,y)| / \max|I^C_{\text{local}}(x,y)|. \tag{C.16}$$

Appendix D

Terhertz Imaging Systems

THIS Appendix provides further detail and specifications on the components of both the pulsed THz and continuous wave (CW) terahertz imaging system. The pulsed approach uses a conventional Ti:sapphire laser and relates to Chapter 2 (Sec. 2.3.1), Chapters 9, 11 and 12. The CW approach uses a THz quantum cascade laser (QCL) and relates to Chapter 2 (Sec. 2.5.2) and Chapter 13. It provides a list of the major hardware components along with their critical specifications and purpose. It also summarises part of the experimental procedure used for pulsed spectroscopy experiments in this Thesis.

D.1 Ultrafast T-ray pulsed imaging

This Section describes experimental equipment used in T-ray pulsed measurements in further detail along with model specifications. Moreover, the software tools that were designed to control the equipment during an experiment and to process the results are also described herein.

D.1.1 Ultrafast laser

The femtosecond laser illustrated in Fig. D.1 is the key part of the pulsed T-ray spectrometer. The Ti:sapphire laser is used for most of the spectroscopy experiments in this Thesis.

D.1.2 Crossed-polariser detection

A fundamental part of electrooptic sampling (EOS, see Section 2.5.1) is the photodiode detection circuit. A photograph of crossed polarisers in electrooptic Sampling used in a series of THz experiments in this Thesis is shown in Fig. D.2. The probe beam, entering the Figure from the left, passes though the EO crystal. The polarisation of the probe beam is modulated by the T-ray power, which, subsequently, causes an intensity modulation by a Wollaston polariser. Depending on the rotation of the probe polarisation, the optical power shifts between the two output beams of the Wollaston. These beams are directed onto two photodiodes.

The two photodiodes are connected to output a *difference current*—common mode fluctuations in the probe power are attenuated, while difference currents produced by polarisation rotation are amplified. A quarter-wave plate is used to balance the power in the two beams to zero for no T-ray power. The T-ray path is blocked and the quarter-wave plate rotated. A DC ammeter is needed to read the output of the balanced circuit for optimisation. Normally during measurement, the output of the preamplifier is attached directly to the LIA.

D.1.3 Hardware specifications

Table D.1 is the description regarding the full system layout of components. This Table lists the components of the full T-ray experiment shown in Fig. D.3, as well as the

NOTE:
This figure is included on page 305 of the print copy of the thesis held in the University of Adelaide Library.

Figure D.1. Photograph of an ultrafast laser. This photograph shows the interior of the femtosecond laser used for a number of THz experiments in this Thesis. Visible in this diagram is the Acousto-Optic Modulator (AOM unit, used to sustain mode-locking (pulsed operation) over long periods of time. The path of the laser beam is marked in red, refracting through the four dispersion-control prisms and into the AOM and output coupler (from left to right). After Mickan (2003).

hardware specifications. Detailed descriptions of the role these components play in the system and the manufacturers of the optics are presented in Table D.2.

D.1.4 Software implementation

A substantial amount of software was developed to support this research. Software tools were designed to control the equipment during an experiment and to process the results. This Appendix describes the major software applications used.

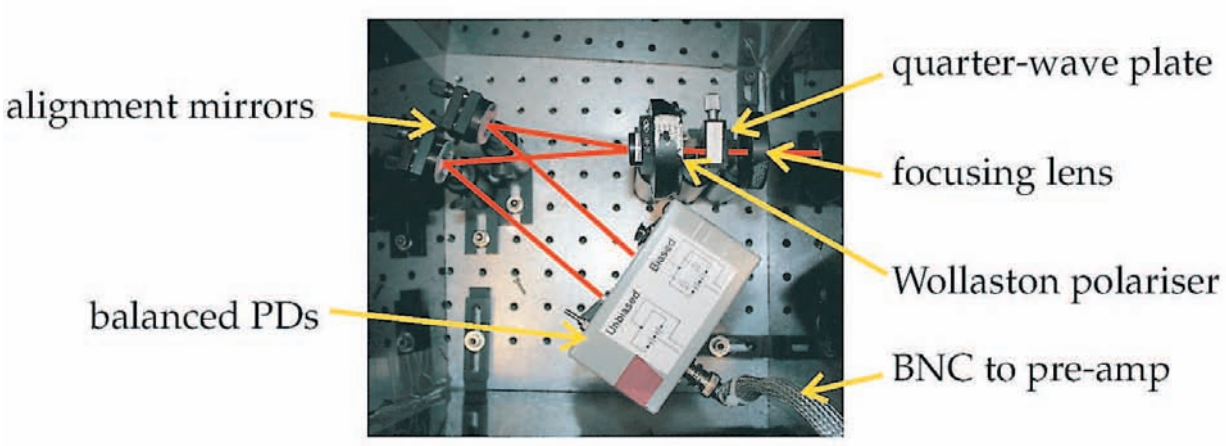

Figure D.2. Photograph of crossed polarisers in electrooptic sampling. The polarisation of the optical probe beam in EOS is detected using crossed polarisers. The probe beam is focused onto the photodiodes using a lens to minimise noise from fluctuations in the alignment of the probe beam. A quarter-wave plate is used to balance the polarisation of the probe beam equally between the s- and p-polarisations when no T-ray field is present.

MFCPentaMax

This application (written in Microsoft Visual C++) was originally developed by Paul Campbell at the Rensselaer Polytechnic Institute. It is used to control the PI Pentamax CCD camera and the motorised motion stages during 2D FSEOS THz imaging. The software is updated by Bradley Ferguson to allow it perform synchronised dynamic subtraction and to control the A200SMC stepper motor controller to allow it to be used for tomography experiments. The software sets up the CCD camera and continuously streams frames from the CCD to a memory buffer, and also controls the motion stages. The software supports CCD pixel binning and dynamic subtraction and accumulation operations. The image data are saved to a file for offline processing and reconstruction, which is performed using Matlab software (see Section 9.3). A screen shot of the MFCPentaMax application is shown in Fig. D.4(a). The code is compiled using Microsoft Visual Studio version 6.

LabView tomography application

National Instruments LabView is used to write general purpose experiment control programs due to the ease of programming and the wide support for equipment drivers. Existing programs written by members of the Department of Physics at Rensselaer

NOTE:
This figure is included on page 307 of the print copy of the thesis held in the University of Adelaide Library.

Figure D.3. Schematic of the femtosecond laser-based T-ray chirped functional imaging system based on a pump-probe configuration. The probe beam is chirped using a diffraction grating to extend its pulse width from 130 fs to 21 ps. The pump beam generates THz pulses via a photoconductive antenna (PCA) emitter. The THz pulses are focused on the sample using parabolic mirrors PM1 and PM2, the transmitted radiation is then focused on the detector using PM3 and PM4. The THz pulse is reflected by an ITO beam splitting mirror, which allows the chirped probe pulse and the THz pulse to propagate collinearly through the ZnTe detector. The wavelength components of the probe beam are then adjusted by a spectrometer and viewed on a CCD camera, revealing the THz temporal profile. The target is then raster scanned to acquire an image. P1,P2=polarizers; ITO=indium tin oxide beam splitter. This experimental setup is used in for THz CT reconstruction, described in Chapter 10. After Ferguson *et al.* (2002a).

Polytechnic Institute are modified to provide the desired functionality. Fig. D.4(b) shows a screen shot of a Labview program designed for performing a T-ray CT experiment. The program allows three translation stages and a rotation stage to be controlled over a GPIB interface and the rotation stage is accessed through the parallel port. A lock-in amplifier is used file is saved to disk for offline processing and reconstruction, which is performed using Matlab software (see Appendix E). The Labview code was written in National Instruments Labview version 6i.

NOTE:
This figure is included on page 308 of the print copy of the thesis held in the University of Adelaide Library.

Figure D.4. Screen shots of the MFCPentamax software and the Labview tomography application. (a) This program is used to control 2D FSEOS THz imaging and tomography experiments. The program records images from the PI Pentamax CCD camera and controls the motorised motion stages to translate and rotate the target. The screen shot shows the CCD options setup page. (b)This program is developed to control T-ray CT experiments. The program allows three translation stages and a rotation stage to be controlled. The motion stages are controlled over a GPIB interface and the rotation stage is accessed through the parallel port. A lock-in amplifier is used to record the THz signal and is accessed over GPIB. The results of the experiment are plotted in the windows shown and may be saved to disk. After Ferguson (2004).

Table D.1. The description regarding the full system layout components, along with the hardware specifications shown in Fig. D.3.

Number	Components	Specifications
1	A Spectra-Physics Mai-Tai Ti:sapphire oscillator	Output power of 0.7 W at 802.3 nm, with a 1 kHz pulse repetition rate and 130 fs pulse width
2	Pneumatic vibration isolated optical tables	Separated mounting holes by 2.54 cm (1")
3	A lock-in amplifier	A stanford Research Systems SRS830 LIA. The lock-in amplifier is synchronised with an optical chopper
4	An optical chopper	Stanford Research Systems SR540, driven using synchronised dynamic subtraction
5	optical mirrors	Newport 10D20ER.2 broadband metallic mirrors
6	Parabolic mirrors	Gold coated off-axis parabolic mirrors
7	Three motorised linear motion stages	Newport stepper motor UR73PP stages.
8	A Newport MM3000 motion controller	200 mm of travel with a resolution of 1 μm
9	A motorised rotation stage	With resolution of 1.8° and a maximum speed of 120 revolutions per minute
10	Double side polished <110> oriented ZnTe crystals	A large 20 mm diameter crystal with the crystal thickness varied between 3 mm and 4 mm
11	Double side polished high-resistivity GaAs wafers	With a 0.6 mm thick, 3 cm diameter GaAs wafer and with metal electrodes separated by 2 cm
12	Quarter and half wave plates	Newport 10RF42-3 broadband wave plates, 1.8° resolution and a maximum speed of 120 revolutions per minute
13	A SPEX 500M spectrometer	A spectral resolution of 0.2 $\AA$ and a dispersion of 3 mm/nm
14	A cubic polarising beam splitter	Anti-reflection coated for 800 nm and its part number was Melles Griot 03 PTA 101
15	Diffraction grating	With grating constant 10 μm, the grating separation of 4mm and the angle of incidence of 51°.
16	A Princeton Instruments EEV 576×384 CCD camera	Air-cooled to -30° with pixel size of 22×22 μm^2,12 bit digitisation, and a frame-transfer period of 15 ms.

Picometrix system software

The T-ray Picometrix 2000 system used for the experiment presented in Section 9.3 is controlled from a LabView program. The computer controls the delay stages via a General Purpose Interface Bus network. Two screen shots regarding the LabView computer interface are shown in Fig. D.5. The two screen shots are the outputs of a couple of example THz measurements in the time domain and the frequency domain, respectively. The controls for the experiment are shown on the left and the bottom and the readouts are in the middle. In the centre is a large time-domain graph (a) and frequency-domain graph (b) of a couple of sampled T-ray waveforms. The smaller graph underneath shows the transforms of the measurements in the frequency domain and the time domain, respectively. The pictures are from the Adelaide laboratory.

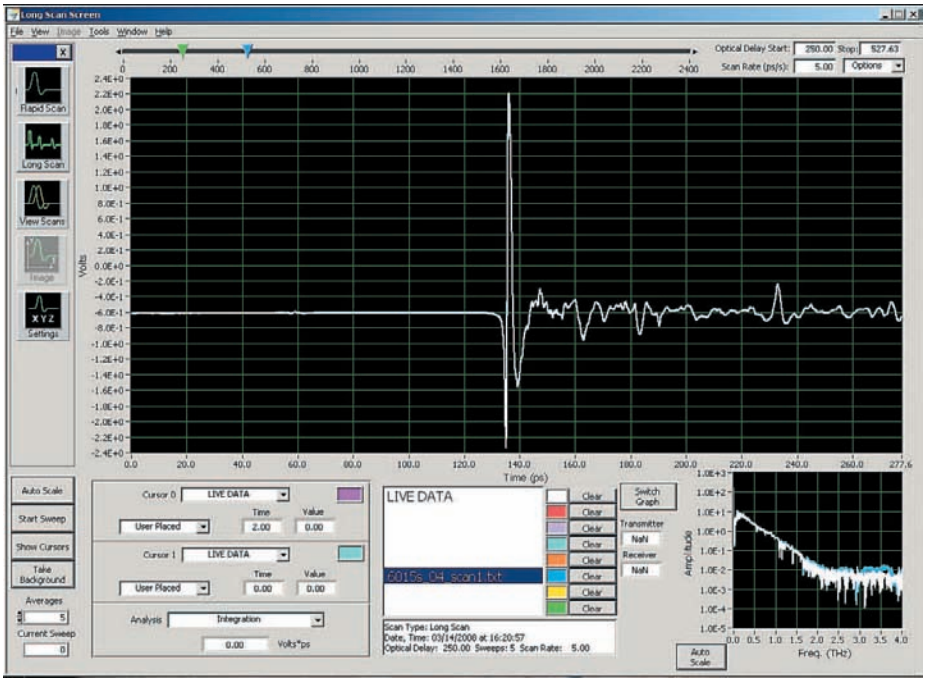

(a)

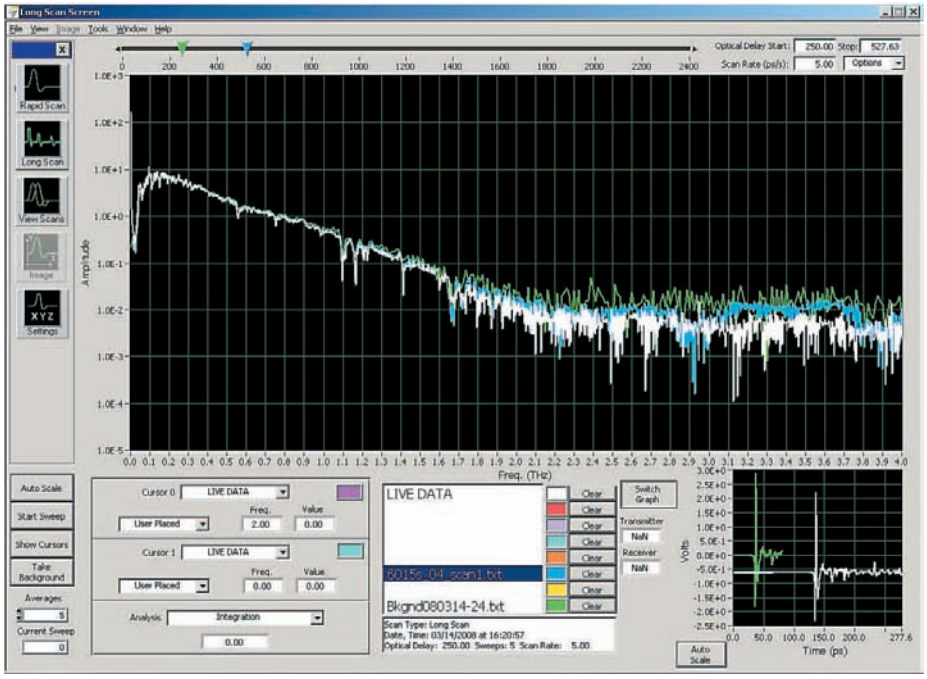

(b)

Figure D.5. Screen shot of control software for operating T-ray TDS experiments via a Picometrix system. These are two screen shots of the LabView computer interface used to control a Picometrix T-ray spectrometer used in Section 9.3. (a) The THz readouts in the time domain. (b) The THz readouts in the frequency domain.

Table D.2. The description regarding the full system layout components, shown in Fig. D.3, including a detailed description of the role these components play in the system, and the manufacturers. The numbers correspond to the items listed in Table D.1.

Number	Functions	Manufacturers
1	The laser is to produce the optical pump and probe beams and therefore to generate and detect THz pulses	
2	The optical table is for optical posts	Newport
3	The LIA is for digitising the detected optical signal and to perform phase sensitive filtering to improve the SNR	
4	The chopper is for amplitude modulated the optical signal; providing manual control of the chopping frequency and a sync output to the lock-in amplifier	
5	The optical mirrors are for the optical adjustment of the NIR pump and probe beams	Newport
6	The parabolic mirrors are to focus and collimate the THz beam	
7	The motion stages are for scanned THz imaging (two for raster scanning the target and a third for the optical delay line). This controller provides front panel control of the stages and GPIB control for remote access from a controller	Newport
8	The motion controller controls the three stages. This controller provided front panel control of the stages and GPIB control for remote access from a controller	Newport
9	The rotation stage is to rotate the imaging target via a NEMA23ESM stepper motor from Mil-Shaf Technologies connected to the parallel port of a computer	
10	The ZnTe crystals generate THz pulses via OR and achieve the detection using EO sampling	eV Products
11	The wafers are to construct photoconductive planar strip lines by gluing two metal electrodes onto the wafer surface using conductive glue	University Wafer Pty. Ltd.
12	The wave plates are to rotate the polarisation of the NIR beam prior to splitting and photo detection	Newport
13	Spectrometer is to disperse the wavelength components of the chirped optical probe pulse for the chirped probe imaging system described in Section 9.3	
14	The splitter is to split the NIR laser pulses into pump and probe beams	
15	The diffraction grating chirps the optical probe pulse and extends its pulse width	
16	The CCD camera is placed in the 2D FSEOS THz imaging system and in the chirped probe system. It provides a sync output signal and allowed external triggering. It is controlled using the serial port of a computer.	

D.2 Continuous wave T-ray imaging via THz QCL

D.2.1 THz QCL imaging

This Section describes the experimental equipment used in T-ray CW imaging via a QCL in further detail along with the relative specifications on these components, which relates to the experiments in Chapter 13. Software tools that are designed to control the equipment during an experiment and to process the results are also described herein. Fig. D.6 is the layout of the THz QCL imaging experiment.

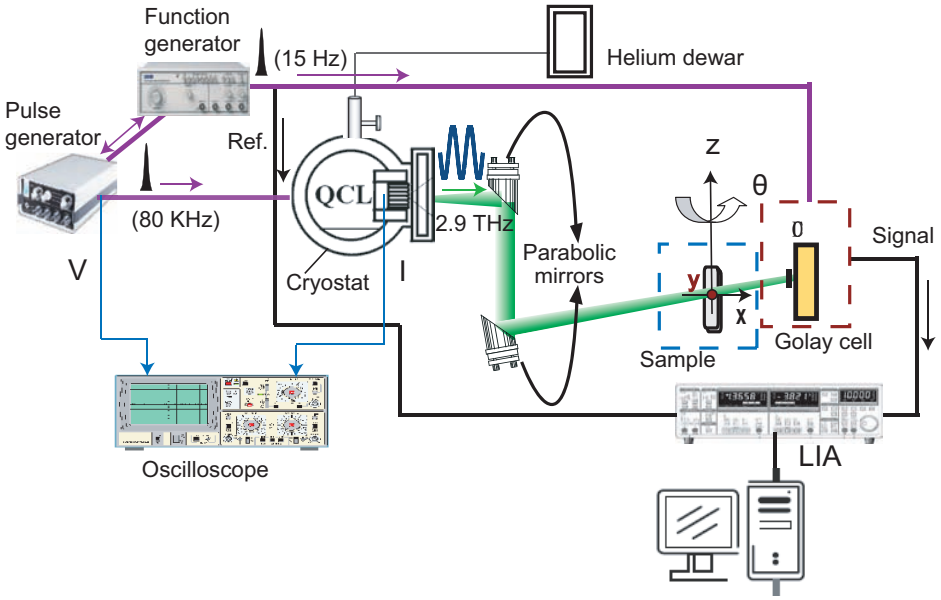

Figure D.6. Experimental apparatus for a terahertz QCL imaging system that is used to realise terahertz CT imaging. The pulse generator supplies pulses at a frequency of 80 kHz to the QCL. The output signal from the pulse generator is usually gated with a 15 Hz, 50% duty cycle slow modulation by an electronic chopper (a function generator of pulses) to match the detector (the Golay cell) response time, and to afford a reference frequency to the lock-in amplifier (LIA). The LIA is used to digitise signals and to significantly improve the signal-to-noise ratio by setting a time constant, over which the input signal is integrated for each data point. The optimal time constant is set to 50 ms and a threshold current density is set as 112 A/cm^2. The emission is collected with a 200" f/1 off-axis parabolic mirror, then focused by a 200" f/6.43 parabolic mirror onto the sample. In practice, the sample is placed on a rotational stage for multi view angles, which is mounted on a xyz linear stage to perform 3D scanning.

D.2.2 Hardware specifications

THz QCL laser illustrated in Fig. D.7(a) is the key part of the CW T-ray spectrometer. The THz QCL is used for the THz continuous wave imaging reconstruction experiment in this Thesis.

In the present experiment carried in Chapter 13, the resolution is determined by the shape of the focused THz beam at the position of the sample and is limited by the optical design. To characterise the beam, the sample is removed and a pin hole with a diameter of 0.5 mm is put in front of the Golay cell, which is moved in the x and z directions to map out the beam shape in the focal plane. The cross-section of the beam

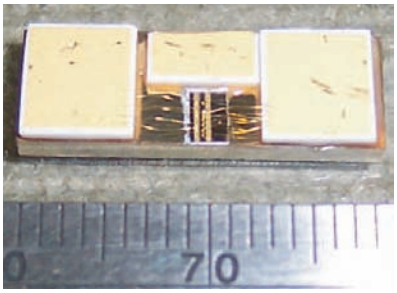

(a)

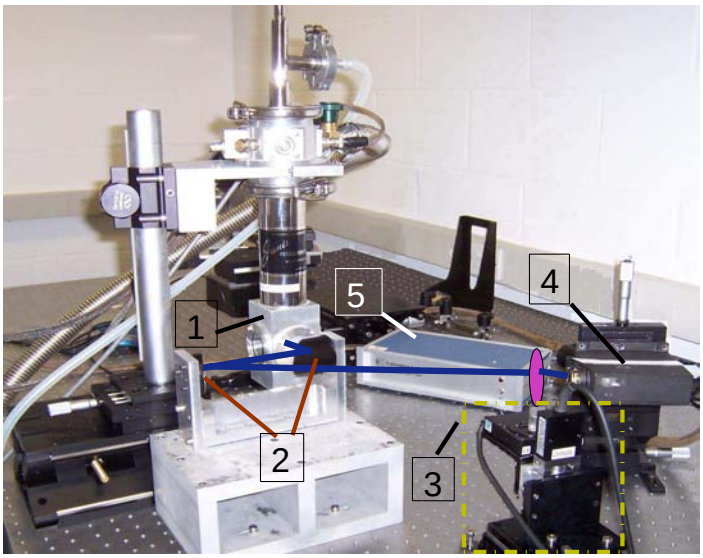

(b)

Figure D.7. Photographs of an THz QCL and its experiment setup for THz CW imaging. (a) The THz QCL used for this project is designed and fabricated by C.H. Worrall, J. Alton *et. al.* in the Semiconductor Physics group, Cavendish Laboratory, Cambridge University, UK. The THz QCL is a GaAs-AlGaAs bound-to-continuum superlattice design, emitting at 2.9 THz (103 μm), and grown by molecular beam epitaxy, and typically operates up to 95K in pulse mode. It delivers 70 mW per facet peak power, with a threshold current density of 112 A/cm^2. The current THz QCL is a GaAs-AlGaAs bound-to-continuum superlattice design, emitting at 2.9 THz (103 μm), and grown by molecular beam epitaxy. After Nguyen *et al.* (2006). (b) Photograph showing the experimental apparatus is outlined in Fig. D.6 that is used to realise terahertz CT imaging. The numbers in the text-boxes from 1 to 5 indicate, respectively, (i) a QCL that is mounted on the cold finger of a continuous-flow helium-cooled cryostat maintaining a heat-sink temperature of 4.2 K, (ii) a pair of parabolic mirrors, (iii) the rotational stage mounted on an xyz translational stage, (iv) a Golay cell detector, and (v) a detector controller.

(a) (b)

Figure D.8. Photograph of right part of the experimental apparatus shown in Fig. D.6. (a) Equipment in the instrument rack from top to bottom is as follows: an EG&G 5210 lock-in amplifier, a Tektronix TDS2014 digital oscilloscope, a TTi TG230 function generator, and an Agilent 8114 A high power pulse generator. (b) A CryoCon model 32 temperature controller, affording two-channel controller designed for fixed cryogenic applications.

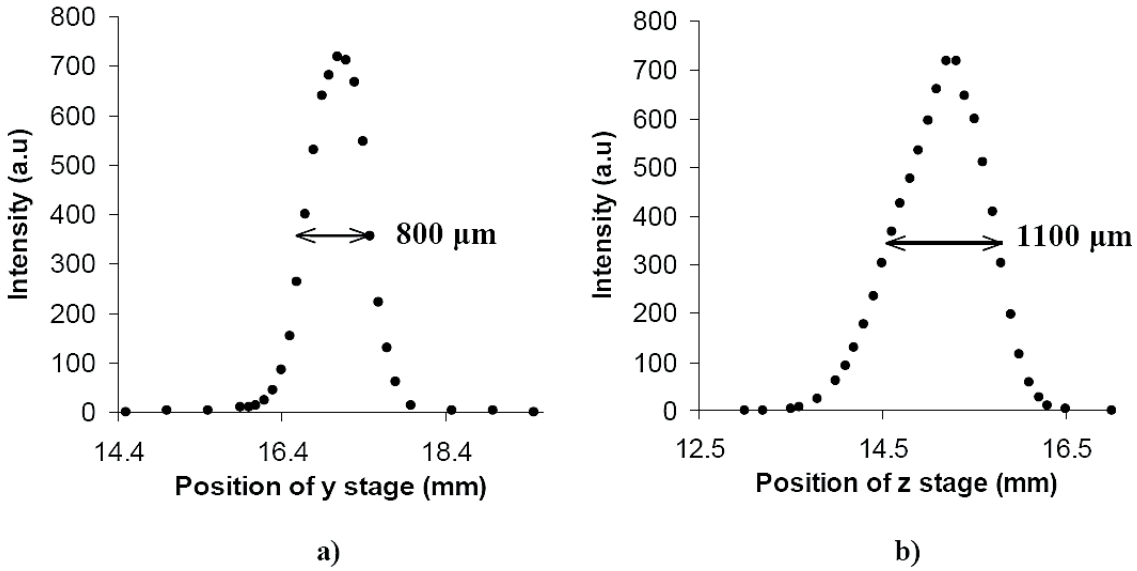

Figure D.9. Mapping the QCL beam shape. (a) Along x direction and (b) Along z direction

(Fig. D.9) is found to be relatively circular, with a full-width-half-maximum (FWHM) varying between 800 μm (x) and 1,100 μm (z).

Table D.1 is the description regarding the full system layout of components associated with the terahertz QCL experiments shown in Fig. D.6.

D.2.3 LabVIEW^{TM} programming implement for data acquisition

The linear and rotational stages on which the sample is mounted are connected to a motion controller (Newport, model: MM4006), which is controlled with a programme written in LabVIEW^{TM} programming language. LabVIEW^{TM} is an increasingly popular graphical development environment for signal acquisition, measurement analysis and data presentation (National Instruments, 2004). A LabVIEW^{TM} programme consists of two components. One is a Front panel, which serves as user interface. The front panel is built with controls and indicators, which are interactive input and output terminals, respectively. Through the front panels of LabVIEW^{TM} programmes, users enter operating parameters. The other is a block diagram, which contains the graphical source code. Objects on the block diagram include terminals, nodes, and functions connected with wires. The block diagram represents the electronic circuits inside physical instruments. The computer controls the delay stages and acquires data

Table D.3. Summary of electronic components of the THz QCL imaging system. Components shown in Fig.D.6.

Items	Manufacturer/model	Functions/Specifications
A THz QCL	Semiconductor Physics group, Cavendish Laboratory, The University of Cambridge	Generation of continuous waves of terahertz radiation with high output power and sample penetration depth.
A pulse generator	Agilent/8144 A	Delivers fast, clean positive or negative pulses up to 100 V at frequencies up to 15 MHz
A cold finger of a continuous-helium-cooled flow cryostat	Janis Research Co. Inc/ ST-300	Maintais a heat-sink temperature of 4.2 K.
An electronic chopper	Thurlby Thandar Instruments (TTI)/TG2000 Series	The main output with a maximum emf of 20 V pk-pk from a 50 Ohmand or 600 Ohm source; A fixed 0 V to +5 V level suitable for driving both TTL and CMOS loads; Each wide sweep range at least 1000:1 either manually or via the sweep control input.
A high performance single phase analog lock-in amplifier	EG&G Princeton Applied Research/5210	A sensitivity vernier control, allowing the full-scale sensitivity to be set to any value between the calibrated values; With an input impedance of down to typically only 25 W the resulting voltage generated across the source by the signal current is minimized for the very best performance.
A 100 MHz 4 channel digital real-time oscilloscope	Tektronix/ TDS2014	With up to 200 MHz bandwidth and 2 GS/s maximum sample rate; providing accurate real-time acquisition up to theirfull bandwidth; offering advanced pulse width triggering and line-selectable video triggering, and 11 standard automatic measurements
A temperature controller	Cryocon/model 32	Two-channel controller designed for fixed cryogenic applications. Platinum RTD sensors allows the use of built-in DIN 43760 (IEC 750) standard curves for 100 W, 1,000 W or 10 KW devices. The standard curve is used for temperatures from 70 K to 1020 K and is extended down to 30 K for cryogenic use. Operation to about 14 K is possible with user-supplied curves.
Parabolic mirrors	Gold coated off-axis parabolic mirrors	A 200" f/1 off-axis parabolic mirror for collecting the THz radiation, then a 200" f/6.43 parabolic mirror is used to focus it onto the sample
Three linear motion stages	Newport/VP-25XA	For scanned THz imaging
A motorised rotation stage	Newport/SR50CC	To rotate a sample for multi-angle imaging
A Golay cell	Cathodean Ltd/IR50	An opto-acoustic detector designed for operation in the spectral range 0.02-20 THz, equipped with a 6 mm diameter polyethylene input window that provides for high transparency at frequencies up to 20 THz. It is mounted on proprietary vibration-isolating bases.

via a General Purpose Interface Bus (GPIB, manufacturer: National Instruments) network. Screen shots of the LabVIEW^{TM} application for the control of linear and rotation stages via front panels and block diagrams are shown in Fig. D.10 and the screen shots regarding front panels and block diagram for the control of a rotation stage are shown in Fig. D.11.

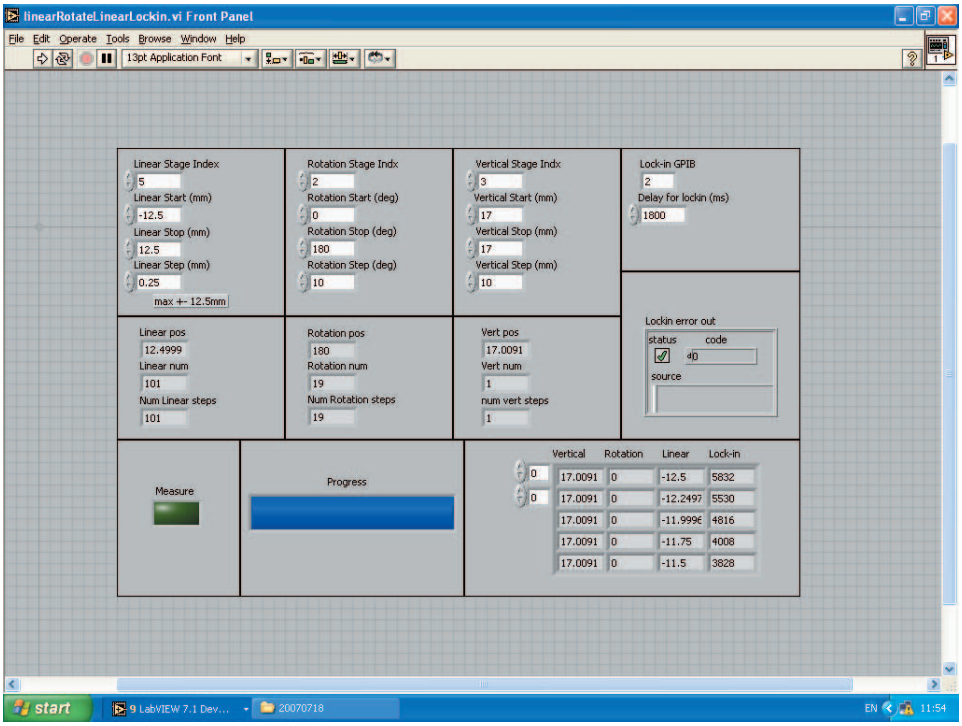

(a)

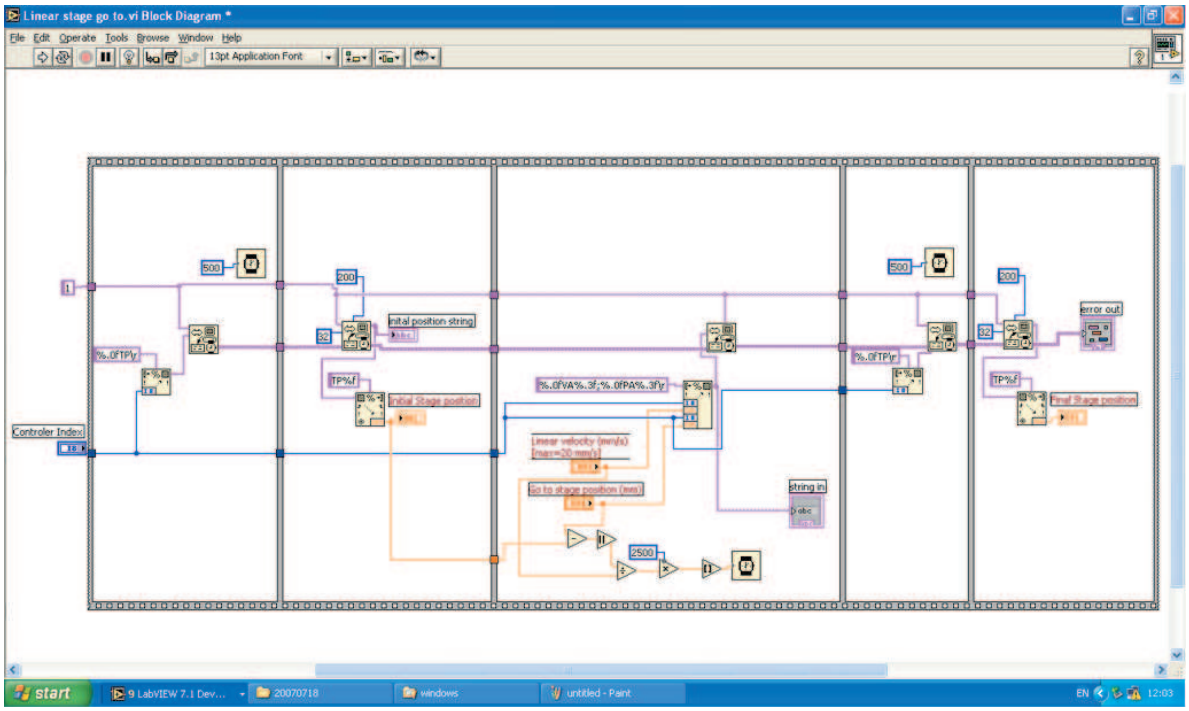

(b)

Figure D.10. Screen shots of LabVIEW^{TM} programme to control motion stages via motion controllers. (a) This controller provides front panel control (a) of the stages and GPIB control via a block diagram interface (b) for remote access from a controller. A lock-in amplifier is used to record the THz signal and is accessed over a GPIB interface.

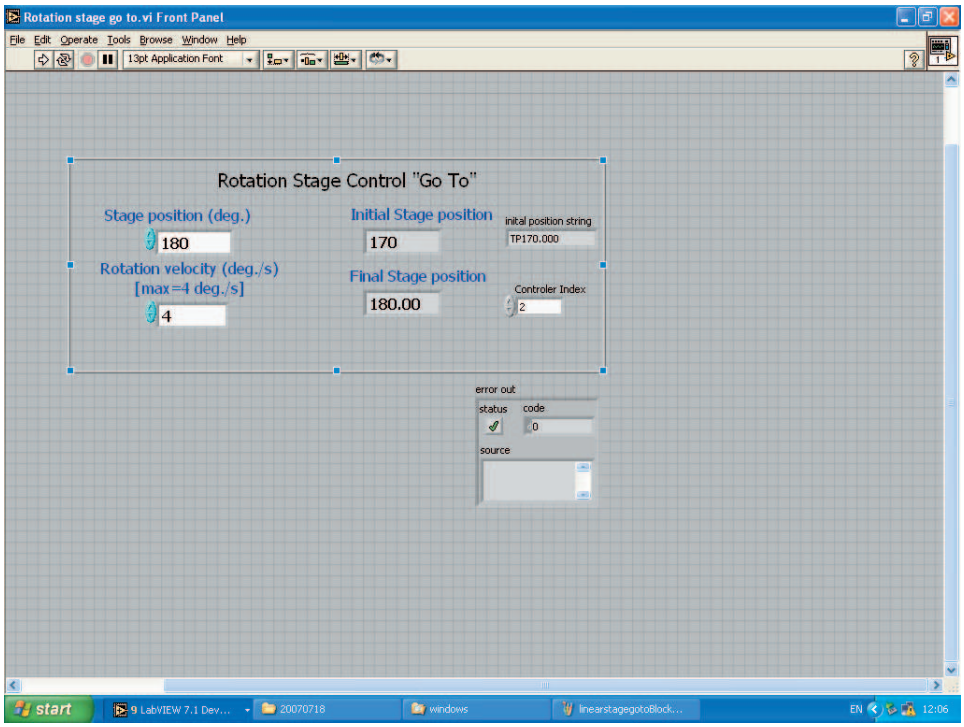

(a)

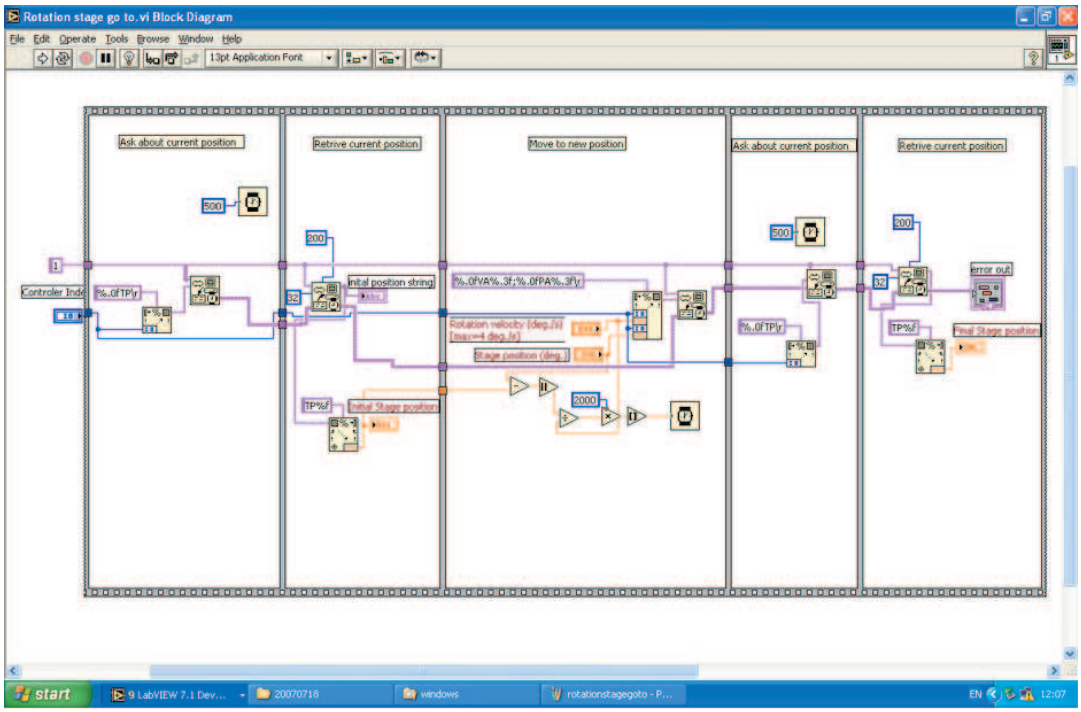

(b)

Figure D.11. Screen shots of LabVIEW^{TM} programme to control rotation stages via motor controllers. (a) This controller provides front panel control (a) of the stage and parallel port control with application of a block diagram interface (b) for remote access of the rotation stage.

Appendix E

Matlab Code

THIS appendix contains some of the algorithms used to achieve computer analysis of the raw T-ray waveforms. These algorithms are implemented in MATLAB (manufacturer: The MathWorks, model:7; URL: http://www.mathworks.com), and are available on the attached CD-ROM, X.X. Yin PhD Thesis/MATLAB Algorithms, as MATLAB files. Also included on the CD-ROM is a directory of raw data files, included as examples of typical T-ray experimental output, and a pdf file of this Thesis.

E.1 Implemented Matlab toolboxes

Matlab 7 is used to implement all the algorithms described in this Thesis. Matlab is an interpreted programming language with built in support for a large number of mathematical functions and data presentation tools. Mathematical derivations in this Thesis are checked using the symbolic Maple toolbox. The following Matlab toolboxes are utilised:

1. the wavelet toolbox
2. the system identification toolbox
3. the SVM and kernel methods matlab toolbox
4. the symbolic toolbox
5. the signal processing toolbox
6. the image processing toolbox.

E.2 Code listings

This Section provides code listings for the Matlab software used to implement many of the algorithms described in this Thesis. This is only a subset of the software developed to support this research. Matlab scripts with little algorithmic content, including those used to parse input data files and generate plots, have not been included. For more details on the software implementation please contact the author.

The attached CD includes copies of the Matlab files described below:

Powder recognition via frequency domain features

- WDHeuSURE.m This function implements the wavelet Soft Heuristic SURE methods to achieve preferred denoised performance of THz pulsed responses, as presented in Chapter 6 (Sec. 6.5). It also demonstrates frequency domain features that are extracted to be as inputs for classification.
- classify.m This function is to apply Mahalanobis classifier to classify different types of powders based on extracted frequency domain features in 3D. This algorithm is described in Chapter 9 (Sec. 9.2 and Section 9.4).

Cancerous cell recognition functions via auto regressive modelling over wavelet subbands

- WPDencorreAR.m This function implements the wavelet packet SURE methods to denoise measured cancerous cell signals *ex vivo*. Auto Regressive (AR) coefficients are calculated over wavelet subbands to extract important features, aiming to identify cancerous cell signals from normal cell THz responses. It relates to Chapter 9 (Sec. 9.4.3)
- PronyCorreARMA.m This function is to apply an improved Prony method to achieve Auto Regressive Moving Average (ARMA) modelling over discrete wavelet subband coefficients. It is also illustrated that the discrete wavelet based Heuristic SURE method is applied in Chapter 9 (Sec. 9.4.3) to achieve denoised THz signals of different types of powder samples.

SVM applications for THz feature subset identification programming

- SVMsDualClas.m The program is realised via applying SVM and kernel methods matlab toolbox, abbreviated as SKMT. Dual classification of THz RNA data is explored. Frequency orientation components are extracted as features to be input to SVMs. It relates to Chapter 9 (Sec. 9.5.4).
- SVMsMulClas.m This program is for multiclass classification, realised via applying One-Against-One algorithms for pairwise classifier designs with use of SKMT. It relates to Chapter 9 (Sec. 9.5.4).

Wavelet Scale Correlation Based Segmentation

WaveSegment.m This function introduces wavelet scale correlation based segmentation for a 3D classification of the nest structure of a plastic tube inserted in a glass vial. The computed tomography is also illustrated. The contents this function involves are described in Chapter 10 and Chapter 11.

Wavelet Based Local Tomography Reconstruction of THz pulsed imaging

- localTomography_PulsedTHz.m This program reconstructs the measured THz pulsed image data along the centered region of interest, via applying wavelet and scaling ramp filters. This relates to Chapter 12. Time domain parameters are extracted via applying correlation algorithms for the sinogram images.

- FFT_scale.m This function describes the algorithm for wavelet and scaling ramp filters for local reconstruction of THz measurements.
- Sepbackproj.m This function performs the inverse Radon transform of wavelet and scaling ramp filtered projections.

Local Reconstruction via THz QCL

THz_QCL_LT.m This program reconstructs and segments the region of interest. Three algorithms are involved: global and local tomography via FBP algorithms, and wavelet based local reconstruction, all of which are applied on THz continuous wave measurements. This relates to Chapter 13.

Frequency Domain Features for THz Recognition Functions

```
function [xd,fXd,aReMatrix,bReMatrix] = WDHeuSURE(inputMatrix,dTime,namePowder,numPixel,genTestPlots);

% This function is used to denoise THz raw responses via wavelet Soft
% Heuristic SURE methods. A few different wavelet families are explored to
% find which one works well on the denoising and classification of THz
% pulsed responses. The outputs include the features in the frequency domain.

% The University of Adelaide
% Xiaoxia Yin
% August 2005

%xd = wden(inputMatrix,'heursure','s','mln',3,'sym8');
xd = wden(inputMatrix,'heursure','s','one',3,'db8');
fXd = fft(xd);
aReMatrix = abs(fXd) ;
bReMatrix = unwrap(angle(fXd));
pReMatrix = 10*log10(aReMatrix.^2);

fX = fft(inputMatrix);
aOrigiMatrix = abs(fX) ;
bOrigiMatrix = unwrap(angle(fX));
pOrigiMatrix = 10*log10(aOrigiMatrix.^2);

timeOri = [0:400]*dTime;
freq = [0:400]/401/dTime;
maxFreq = 3; % THz;
maxI = ceil(maxFreq/freq(2));
time = timeOri(1:maxI);

if (nargin >= 5)
    TestPlots = genTestPlots;
else
    TestPlots = 0;
end

if (TestPlots == 1)
    % plot several of the responses to see what they look like.
    if (numPixel == 1)

        figure(gcf+1);clf;
        plot(time,inputMatrix(1: maxI, numPixel), time, xd(1: maxI, numPixel));
        formatImage(1);
        xlabel('Time (ps)');
        ylabel('THz Magnitude (a.u.)');
        legend('original signal','denoised signal');
        title('comparison of time domain spectrum ');

        figure(gcf+1);clf;
        plot(freq(1:maxI),fX(1:maxI,numPixel), freq(1:maxI),fXd(1:maxI,numPixel));
        formatImage(1);
        xlabel('Frequency (THz)');
```

```
        ylabel('THz Magnitude (a.u.)');
        legend('original signal','denoised signal');
        title('comparison of frequency domain spectrum ');

        figure(gcf+1);clf;
        plot(freq(1:maxI),pOrigiMatrix(1:maxI,numPixel),freq(1:maxI),pReMatrix(1:maxI,numPixel));
        formatImage(1);
        xlabel('Frequency (THz)');
        ylabel('THz Power(dB)');
        legend('original signal','reconstrcted signal');
        title('the comparison of power spectrum');

        figure(gcf+1);clf;
        plot(freq(1:maxI),bOrigiMatrix(1:maxI,numPixel),freq(1:maxI),bReMatrix(1:maxI,numPixel));
        formatImage(1);
        xlabel('Frequency( THz)');
        ylabel('THz phase');
        legend('original signal','denoised signal');
        title('the comparison of phase spectrum');

    end
end
```

```
function class = classify(sample,training,group)
%   This function is used to achieve linear discriminant analysis.
%   CLASS = CLASSIFY(SAMPLE,TRAINING,GROUP) classifies each row
%   of the data in SAMPLE into one of the values of the vector
%   GROUP. GROUP contains integers from one to the number of
%   groups in the training set, which is the matrix, TRAINING.
%
%   SAMPLE and TRAINING must have the same number of columns.
%   TRAINING and GROUP must have the same number of rows.
%   CLASS is a vector with the same number of rows as SAMPLE.


[gr,gc] = size(group);
if min(gr,gc) ~= 1
   error('Requires the third argument to be a vector.');
end

if gc ~= 1,
   group = group(:);
   gr = gc;
end

if any(group - round(group)) | any(group < 1)
  error('The third input argument must be positive integers.');
end
maxg = max(group);

[tr,tc] = size(training);
```

```
if tr ~= gr,
  error('The number of rows in the second and third input arguments must match.');
end

[sr,sc] = size(sample);
if sc ~= tc
  error('The number of columns in the first and second input arguments must match.');
end

d = zeros(sr,maxg);
for k = 1:maxg
   groupk = training(find(group == k),:);
  % d(:,k) = mahal(sample,groupk);
  d(:,k) = mahaldist(sample,groupk);
end
[tmp, class] = min(d');
class = class';
```

Auto Regressive Over Wavelet Subband for THz Recognition Functions

```
function [A1,A2,A3,xwpd,snr] = WPDen-correlationAR.m(inputMatrix,dTime);
% This function is to realize an AR modeling using autocorrelation method.
% This AR modelling coefficients are calculated on wavelet Packet subbands.
% numpix, nominitedPowder, genScalePlots, genTestPlots, are used to control
% the plot activity, order is the order of AR models;

% Xiaoxia Yin
% Janury 2006

%using wavelet package to denoise T-ray signal
n=length(inputMatrix);
thr=sqrt(2*log(n*log(n)/log(2)));
xwpd=wpdencmp(inputMatrix,'s',3,'bior6.8','sure',thr,1);% 87.50%
%xwpd=wpdencmp(inputMatrix,'s',3,'db4','sure',thr,1);%93.06%
%xwpd=wpdencmp(inputMatrix,'s',3,'sym4','sure',thr,1);
freq = [0:200]/201/dTime/1e12; time = [0:200]*dTime*1e-12;
maxFreq = 2.5; % THz;
maxI = ceil(maxFreq/freq(2));
err=xwpd(1:maxI)-inputMatrix(1:maxI);
snr=20*log10(norm(inputMatrix)/norm(err));
if 1==0

    figure(gcf+1);clf; %plot wavelet package tree
    wpt = wpdec(xwpd,3,'sym4');
    plot(wpt);

    xd = wden(inputMatrix,'heursure','s','mln',3,'db1');
    figure(gcf+1);clf;
    % plot(time(1: maxI)',inputMatrix(1: maxI), time(1: maxI)', xwpd(1: maxI));
    plot(time',inputMatrix, time', xwpd, time',xd);
    formatImage(1);
```

```
    xlabel('Time (ps)');
    ylabel('THz Amplitude (a.u.)');
    legend('original signal','WPT denoised signal','DWT denoised signal');
    title('comparison of time domain spectrum ');

    figure(gcf+1);clf;
    % plot(time(1: maxI)',inputMatrix(1: maxI), time(1: maxI)', xwpd(1: maxI));
    subplot(311),plot(time',inputMatrix);
    formatImage(1);
    %  xlabel('Time (ps)');
    % ylabel('THz Amplitude (a.u.)');
    title('original signal');
    subplot(312),plot(time',xwpd);
    formatImage(1);
    % xlabel('Time (ps)');
    ylabel('THz Amplitude (a.u.)');
    title('WPT denosing signal');
    subplot(313),plot(time',xd);
    formatImage(1);
    xlabel('Time (ps)');
    % ylabel('THz Amplitude (a.u.)');
    title('DWT denoising signal');

    figure(gcf+1);clf;
    % plot(time(1: maxI)',inputMatrix(1: maxI), time(1: maxI)', xwpd(1: maxI));
    plot(time',inputMatrix);
    formatImage(1);
    %  xlabel('Time (ps)');
    % ylabel('THz Amplitude (a.u.)');
    title('original signal');
    plot(time',inputMatrix);
    formatImage(1);
    % xlabel('Time (ps)');
    ylabel('THz Amplitude (a.u.)');
    title('WPT denosing signal');
    plot(time',inputMatrix);
    formatImage(1);
    xlabel('Time (ps)');
    % ylabel('THz Amplitude (a.u.)');
    title('DWT denoising signal');

    err=xwpd(1:maxI)-inputMatrix(1:maxI);
    snr=20*log10(norm(inputMatrix)/norm(err));
end

wpt=wpdec(xwpd,3,'bior6.8');
%using wavelet package tree to decompose the x to 3 levels based on shannon entropy
% plot(wpt); %plot wavelet package tree
cfs10=wpcoef(wpt,[1 0]); % read the coefficients of wavelet package tree at a node [1 0]
cfs11=wpcoef(wpt,[1 1]);
cfs20=wpcoef(wpt,[2 0]);
cfs21=wpcoef(wpt,[2 1]);
cfs22=wpcoef(wpt,[2 2]);
```

```
cfs23=wpcoef(wpt,[2 3]);
cfs30=wpcoef(wpt,[3 0]);
cfs31=wpcoef(wpt,[3 1]);
cfs32=wpcoef(wpt,[3 2]);
cfs33=wpcoef(wpt,[3 3]);
cfs34=wpcoef(wpt,[3 4]);
cfs35=wpcoef(wpt,[3 5]);
cfs36=wpcoef(wpt,[3 6]);
cfs37=wpcoef(wpt,[3 7]);

xdCA1=vertcat(cfs10); % the first level wavelet package coarse coefficients
xdCA2=vertcat(cfs20);
xdCA3=vertcat(cfs30,cfs31);
xdCD1=vertcat(cfs11);
xdCD2=vertcat(cfs22,cfs23);
xdCD3=vertcat(cfs34,cfs35,cfs36,cfs37);

A=zeros(9,8);
for order=2:8
    %xdCAExtend=zeros(8+xdCAlenghth,3);
    xdCAlenghth=length(xdCA1);correMatrixExch=zeros(order+1,1);
    xdCAExtend=zeros(order+xdCAlenghth,order);
    for i=0:order
        numberZero2=zeros(1,order-i)';
        numberZero1=zeros(1,i)';
        %xdCAExtend(:,i) = vertcat(numberZero1,xdCA(:,orderCA),numberZero2);
        xdCAExtend(:,i+1) = vertcat(numberZero1,xdCA1,numberZero2);
        %correlation matrix is calculated based on equation: correMatrix = X'X
    end

    X=xdCAExtend;
    correMatrix=X'*X;
    %correMatrix=X'*X./(1.0e-015);
    storVector=correMatrix(:,1);
    vecMinisumTrans=zeros(order,1);
    vecMiniSum=vertcat(-1,vecMinisumTrans);
    correMatrixExch(:,1)=vecMiniSum;
    vecMiniSumExch=-1*storVector;
    correMatrix= horzcat(correMatrixExch(:,1),correMatrix(:,2:end));
    lengthA=length(correMatrix\vecMiniSumExch); lengthAZeros=zeros(9-lengthA,1);
    A1(:,order-1)=vertcat(correMatrix\vecMiniSumExch,lengthAZeros);
%A1(1,1)is the minimum sum, A1(2:end)are the coefficients of AR
    %A(:,order-1)=correMatrix\vecMiniSumExch;
    errorVariance1(1,order-1)=(length(xdCA1)-1+1)^(-1)*A1(1,order-1); %squred error variance
end

for order=2:8
    %xdCAExtend=zeros(8+xdCAlenghth,3);
    xdCAlenghth=length(xdCA2);correMatrixExch=zeros(order+1,1);
    xdCAExtend=zeros(order+xdCAlenghth,order);
    for i=0:order
        numberZero2=zeros(1,order-i)';
        numberZero1=zeros(1,i)';
```

```
        %xdCAExtend(:,i) = vertcat(numberZero1,xdCA(:,orderCA),numberZero2);
        xdCAExtend(:,i+1) = vertcat(numberZero1,xdCA2,numberZero2);
        %correlation matrix is calculated based on equation: correMatrix = X'X
    end

    X=xdCAExtend;
    %correMatrix=X'*X./(1.0e-015);
    correMatrix=X'*X;
    storVector=correMatrix(:,1);
    vecMinisumTrans=zeros(order,1);
    vecMiniSum=vertcat(-1,vecMinisumTrans);
    correMatrixExch(:,1)=vecMiniSum;
    vecMiniSumExch=-1*storVector;
    correMatrix(:,1)=correMatrixExch(:,1);
    lengthA=length(correMatrix\vecMiniSumExch); lengthAZeros=zeros(9-lengthA,1);
    A2(:,order-1)=vertcat(correMatrix\vecMiniSumExch,lengthAZeros);
    %A(:,order-1)=correMatrix\vecMiniSumExch;
    errorVariance2(1,order-1)=(length(xdCA2)-1+1)^(-1)*A2(1,order-1);
end

for order=2:8
    %xdCAExtend=zeros(8+xdCAlenghth,3);
    xdCAlenghth=length(xdCA3);correMatrixExch=zeros(order+1,1);
    xdCAExtend=zeros(order+xdCAlenghth,order);
    for i=0:order
        numberZero2=zeros(1,order-i)';
        numberZero1=zeros(1,i)';
        %xdCAExtend(:,i) = vertcat(numberZero1,xdCA(:,orderCA),numberZero2);
        xdCAExtend(:,i+1) = vertcat(numberZero1,xdCA3,numberZero2);
        %correlation matrix is calculated based on equation: correMatrix = X'X
    end

    X=xdCAExtend;
    %correMatrix=X'*X./(1.0e-015);
    correMatrix=X'*X;
    storVector=correMatrix(:,1);
    vecMinisumTrans=zeros(order,1);
    vecMiniSum=vertcat(-1,vecMinisumTrans);
    correMatrixExch(:,1)=vecMiniSum;
    vecMiniSumExch=-1*storVector;
    correMatrix(:,1)=correMatrixExch(:,1);
    lengthA=length(correMatrix\vecMiniSumExch); lengthAZeros=zeros(9-lengthA,1);
    A3(:,order-1)=vertcat(correMatrix\vecMiniSumExch,lengthAZeros);
    %A(:,order-1)=correMatrix\vecMiniSumExch;
    errorVariance3(1,order-1)=(length(xdCA3)-1+1)^(-1)*A3(1,order-1);
end
```

```
function [A1,A2,A3,B1,B2,B3] = PronyCorrelationARMA (inputMatrix,dTime,numPixel,nominitedPowder,...
                                genScalePlots,genTestPlots);
```

```
% This function is to realize an ARMA modeling using an improved Prony method
% Variables: numpix, nominitedPowder, genScalePlots, genTestPlots, are used to control
% the plot activity, order is the order of AR models;

%denoise T-ray pulses using soft threshold
xd = wden(inputMatrix,'heursure','s','mln',3,'db8');
%[c1,l1]=wavedec(inputMatrix,1,'db8');
%[c2,l2]=wavedec(inputMatrix,2,'db8');
%[c3,l3]=wavedec(inputMatrix,3,'db8');

%DWT denoised T-ray pulses into 3 levels
[CA1,CD1] = dwt (inputMatrix,'db8');
[CA2,CD2] = dwt (CA1,'db8');
[CA3,CD3] = dwt (CA2,'db8');
[xdCA1,xdCD1] = dwt (xd,'db8');
[xdCA2,xdCD2] = dwt (xdCA1,'db8');
[xdCA3,xdCD3] = dwt (xdCA2,'db8');

%the order of ARMA modeling: P,Q=2,3,4...8

%A=zeros(9,8);
% level 2 of the average coefficients of ARMA at the order from 2 to 8
%first to calculate the coefficients of AR using autocorrelation method
for order=2:8
    %xdCAExtend=zeros(8+xdCAlenghth,3);
    xdCAlenghth=length(xdCA1);correMatrixExch=zeros(order+1,1);
    xdCAExtend=zeros(order+xdCAlenghth,order+1);
    for i=0:order
        numberZero2=zeros(1,order-i)';
        numberZero1=zeros(1,i)';
        %xdCAExtend(:,i) = vertcat(numberZero1,xdCA(:,orderCA),numberZero2);
        xdCAExtend(:,i+1) = vertcat(numberZero1,xdCA1,numberZero2);
        %correlation matrix is calculated based on equation: correMatrix = X'X
    end

    X=xdCAExtend;
    correMatrix=X'*X;
    storVector=correMatrix(:,1);
    vecMinisumTrans=zeros(order,1);
    vecMiniSum=vertcat(-1,vecMinisumTrans);
    correMatrixExch(:,1)=vecMiniSum;
    vecMiniSumExch=-1*storVector;
    correMatrix= horzcat(correMatrixExch(:,1),correMatrix(:,2:end));
    lengthA=length(correMatrix\vecMiniSumExch); lengthAZeros=zeros(9-lengthA,1);
    A1(:,order-1)=vertcat(correMatrix\vecMiniSumExch,lengthAZeros);
    %A1(1,1)is the minimum sum, A1(2:end)are the coefficients of AR
    %A(:,order-1)=correMatrix\vecMiniSumExch;
    errorVariance1(1,order-1)=(length(xdCA1)-1+1)^(-1)*A1(1,order-1); %squred error variance

    %The coefficients for MA modeling
    %The first stage to use autocorelation methods to calculate AR coefficients by choosing
    %an order L, which is the five times the order of the desired MA modeling
```

```
    L=5*order; xdCAlenghth=length(xdCA1);correMatrixExchARMA=zeros(L+1,1);
    xdCAExtend=zeros(L+xdCAlenghth,L+1);G1=zeros(41,7);
    for i=0:L
        numberZero2=zeros(1,L-i)';
        numberZero1=zeros(1,i)';
        %xdCAExtend(:,i) = vertcat(numberZero1,xdCA(:,orderCA),numberZero2);
        xdCAExtend(:,i+1) = vertcat(numberZero1,xdCA1,numberZero2);
        %correlation matrix is calculated based on equation: correMatrix = X'X
    end

    X=xdCAExtend;
    correMatrix=X'*X;
    %storVector=correMatrix(:,1);
    vecMinisumTrans=zeros(L,1);
    vecMiniSum=vertcat(1,vecMinisumTrans);
    %correMatrixExchARMA(:,1)=vecMiniSum;
    %vecMiniSumExch=-1*storVector;
    %correMatrix= horzcat(correMatrixExchARMA(:,1),correMatrix(:,2:end));
    lengthG=length(correMatrix\vecMiniSum); lengthGZeros=zeros(41-lengthG,1);
    G1(:,L/5-1)=vertcat(correMatrix\vecMiniSum,lengthGZeros);
    %G1 is the coefficient vector of first stage of AR modeling
    %correlation Matrix for the second stage of AR model (of order Q)
    %the value gain is extracted from the first value of vector G1
    gain1=G1(1,L/5-1)^(1/2); % L/5-1=order-1 with the AR order starting from 2

    correMatrixExch=zeros(order+1,1);
    xdCAExtend=zeros(order+L+1,order+1);
    for i=0:order
        numberZero2=zeros(1,order-i)';
        numberZero1=zeros(1,i)';
        %xdCAExtend(:,i) = vertcat(numberZero1,xdCA(:,orderCA),numberZero2);
        xdCAExtend(:,i+1) = vertcat(numberZero1,G1(1:L+1,L/5-1),numberZero2);
        %correlation matrix is calculated based on equation: correMatrix = X'X
    end

    Xg=xdCAExtend.*(1/gain1);
    %Xg is the data matrix of G1 with the order of this stage of Q
    %correMatrixMA=Xg'*Xg./(1.0e-015);
    correMatrixMA=Xg'*Xg;
    %storVector=correMatrixMA(:,1);
    vecMinisumTrans=zeros(order,1);
    vecMiniSum=vertcat(1,vecMinisumTrans);
    %correMatrixExch(:,1)=vecMiniSum;
    %vecMiniSumExch=-1*storVector;
    %correMatrixMA= horzcat(correMatrixExch(:,1),correMatrixMA(:,2:end));
    lengthB=length(correMatrixMA\vecMiniSum); lengthBZeros=zeros(9-lengthB,1);%9=order+1
    B1(:,order-1)=vertcat(correMatrixMA\vecMiniSum,lengthBZeros);
    %AR and ARMA have the same error covariance
end

% level 2 of the average coefficients of ARMA at the order from 2 to 8

for order=2:8
```

```
%xdCAExtend=zeros(8+xdCAlenghth,3);

xdCAlenghth=length(xdCA2);correMatrixExch=zeros(order+1,1);
xdCAExtend=zeros(order+xdCAlenghth,order);
for i=0:order
    numberZero2=zeros(1,order-i)';
    numberZero1=zeros(1,i)';
    %xdCAExtend(:,i) = vertcat(numberZero1,xdCA(:,orderCA),numberZero2);
    xdCAExtend(:,i+1) = vertcat(numberZero1,xdCA2,numberZero2);
    %correlation matrix is calculated based on equation: correMatrix = X'X
end

X=xdCAExtend;
correMatrix=X'*X;
storVector=correMatrix(:,1);
vecMinisumTrans=zeros(order,1);
vecMiniSum=vertcat(-1,vecMinisumTrans);
correMatrixExch(:,1)=vecMiniSum;
vecMiniSumExch=-1*storVector;
correMatrix(:,1)=correMatrixExch(:,1);
lengthA=length(correMatrix\vecMiniSumExch); lengthAZeros=zeros(9-lengthA,1);
A2(:,order-1)=vertcat(correMatrix\vecMiniSumExch,lengthAZeros);
%A(:,order-1)=correMatrix\vecMiniSumExch;
errorVariance2(1,order-1)=(length(xdCA2)-1+1)^(-1)*A2(1,order-1);

%The coefficients for MA modeling
%the first stage to use autocorelation methods to calculate AR coefficients by choosing an order L,
%which is the five times the order of the desired MA modeling

L=5*order; xdCAlenghth=length(xdCA2);correMatrixExchARMA=zeros(L+1,1);
xdCAExtend=zeros(L+xdCAlenghth,L+1); G2=zeros(41,7);
for i=0:L
    numberZero2=zeros(1,L-i)';
    numberZero1=zeros(1,i)';
    %xdCAExtend(:,i) = vertcat(numberZero1,xdCA(:,orderCA),numberZero2);
    xdCAExtend(:,i+1) = vertcat(numberZero1,xdCA2,numberZero2);
    %correlation matrix is calculated based on equation: correMatrix = X'X
end

X=xdCAExtend;
correMatrix=X'*X;
%storVector=correMatrix(:,1);
vecMinisumTrans=zeros(L,1);
vecMiniSum=vertcat(1,vecMinisumTrans);
%correMatrixExchARMA(:,1)=vecMiniSum;
%vecMiniSumExch=-1*storVector;
%correMatrix= horzcat(correMatrixExchARMA(:,1),correMatrix(:,2:end));
lengthG=length(correMatrix\vecMiniSum); lengthGZeros=zeros(41-lengthG,1);
G2(:,L/5-1)=vertcat(correMatrix\vecMiniSum,lengthGZeros);
%G1 is the coefficient vector of first stage of AR modeling
%correlation Matrix for the second stage of AR model (of order Q)
%the value gain is extracted from the first value of vector G1
gain2=G2(1,L/5-1)^(1/2);
```

```
    %Xg is the data matrix of G1; the order of this stage is Q

    correMatrixExch=zeros(order+1,1);
    xdCAExtend=zeros(order+L+1,order+1);
    for i=0:order
        numberZero2=zeros(1,order-i)';
        numberZero1=zeros(1,i)';
        %xdCAExtend(:,i) = vertcat(numberZero1,xdCA(:,orderCA),numberZero2);
        xdCAExtend(:,i+1) = vertcat(numberZero1,G2(1:L+1,L/5-1),numberZero2);
        %correlation matrix is calculated based on equation: correMatrix = X'X
    end

    Xg=xdCAExtend.*(1/gain2);
    %correMatrixMA=Xg'*Xg./(1.0e-015);
    correMatrixMA=Xg'*Xg;
    %storVector=correMatrixMA(:,1);
    vecMinisumTrans=zeros(order,1);
    vecMiniSum=vertcat(1,vecMinisumTrans);
    %correMatrixExch(:,1)=vecMiniSum;
    %vecMiniSumExch=-1*storVector;
    %correMatrixMA= horzcat(correMatrixExch(:,1),correMatrixMA(:,2:end));
    lengthB=length(correMatrixMA\vecMiniSum); lengthBZeros=zeros(9-lengthB,1);
    B2(:,order-1)=vertcat(correMatrixMA\vecMiniSum,lengthBZeros);
    %AR and ARMA have the same error covariance
end


% level 3 of the average coefficients of ARMA at the order from 2 to 8
for order=2:8
    %xdCAExtend=zeros(8+xdCAlenghth,3);
    xdCAlenghth=length(xdCA3);correMatrixExch=zeros(order+1,1);
    xdCAExtend=zeros(order+xdCAlenghth,order);
    for i=0:order
        numberZero2=zeros(1,order-i)';
        numberZero1=zeros(1,i)';
        %xdCAExtend(:,i) = vertcat(numberZero1,xdCA(:,orderCA),numberZero2);
        xdCAExtend(:,i+1) = vertcat(numberZero1,xdCA3,numberZero2);
        %correlation matrix is calculated based on equation: correMatrix = X'X
    end

    X=xdCAExtend;
    correMatrix=X'*X;
    storVector=correMatrix(:,1);
    vecMinisumTrans=zeros(order,1);
    vecMiniSum=vertcat(-1,vecMinisumTrans);
    correMatrixExch(:,1)=vecMiniSum;
    vecMiniSumExch=-1*storVector;
    correMatrix(:,1)=correMatrixExch(:,1);
    lengthA=length(correMatrix\vecMiniSumExch); lengthAZeros=zeros(9-lengthA,1);
    A3(:,order-1)=vertcat(correMatrix\vecMiniSumExch,lengthAZeros);
    %A(:,order-1)=correMatrix\vecMiniSumExch;
    errorVariance3(1,order-1)=(length(xdCA3)-1+1)^(-1)*A3(1,order-1);
```

```
    %The coefficients for MA modeling
    %the first stage to use autocorelation methods to calculate AR coefficients by choosing an order L,
    %which is the five times the order of the desired MA modeling

    L=5*order; xdCAlenghth=length(xdCA3);correMatrixExchARMA=zeros(L+1,1);
    xdCAExtend=zeros(L+xdCAlenghth,L+1); G3=zeros(41,7);
    for i=0:L
        numberZero2=zeros(1,L-i)';
        numberZero1=zeros(1,i)';
        %xdCAExtend(:,i) = vertcat(numberZero1,xdCA(:,orderCA),numberZero2);
        xdCAExtend(:,i+1) = vertcat(numberZero1,xdCA3,numberZero2);
        %correlation matrix is calculated based on equation: correMatrix = X'X
    end

    X=xdCAExtend;
    correMatrix=X'*X;
    %storVector=correMatrix(:,1);
    vecMinisumTrans=zeros(L,1);
    vecMiniSum=vertcat(1,vecMinisumTrans);
    %correMatrixExchARMA(:,1)=vecMiniSum;
    %vecMiniSumExch=-1*storVector;
    %correMatrix= horzcat(correMatrixExchARMA(:,1),correMatrix(:,2:end));
    lengthG=length(correMatrix\vecMiniSum); lengthGZeros=zeros(41-lengthG,1);
    G3(:,L/5-1)=vertcat(correMatrix\vecMiniSum,lengthGZeros);
     %G1 is the coefficient vector of first stage of AR modeling
    %correlation Matrix for the second stage of AR model (of order Q)
    %the value gain is extracted from the first value of vector G1
    gain3=G3(1,L/5-1)^(1/2);

    correMatrixExch=zeros(order+1,1);
    xdCAExtend=zeros(order+L+1,order+1);
    for i=0:order
        numberZero2=zeros(1,order-i)';
        numberZero1=zeros(1,i)';
        %xdCAExtend(:,i) = vertcat(numberZero1,xdCA(:,orderCA),numberZero2);
        xdCAExtend(:,i+1) = vertcat(numberZero1,G3(1:L+1,L/5-1),numberZero2);
        %correlation matrix is calculated based on equation: correMatrix = X'X
    end

    Xg=xdCAExtend.*(1/gain3);
    %correMatrixMA=Xg'*Xg./(1.0e-015);
    correMatrixMA=Xg'*Xg;
    %storVector=correMatrixMA(:,1);
    vecMinisumTrans=zeros(order,1);
    vecMiniSum=vertcat(1,vecMinisumTrans);
    %correMatrixExch(:,1)=vecMiniSum;
    %vecMiniSumExch=-1*storVector;
    %correMatrixMA= horzcat(correMatrixExch(:,1),correMatrixMA(:,2:end));
    lengthB=length(correMatrixMA\vecMiniSum); lengthBZeros=zeros(9-lengthB,1);
    B3(:,order-1)=vertcat(correMatrixMA\vecMiniSum,lengthBZeros);
    %AR and ARMA have the same error covariance
end
```

SVMs for THz Recognition Programming

SVMsDualClas.m

```
% The THz classification system was used to classify
% RNA sample: Poly-A and Poly-C
% dual classification is finished via svms

% Xiaoxia Yin
% June 2006
clear;tic
load testamp_matrix.dat;

imagesc(testamp_matrix);
grid;

figure(gcf+1);grid;imagesc(testamp_matrix);
axis( [7 13 15 21]);

filePath = 'D:\MATLAB6p5\work\Data\Burnd data\biochip';

[mpolyC1,bpolyC1,polyC1] = openLIACTFile_yxx('biochip1_1_10x34c','biochip1_1_1x1c');
% omitting the reading of the remaining RNA data files.

% the feature matrix from meaured image data corresponding to each pixel of PolyA
mpolyA=[mpolyA1,mpolyA2,mpolyA3,mpolyA4,mpolyA5,mpolyA6,mpolyA7,mpolyA8,mpolyA9,mpolyA10,mpolyA11,mpolyA12,...
    mpolyA13,mpolyA14,mpolyA15,mpolyA16,mpolyA17,mpolyA18,mpolyA19,mpolyA20,mpolyA21,mpolyA22,mpolyA32,mpolyA24,...
    mpolyA25,mpolyA26,mpolyA27,mpolyA28,mpolyA29,mpolyA30,mpolyA31,mpolyA32,mpolyA33,mpolyA34,mpolyA35,mpolyA36,...
    mpolyA37,mpolyA38,mpolyA39,mpolyA40,mpolyA41,mpolyA42,mpolyA43,mpolyA44,mpolyA45,mpolyA46,mpolyA47,mpolyA48];

bpolyA=[bpolyA1,bpolyA2,bpolyA3,bpolyA4,bpolyA5,bpolyA6,bpolyA7,bpolyA8,bpolyA9,bpolyA10,bpolyA11,bpolyA12,...
    bpolyA13,bpolyA14,bpolyA15,bpolyA16,bpolyA17,bpolyA18,bpolyA19,bpolyA20,bpolyA21,bpolyA22,bpolyA32,bpolyA24,...
    bpolyA25,bpolyA26,bpolyA27,bpolyA28,bpolyA29,bpolyA30,bpolyA31,bpolyA32,bpolyA33,bpolyA34,bpolyA35,bpolyA36,...
    bpolyA37,bpolyA38,bpolyA39,bpolyA40,bpolyA41,bpolyA42,bpolyA43,bpolyA44,bpolyA45,bpolyA46,bpolyA47,bpolyA48];

polyA=[polyA1,polyA2,polyA3,polyA4,polyA5,polyA6,polyA7,polyA8,polyA9,polyA10,polyA11,polyA12,...
    polyA13,polyA14,polyA15,polyA16,polyA17,polyA18,polyA19,polyA20,polyA21,polyA22,polyA32,polyA24,...
    polyA25,polyA26,polyA27,polyA28,polyA29,polyA30,polyA31,polyA32,polyA33,polyA34,polyA35,polyA36,...
    polyA37,polyA38,polyA39,polyA40,polyA41,polyA42,polyA43,polyA44,polyA45,polyA46,polyA47,polyA48];

% omitting the feature matrices regarding polyC

mpolyC=mpolyC(:,1:48);
bpolyC=bpolyC(:,1:48);
polyC=polyC(:,1:48);

[larpolyC,C] = max(polyC,[],1); length(larpolyC)
[larpolyA,A] = max(polyA,[],1); length(larpolyA)

LmpolyC=mpolyC(335,:);%C=335;
LbpolyC=bpolyC(335,:);

LmpolyA=mpolyA(335,:);%C=335;
```

```
LbpolyA=bpolyA(335,:);
%
% figure(11);clf;
% plot(larpolyC,'b.');hold on;
% plot(larpolyA,'r.');

if 1==0
    figure(11);clf;
    plot(LmpolyC,LbpolyC,'b.');hold on;
    plot(LmpolyA,LbpolyA,'r.');
end
timestep=0.0667*10^(-12);

normalizeSpectra = 0;
maxFreqI = 70;

lambda = 1e-7;
C =10;
% C =1;
kernel='gaussian';
kerneloption=30;

l=size(mpolyC,1);
if 1==1

    tt1=cputime;
    %-----train svms-------
    wrong=[];    corre=[];
    % for u=2:120
    u=335;
    % holdout method for classification design
    for k=12
        Xapp=[mpolyA(u,1:24+k)',bpolyA(u,1:24+k)';mpolyC(u,1:24+k)',bpolyC(u,1:24+k)'];
% 2 features and 51 vectors for each of two classes before denoising
        yapp=[-ones(24+k,1);ones(24+k,1)];
        [xsup,w,w0,pos,tps,alpha] = svmclass(Xapp,yapp,C,lambda,kernel,kerneloption);
        %[xsup,w,w0,pos,tps,alpha] = svmclassLS(Xapp,yapp,C,lambda,kernel,kerneloption,1,1,100);

 %-----test svms-------

        xtesta1=mpolyA(u,24+k+1:end)';
        xtesta2=bpolyA(u,24+k+1:end)';

        xtest=[xtesta1, xtesta2];
        ypred = svmval(xtest,xsup,w,w0,kernel,kerneloption);
        ypredmat=ypred;

        % ypredapp = svmval(Xapp,xsup,w,,kernel,kerneloption,1);

        %------------Classification accuracy----------------------

        %     ind1=find(ypred>0); wrong(u,k)=length(ind1)/(24-k);
        %     indm1=find(ypred<0);corre(u,k)=length(indm1)/(24-k);
```

```
        ind1=find(ypred>0); wrong(1,k/2)=length(ind1)/(24-k);
        indm1=find(ypred<0);corre(1,k/2)=length(indm1)/(24-k);
        length(ind1)
        ind1C=find(ypred<0); wrongC(1,k/2)=length(ind1C)/(24-k);
        indm1C=find(ypred>0);correC(1,k/2)=length(indm1C)/(24-k);
        length(ind1C)
    end

end

toc
size(pos)
```

SVMsMulClas.m

```
%
% Powder MultiClass SVM Classifiction
% "One against One"
%
close all
clear all
tic
%-------------------------------------------------
% The THz imaging system was used to obtain the THz response of
% several different powders with thickness of 2mm.
% We then attempted to classify the images.
%
% Xiaoxia (Sunny) Yin
% May 2006

    % 1D images of the powders.
    %

    [mFree2mm,nX,nY,nTime,nAngle,dX,dY,dTime,dAngle] = openLIACTFile('THzFreeSpace2mm1529');
    [mFree2mm,nX,nY,nTime,nAngle,dX,dY,dTime,dAngle] = openLIACTFile('THzFreeSpace2mm1529');

    mSand2mm = openLIACTFile('ChinesePowder2mm1755');
    mTalc2mm = openLIACTFile('TalcumPowder2mm1939');
    mSalt2mm = openLIACTFile('SaltPowder2mm2127');
    mPowSugar2mm = openLIACTFile('PowderSuger2mm2237');
    mSugar2mm = openLIACTFile('Suger2mm2337');
    %
    mRef2 = openLIACTFile('THzRef1356');

    mFlour2mm = openLIACTFile('2mnmflour2207');
    mSoda2mm = openLIACTFile('2mmSoda2313');
    mSugar2mm = openLIACTFile('2mmSugar2037');

    % normalization:
    mRef2_avg = mean(mRef2,2);
    mFree2mm_avg = mean(mFree2mm,2);
```

```
    [ref1Max,ref1Timing] = max(mFree2mm_avg);
    [ref2Max,ref2Timing] = max(mRef2_avg);
    ampFactor = ref1Max/ref2Max;
    timingFactor = ref1Timing-ref2Timing;

    % truncate all the signals so that they are all the same size.
    mFree2mm = mFree2mm(1:401,:);
    mSand2mm = mSand2mm(1:401,:);
    mTalc2mm = mTalc2mm(1:401,:);
    mSalt2mm = mSalt2mm(1:401,:);
    mSalt4mm = mSalt4mm(1:401,:);

    time = [0:400]*dTime;

    freq = [0:400]/401/3/dTime;
    maxFreq = 3; % THz;
    maxI = ceil(maxFreq/freq(2));

% first normalize the responses.
% scale the amplitude in the time domain
normalizeResponses = 0;
if (normalizeResponses == 1)
    mFree2mm = normalizeTHz(mFree2mm,mFree2mm(:,2));
    mSalt2mm = normalizeTHz(mSalt2mm,mFree2mm(:,2));
    mSand2mm = normalizeTHz(mSand2mm,mFree2mm(:,2));
    mTalc2mm = normalizeTHz(mTalc2mm,mFree2mm(:,2));
    mPowSugar2mm = normalizeTHz(mPowSugar2mm,mFree2mm(:,2));
    mSugar2mm = normalizeTHz(mSugar2mm,mFree2mm(:,2));
end

% now deconvolve.
% construct a symmetric structure, same as m*m, to plot
numPix=size(mFree2mm,2);
for i = 1:numPix
    %[aSoda3mm(:,i),pSoda3mm(:,i),c,d]=deconvolve(mSoda3mm(:,i),mRef3(:,25),dTime*1e-12,3,0,1,1,1);

    [aFree2mm(:,i),pFree2mm(:,i),c,d]=deconvolveBrad(mFree2mm(:,i),mFree2mm(:,1),dTime*1e-12,3,0,0,0,1,0);
    [aSalt2mm(:,i),pSalt2mm(:,i),c,d]=deconvolveBrad(mSalt2mm(:,i),mFree2mm(:,1),dTime*1e-12,3,0,0,0,1,0);
    [aSand2mm(:,i),pSand2mm(:,i),c,d]=deconvolveBrad(mSand2mm(:,i),mFree2mm(:,1),dTime*1e-12,3,0,0,0,1,0);
    [aTalc2mm(:,i),pTalc2mm(:,i),c,d]=deconvolveBrad(mTalc2mm(:,i),mFree2mm(:,1),dTime*1e-12,3,0,0,0,1,0);
    [aPowSugar2mm(:,i),pPowSugar2mm(:,i),c,d]=deconvolveBrad(mPowSugar2mm(:,i),mFree2mm(:,1), ...
                                                                    dTime*1e-12,3,0,0,0,1,0);

    [aSugar2mm(:,i),pSugar2mm(:,i),c,d]=deconvolveBrad(mSugar2mm(:,i),mRef3(:,25),dTime*1e-12,3,0,0,0,1,0);
    [aFlour2mm(:,i),pFlour2mm(:,i),c,d]=deconvolveBrad(mFlour2mm(:,i),mRef3(:,25),dTime*1e-12,3,0,0,0,1,0);
    [aSoda2mm(:,i),pSoda2mm(:,i),c,d]=deconvolveBrad(mSoda2mm(:,i),mRef3(:,25),dTime*1e-12,3,0,0,0,1,0);

end
toc
normalizeSpectra = 0;
maxFreqI = 70;
maxFreqI = 70;
```

```
%-----------------------------------------------------
%   Learning and Learning Parameters
c =1000;
lambda = 1e-7;
kerneloption=4;
%     kernel='gaussian';
kernel='poly';
verbose = 0;
%-------------powder at 2mm to test svms using LOO--------

if 1==1
    tt13=cputime;
    leng1=[];  leng2=[];  leng3=[];  leng4=[];  leng5=[];  leng6=[];

    n= numPix-2 ;
    for i=2: numPix-1  % LOO
        %for i=30: 50
        posFre=[1:i-1,i+1:numPix];
        xapp=[aSalt3mm(2,posFre) aSand3mm(2,posFre) aTalc3mm(2,posFre) aSugar3mm(2,posFre) ...
           aFlour3mm(2,posFre) aSoda3mm(2,posFre); pSalt3mm(2,posFre) pSand3mm(2,posFre) ...
           pTalc3mm(2,posFre) pSugar3mm(2,posFre) pFlour3mm(2,posFre) pSoda3mm(2,posFre)]';
        yapp=[1*ones(1,numPix-1) 2*ones(1,numPix-1) 3*ones(1,numPix-1) 4*ones(1,numPix-1) ...
           5*ones(1,numPix-1) 6*ones(1,numPix-1) ]';
        nbclass=6;

        [n1, n2]=size(xapp);

        % ----------------------------------------
        % %   Learning and Learning Parameters
        % c = 1000;
        % lambda = 1e-7;
        % kerneloption= 1;
        % kernel='gaussian'; % kernel='poly';
        % verbose = 0;

        %--------------------One Against One algorithms----------------

        nbclass=6;
               [xsup,w,b,nbsv,classifier]=svmmulticlassoneagainstone(xapp,yapp,nbclass,c,lambda,...
                           kernel,kerneloption,verbose);
        size(xsup)
        xtesta1=aSalt3mm(2,i);
        xtesta2=pSalt3mm(2,i);
        xtest=[xtesta1; xtesta2]';
        [ypred,maxi] = svmmultivaloneagainstone(xtest,xsup,w,b,nbsv,kernel,kerneloption);
        leng1(i)=ypred;

        xtesta1=aSand3mm(2,i);% 100% before denoising 100% after denoising
        xtesta2=pSand3mm(2,i);
        xtest=[xtesta1; xtesta2]';
        [ypred,maxi] = svmmultivaloneagainstone(xtest,xsup,w,b,nbsv,kernel,kerneloption);
        leng2(i)=ypred;
```

```
        xtesta1=aTalc3mm(2,i);% 92% before denoising 96% after denoising
        xtesta2=pTalc3mm(2,i);
        xtest=[xtesta1; xtesta2]';
        [ypred,maxi] = svmmultivaloneagainstone(xtest,xsup,w,b,nbsv,kernel,kerneloption);
        leng3(i)=ypred;

        xtesta1=aSugar3mm(2,i);% 96% before denoising 96% after denoising
        xtesta2=pSugar3mm(2,i);
        xtest=[xtesta1; xtesta2]';
        [ypred,maxi] = svmmultivaloneagainstone(xtest,xsup,w,b,nbsv,kernel,kerneloption);
        leng4(i)=ypred;

        xtesta1=aFlour3mm(2,i);% 92% before denoising 84% after denoising
        xtesta2=pFlour3mm(2,i);
        xtest=[xtesta1; xtesta2]';
        [ypred,maxi] = svmmultivaloneagainstone(xtest,xsup,w,b,nbsv,kernel,kerneloption);
        leng5(i)=ypred;

        xtesta1=aSoda3mm(2,i);% 100% before denoising 100% after denoising
        xtesta2=pSoda3mm(2,i);
        xtest=[xtesta1; xtesta2]';
        [ypred,maxi] = svmmultivaloneagainstone(xtest,xsup,w,b,nbsv,kernel,kerneloption);
        leng6(i)=ypred;
        % i
    end

    ACla1=length(find(leng1==1))/n;   ACla2=length(find(leng2==2))/n;   ACla3=length(find(leng3==3))/n;
    ACla4=length(find(leng4==4))/n;   ACla5=length(find(leng5==5))/n;   ACla6=length(find(leng6==6))/n;
    accuracy=[ACla1 ACla2 ACla3 ACla4 ACla5 ACla6];
    % tt23=cputime;
end
toc

        %-------------------------------plot-----------------------------

        [xtesta1,xtesta2]=meshgrid([0:0.25:5],[-2:0.1:0]);
        [na,nb]=size(xtesta1);
        xtest1=reshape(xtesta1,1,na*nb);
        xtest2=reshape(xtesta2,1,na*nb);
        xtest=[xtest1;xtest2]';

        [ypred,maxi] = svmmultivaloneagainstone(xtest,xsup,w,b,nbsv,kernel,kerneloption);

        ypredmat=reshape(ypred,na,nb);

        figure(1);clf;
        contourf(xtesta1,xtesta2,ypredmat*3,30);shading flat
        hold on;
        [cs,h]=contour(xtesta1,xtesta2,ypredmat,[1 2 3 4 5 6]);
        clabel(cs,h);hold on;

        style=['x+*x+o'];
```

```
        color=['kcgrbm'];
        for i=0:nbclass-1
            h=plot(xapp(i*n+1:(i+1)*n,1),xapp(i*n+1:(i+1)*n,2),[style(i+1) color(i+1)]);
            set(h,'LineWidth',2);
            hold on
        end;
        %grid off;
        %formatImage(1);
        xlabel('THz Amplitude (a.u.)');
        ylabel('THz Phase (radians)');

        hold on;
        h=plot(xsup(:,1),xsup(:,2),'.r');
        set(h,'LineWidth',2);
        axis( [ 0 5 -2 0]);
        legend('Salt2mm','Sand2mm','Talc2mm', 'Sugar2mm','Flour2mm','Soda2mm','Support Vector');
        hold off

    end
```

Wavelet Scale Correlation Based Segmentation

```
function [numXVial1, numYVial1, numXtube1, numYtube1, numXair1,numYair1] = WaveSegment...
                        (allData,refPulse,stepAngle,methodIn,debugPlotin,savePathin)
% THZ CT Computes the inverse radon transform for the slice of data files
%
%   This function opens the THz files CT angle files and
%   computes the inverse Radon Transform to obtain an image of
%   the slice.
%
%   Wavelet based segmentation is used to find the position of each pixels for classification application
%
%  Sunny Yin
%  Novemver 2006

useVial = 1;
figure(1);clf;

if (nargin >= 4)
    method = methodIn;
else
    method = 1;
end

if (nargin >= 5)
    debugPlot = debugPlotin;
else
    debugPlot = 0;
end

if (nargin >= 6)
```

```
    printPlots = 1;
    savePath = savePathin;
else
    printPlots = 0;
    savePath = '';
end

methodIndex=1;

printOpts = '-deps2c';
nX = size(allData,2);
nAngle = size(allData,4);
nY = size(allData,3);

% refPulse = allData(:,1,1,1);

useVial = 1;
refPulse = allData(:,2,2,2);

% use only y = 2
y = floor(nY/2)+1;

for y=5:9
    %for y=7

    pad = 2;
    fallData = fft(allData(:,:,y,:),size(allData,1)*pad);
    refFFT = fallData(:,2,2);

    imagData = imag(fallData);
    absData = abs(fallData);

    imagRef = ones(size(refFFT)); %imag(refFFT);
    absRef = ones(size(refFFT));
    if 1==1
        imagRef = imag(refFFT);
        absRef = abs(refFFT);
    end

    % image fusion and 2D wavelet energy for segment detection
    % Sunny Yin
    % Feb.2006
    figure(gcf+1);
    nF= size(fallData,1);
    nF=200;
    f=1:nF;
    for nf =1:nF
        R = reshape(fallData(f(nf),:,:),nX,nAngle);
        R = -log(R / refFFT(f(nf)));
        a = iradon(real(R),stepAngle,45,'spline','Hamming');%,'Hamming');
        %interp2(b,1)
        % invert and threshold a
        b = normMatrix(a);
```

```
    b=threshMatrix(b,0.1,0.7);
    b = wiener2(b,[3 3]);
    bI(:,:,nf)=interp2(b,1);
end

figure(gcf+1);    fusbIclsSum1=bI(:,:,2)/15+bI(:,:,3)/15+bI(:,:,4)/15+bI(:,:,5)/15+bI(:,:,6)/15+...
   bI(:,:,7)*2/15+bI(:,:,8)*2/15+bI(:,:,9)*2/15+bI(:,:,10)*2/15+bI(:,:,11)*2/15;
fusbIclsSum(:,:,nf)=fusbIclsSum1;
imagesc([size(fusbIclsSum1,2):-1:0],[0:size(fusbIclsSum1,1)],interp2(fusbIclsSum1,1));
colormap('default');formatImage(2); grid off;
colormap('default'); xlabel('mm'); ylabel('mm');

[cA,cH,cV,cD]=dwt2(fusbIclsSum1,'db4');%2D wavelet decomposition to 2 levels;
[cA1,cH1,cV1,cD1]=dwt2(cA,'db4');

[c,s]=wavedec2(fusbIclsSum1,4,'db4');
siz=s(size(s,1),:);

ca1=appcoef2(c,s,'db4',1);%subtract the low pass coeffi;
a1=upcoef2('a',ca1,'db4',1,siz);%reconstruction the low pass

figure (gcf+1);clf;
subplot(2,2,1);%plot
imagesc([size(a1,2):-1:0],[0:size(a1,1)],interp2(a1,1));formatImage(2); grid off;
colormap('default');
title('approximation coef. recons.'); xlabel('mm'); ylabel('mm');

chd1=detcoef2('h',c,s,1);
hd1=upcoef2('h',chd1,'db4',1,siz);

subplot(2,2,2)
imagesc([size(hd1,2):-1:0],[0:size(hd1,1)],interp2(hd1,1));formatImage(2); grid off;
colormap('default');
title('horizontal detail coef. recons.');
xlabel('mm'); ylabel('mm');

cvd1=detcoef2('v',c,s,1);
vd1=upcoef2('h',cvd1,'db4',1,siz);

subplot(2,2,3)
imagesc([size(vd1,2):-1:0],[0:size(vd1,1)],interp2(vd1,1));formatImage(2); grid off;
colormap('default')
title('vertical detail coef. recons.'); xlabel('mm'); ylabel('mm');

cdd1=detcoef2('d',c,s,1);
dd1=upcoef2('d',cdd1,'db4',1,siz);

subplot(2,2,4)
imagesc([size(dd1,2):-1:0],[0:size(dd1,1)],interp2(dd1,1));formatImage(2); grid off;
colormap('default')
title('diagonal detail coef. recons.'); xlabel('mm'); ylabel('mm');

%second level of reconstruction
```

```
ca2=appcoef2(c,s,'db4',2);%subtract the low pass coeffi;
a2=upcoef2('a',ca2,'db4',2,siz);%reconstruction the low pass

figure (gcf+1);
subplot(2,2,1);%plot
imagesc([size(a2,2):-1:0],[0:size(a2,2)],interp2(a2,2));formatImage(2); grid off;
colormap('default');
title('approximation coef. recons.'); xlabel('mm'); ylabel('mm');

chd2=detcoef2('h',c,s,2);
hd2=upcoef2('h',chd2,'db4',2,siz);

subplot(2,2,2)
imagesc([size(hd2,2):-1:0],[0:size(hd2,1)],interp2(hd2,1));formatImage(2); grid off;
colormap('default');
title('horizontal detail coef. recons.'); xlabel('mm'); ylabel('mm');

cvd2=detcoef2('v',c,s,2);
vd2=upcoef2('h',cvd2,'db4',2,siz);

subplot(2,2,3)
imagesc([size(vd2,2):-1:0],[0:size(vd2,1)],interp2(vd2,1));formatImage(2); grid off;
colormap('default')
title('vertical detail coef. recons.'); xlabel('mm'); ylabel('mm');

cdd2=detcoef2('d',c,s,2);
dd2=upcoef2('d',cdd2,'db4',2,siz);

subplot(2,2,4)
imagesc([size(dd2,2):-1:0],[0:size(dd2,1)],interp2(dd2,1));formatImage(2); grid off;
colormap('default')
title('diagonal detail coef. recons.'); xlabel('mm'); ylabel('mm');

ca3=appcoef2(c,s,'db4',3);%subtract the low pass coeffi;
a3=upcoef2('a',ca3,'db4',3,siz);%reconstruction the low pass

figure (gcf+1);
subplot(2,2,1);%plot
imagesc([size(a3,2):-1:0],[0:size(a3,2)],interp2(a3,2));formatImage(2); grid off;
colormap('default');
title('approximation coef. recons.'); xlabel('mm'); ylabel('mm');

chd3=detcoef2('h',c,s,3);
hd3=upcoef2('h',chd3,'db4',3,siz);

subplot(2,2,2)
imagesc([size(hd3,2):-1:0],[0:size(hd3,1)],interp2(hd3,1));formatImage(2); grid off;
colormap('default');
title('horizontal detail coef. recons.'); xlabel('mm'); ylabel('mm');

cvd3=detcoef2('v',c,s,3);
vd3=upcoef2('h',cvd3,'db4',3,siz);
```

```
subplot(2,2,3)
imagesc([size(vd3,2):-1:0],[0:size(vd3,1)],interp2(vd3,1));formatImage(2); grid off;
colormap('default')
title('vertical detail coef. recons.'); xlabel('mm'); ylabel('mm');

cdd3=detcoef2('d',c,s,3);
dd3=upcoef2('d',cdd3,'db4',3,siz);

subplot(2,2,4)
imagesc([size(dd3,2):-1:0],[0:size(dd3,1)],interp2(dd3,1));formatImage(2); grid off;
colormap('default')
title('diagonal detail coef. recons.'); xlabel('mm'); ylabel('mm');

[c,s]=wavedec2(fusbIclsSum1,4,'db4');
siz=s(size(s,1),:);

ca1=appcoef2(c,s,'db4',1);%subtract the low pass coeffi;
a1=upcoef2('a',ca1,'db4',1,siz);

ca2=appcoef2(c,s,'db4',2);%subtract the low pass coeffi;
a2=upcoef2('a',ca2,'db4',2,siz);

ca3=appcoef2(c,s,'db4',3);%subtract the low pass coeffi;
a3=upcoef2('a',ca3,'db4',3,siz);

------Wavelet scale correlation based segmentation------

[Ea,Eh,Ev,Ed] =wenergy2(c,s);
[Ea,EDetails]=wenergy2(c,s);

coeCor12=a1.*a2;
coeCor23=a2.*a3;

coePW1=sum(sum(a1.^2));
coePW2=sum(sum(a2.^2));

coePC1=sum(sum(coeCor12.^2));
coePC2=sum(sum(coeCor23.^2));

coeRWCor1=(coePW1/coePC1).^(1/2);
coeRWCor2=(coePW2/coePC2).^(1/2);

coeNCor1=coeCor12 * coeRWCor1;
coeNCor2=coeCor23* coeRWCor2;

coeNCor1Den=(abs(coeNCor1)>=a1) .* coeNCor1;
coeNCor2Den=(abs(coeNCor2)>=a2) .* coeNCor2;

figure (gcf+1);clf;
subplot(2,2,1)
imagesc([size(coeNCor1Den,2):-1:0],[0:size(coeNCor1Den,1)],interp2(coeNCor1Den,1));
formatImage(2); grid off; colormap('default')
```

```
title('ampl. covolu. between levels 1 and 2');   xlabel('mm'); ylabel('mm');

subplot(2,2,2)
imagesc([size(coeNCor2Den,2):-1:0],[0:size(coeNCor2Den,1)],interp2(coeNCor2Den,1));
formatImage(2); grid off; colormap('default')
title('ampl. covolu. between levels 2 and 3');     xlabel('mm'); ylabel('mm');

coeNCor1DenThr= (coeNCor1Den>0);
copyCoeNCor1DenThr=coeNCor1DenThr;
coeNCor1DenThrAir= (coeNCor1Den<=0);
norModSubBIThAir=coeNCor1DenThrAir;

subplot(2,2,3)
imagesc([size(copyCoeNCor1DenThr,2):-1:0],[0:size(copyCoeNCor1DenThr,1)],...
   interp2(copyCoeNCor1DenThr,1)); formatImage(2);
grid off; colormap('default')
title('subtract segments');  xlabel('mm'); ylabel('mm');

copyCoeNCor1DenThrCan =edge(copyCoeNCor1DenThr,'canny');

subplot(2,2,4)
imagesc([size(copyCoeNCor1DenThrCan,2):-1:0],[0:size(copyCoeNCor1DenThrCan,1)],...
   interp2(copyCoeNCor1DenThrCan,1)); formatImage(2); grid off; colormap('default')
title('subtract segments');  xlabel('mm'); ylabel('mm');

[xSubBITh,ySubBITh] = find(copyCoeNCor1DenThrCan);
numSubBITh =length(xSubBITh);

xSubBIThMaxPosi=max(xSubBITh);
xSubBIThMinPosi=min(xSubBITh);
xSubBIThCentrPosi=(xSubBIThMaxPosi-xSubBIThMinPosi)/2;
% central point coordination is very important which
% determine the modulus and the color match for the different circle
xSubBIThCentrPosi=xSubBIThCentrPosi+xSubBIThMinPosi;

ySubBIThMaxPosi=max(ySubBITh);
ySubBIThMinPosi=min(ySubBITh);
ySubBIThCentrPosi=(ySubBIThMaxPosi-ySubBIThMinPosi)/2;
ySubBIThCentrPosi=ySubBIThCentrPosi+ySubBIThMinPosi;

% coordination of central position: (47,40)
% calculate the modulus between the central position and edge of the vial
% and the tube

[xAxisMod,yAxisMod]=size(copyCoeNCor1DenThrCan);
ModSubBITh=zeros(xAxisMod,yAxisMod);
theta=zeros(xAxisMod,yAxisMod);
for k=1:numSubBITh

    ModSubBITh(xSubBITh(k),ySubBITh(k))=((xSubBITh(k)-xSubBIThCentrPosi)^2+...
       (ySubBITh(k)-ySubBIThCentrPosi)^2).^(1/2);% modulus
    theta(ySubBITh(k),ySubBITh(k))=atan((ySubBITh(k)-ySubBIThCentrPosi)/...
    (xSubBITh(k)-xSubBIThCentrPosi));%angle between the
```

```
    %calculated modulus vector and the  x axis

end

figure(gcf+1)
subplot(2,2,1);
imagesc([size(ModSubBITh,2):-1:0],[size(ModSubBITh,1):-1:0],interp2(ModSubBITh,2));
set(gca,'YDir','normal');
formatImage(2); grid off;
colormap('default')
xlabel('mm'); ylabel('mm')

norModSubBITh=ModSubBITh./max(max(ModSubBITh));

subplot(2,2,2);
%use histogram to find the threshold
h=imhist(norModSubBITh);
%p=h/numel(fusbIclsSum2);
h1=h(1:255);
horz=1:255;
bar(horz,h1)
%stem(horz,h1,'b--','fill')
axis([0 255 0 30])
set(gca,'xtick',0:30:255)
set(gca,'ytick',0:10:30)

TTube=graythresh(norModSubBITh);
% a little adjustment of threshold for the target image with blurred boundary.
%if y==7
% TTube=TTube-0.2;
% end

norModSubBIThVial=(norModSubBITh >TTube+0.04*(y-5));  % test if there are some other points left
if y==5
    norModSubBIThVial=(norModSubBITh >TTube+0.2);
end
subplot(2,2,3);
imagesc([size(norModSubBIThVial,2):-1:0],[size(norModSubBIThVial,1):-1:0],interp2(norModSubBIThVial,2));
set(gca,'YDir','normal');
formatImage(2); grid off;
colormap('default')
xlabel('mm'); ylabel('mm')

norModSubBIThVialTub=(norModSubBITh >0);  % test if there are some other points left
norModSubBIThTub=norModSubBIThVialTub-norModSubBIThVial;

subplot(2,2,4);
imagesc([size(norModSubBIThTub,2):-1:0],[size(norModSubBIThTub,1):-1:0],interp2(norModSubBIThTub,2));
set(gca,'YDir','normal');
formatImage(2); grid off;
colormap('default')
xlabel('mm'); ylabel('mm')
copynorModSubBIThTub = norModSubBIThTub;
```

```
nYbI=size(norModSubBIThTub,2);

[xx,yy]=find(norModSubBIThTub);
leng=length(xx);
for jj=1:leng% xx(jj) record the x axis position
    maxYY=max(yy(xx==xx(jj)));
    minYY=min(yy(xx==xx(jj)));
    for RR=0:nYbI
        if RR<=maxYY & RR>=minYY
            norModSubBIThTub(xx(jj),RR)=1;
        end
    end
end

figure(gcf+1)
subplot(2,2,1);
imagesc([size(copynorModSubBIThTub,2):-1:0],[size(copynorModSubBIThTub,1):-1:0],...
     interp2(copynorModSubBIThTub,2));  set(gca,'YDir','normal');
formatImage(2); grid off;
colormap('default')
xlabel('mm'); ylabel('mm')

subplot(2,2,2);
imagesc([size(norModSubBIThTub,2):-1:0],[size(norModSubBIThTub,1):-1:0],interp2(norModSubBIThTub,2));
set(gca,'YDir','normal');
formatImage(2); grid off;
colormap('default')
xlabel('mm'); ylabel('mm')

norModSubBIThVial=((coeNCor1DenThr- norModSubBIThTub)>0);
subplot(2,2,3);
imagesc([size(norModSubBIThVial,2):-1:0],[size(norModSubBIThVial,1):-1:0],interp2(norModSubBIThVial,2));
set(gca,'YDir','normal');
formatImage(2); grid off;
colormap('default')
xlabel('mm'); ylabel('mm')

subplot(2,2,4);
imagesc([size( norModSubBIThAir,2):-1:0],[size( norModSubBIThAir,1):-1:0],interp2( norModSubBIThAir,2));
set(gca,'YDir','normal');
formatImage(2); grid off;
colormap('default')
xlabel('mm'); ylabel('mm')

%   --------------record segements for classification application---------------
claBIairSub= norModSubBIThAir;
subBIThTube= norModSubBIThTub;
segVialBITh= norModSubBIThVial;

% select the same number of pixels from each segment
[XposClaBIair,YposClaBIair]=find(claBIairSub);
%numAir=length(XposClaBIair);% 6381 ---  5748
```

```
    %cut down and keep 50 pixels of the image data
    numXair1(:,y-4)=XposClaBIair(1:34:3400);
    numYair1(:,y-4)=YposClaBIair(1:34:3400);
    numAir(y-4)=length(numXair1);
    %numXair(:,y-5)=numXair1;
    %numYair(:,y-5)=numYair1;
    %find the tube data
    [XposClaBItube,YposClaBItube]=find(subBIThTube);
    %numTube=length(XposClaBItube);% 381
    numXtube1(:,y-4)=XposClaBItube(1:2:200);
    numYtube1(:,y-4)=YposClaBItube(1:2:200);
    numTube(y-4)=length(numXtube1);
    %numXTube(:,y-5)=numXtube1;
    %numYTube(:,y-5)=numYtube1;
    %find the vial data
    [XposClaBIVial,YposClaBIVial]=find(segVialBITh);
    %numVial=length(XposClaBIVial);% 1183
    numXVial1(:,y-4)=XposClaBIVial(1:6:600);
    numYVial1(:,y-4)=YposClaBIVial(1:6:600);
    numVial(y-4)=length(numXVial1);
    %numXVial(:,y-5)=numXVial1;
    %numYVial(:,y-5)=numYVial1;
    bIcla(:,:,:,y-4)=bI;
end
```

Wavelet Based Local Tomography via THz Pulsed Measurements

localTomography_PulsedTHz.m

```
% THz CT with a LIA was used to obtain a 1D image of a polystyrene sample.
%
% wavelet based local tomography on the centered area of interests
%
% Time domain parameter is extracted via applying correlation algorithms
% for the sinogram images (Radon transforms)
%
% The Unviersity of Adelaide
% Xiaoxia Yin
% January 2007

clear;
figure(1); clf;

    % open the file and read the header information
    fid = fopen(fileName,'r','n');
    mHeader = fscanf(fid,'%f',8); % 6,'int32')

    mDat = fscanf(fid,'%f');
    fclose(fid);

    nX = ceil(mHeader(1)/mHeader(2))+1;
    dX = mHeader(2) / 1000;  % mm
```

```
    nY = ceil(mHeader(3)/mHeader(4))+1;
    dY = mHeader(4) / 1000;  % mm
    nTime = ceil(mHeader(5)/mHeader(6))+1;
    dTime = mHeader(6) / 1.5e8 * 1e6; % ps
    time = [0:nTime-1]*dTime;

    nAngle = ceil(mHeader(7)/mHeader(8));
    dAngle = mHeader(8); % degrees

    mDat = reshape(mDat,nAngle,nTime,nX*nY);

    truncateData = 0;
    if (truncateData == 1)
        mDat = mDat(:,1:29,:);
        nTime = size(mDat,2);
        time = [0:nTime-1]*dTime;
    end

    [amp,delay]=max(mDat(:,1:1:end,:),[],2);

    amp = reshape(amp,nAngle,nX*nY);
    delay = reshape(delay,nAngle,nX*nY);
end

if (crossCorr == 1)
    % use cross-correlation to get the delay.
    interpFactor = 10;
    subsampleTime = 2; % set to 2 to skip every second sample

    % first we interpolate the signals to improve the resolution
    refInterp = interpft(mDat(2,1:subsampleTime:end,2),nTime*interpFactor);
    interpDelay = zeros(nAngle,nX);
    for i = 1:nAngle
        g = interpft(mDat(i,1:subsampleTime:end,:),nTime*interpFactor);

        % note xcorr2 is much slower than this loop
        for j = 1:nX*nY
            h = xcorr(g(:,:,j),refInterp);
            % h = abs(h);
            % apply some smoothing to h
            h = boxfilt(h,60);
            [a,b] = max(h);
            interpDelay(i,j) = b;
        end
    end

    figure(gcf+1);clf;
    imagesc([0:nX*nY-1]*dY,[0:nAngle-1]*dAngle,interpDelay);
    formatImage(2);
    title('XCorr Timing Sinogram');
    ylabel('Angle (degrees)');
    xlabel('X (mm)');
```

```
    if (printPlots)
        print(printOpts,strcat(printName,'xCorrSinogram'));
    end

end

if 1==1
    sinogramOut = interpDelay;

    % preprocess the sinogram
    if (interpMin ~= 0)
        sinogramOut = interpDelay - min(min(interpDelay));
        sinogramOut(sinogramOut < interpMin) = 0;
    end

    filtSinogram = 1;
    if (filtSinogram == 1)
        % wrap around the top and bottom rows of the delay and wiener filter
        wrapSinogram = [sinogramOut(end,:);sinogramOut;sinogramOut(1,:)];
        filtSinogram = wiener2(wrapSinogram,[2,2]);
        sinogramOut = filtSinogram(2:end-1,:);
    end

    debugPlot = 1;
    if (debugPlot == 1)
        figure(gcf+1);clf;
        imagesc([0:size(sinogramOut,1)-1]*dAngle,[0:size(sinogramOut,2)-1]*dY,sinogramOut');
        formatImage(2);
        title('Sinogram');
        ylabel('Y (mm)');
        xlabel('Angle (degrees)');
    end
    AA=zeros(34,nAngle);
    sinogramOut1=sinogramOut';
    if localCT==1;     %local tomography of the centered interest area
        AA=zeros(29,nAngle);
        sinogramOut1 =[AA;sinogramOut1(30:72,1:end);AA];
        reconCT = iradon(sinogramOut1,[],'linear','Ram-Lak',100);
    else
        reconCT = iradon(sinogramOut1,[],'linear','Ram-Lak',100);
    end
    % if (reconThresh == 1)
    %     reconCT = normMatrix(reconCT);
    %     reconCT = threshMatrix(reconCT,reconLowThresh,reconHighThresh,1);
    % end
    %

    debugPlot = 1;
    if (debugPlot == 1)
        figure(gcf+1);clf;
        %     imagesc([0:size(reconCT,1)]*dX,[0:size(reconCT,2)]*dX,interp2(abs(reconCT)));
        reconCT=interp2(reconCT,1);
        imagesc([0:size(reconCT,1)]*dX,[0:size(reconCT,2)]*dX,abs(reconCT));
```

```
        xlabel('X (mm)');
    end
end

p=sinogramOut1;
len=size(p,1);
order = max(64,2^nextpow2(2*len));

% First create a ramp filter - go up to the next highest
% power of 2.

filt = 2*( 0:(order/2) )./order;
w = 2*pi*(0:size(filt,2)-1)/order;   % frequency axis up to Nyquist

d=1;
filt(w>pi*d) = 0;                      % Crop the frequency response
filt = [filt' ; filt(end-1:-1:2)'];    % Symmetry of the filter


H=filt;Nfft=length(H);

p(length(H),1)=0;  % Zero pad projections

% In the code below, I continuously reuse the array p so as to
% save memory.  This makes it harder to read, but the comments
% explain what is going on.

pF = fft(p,Nfft);    % p holds fft of projections

for i = 1:size(pF,2)
    pp(:,i) = pF(:,i).*H; % frequency domain filtering
end
figure(gcf+1); clf;
plot(real(pp(:,2)));hold on;
plot(real(pF(:,2)),'r');

if 1==1
    pt = real(ifft(pp));     % p is the filtered projections
    pt(len+1:end,:) = [];   % Truncate the filtered projections
    figure(gcf+1);clf;
    plot(pt(:,i)); hold on;
    plot(sinogramOut1;(:,i),'r');
    figure(gcf+1);clf;
    sinogramOut1 =[repmat(pt(36,1:end),35,1);pt(36:67,1:end); repmat(pt(67,1:end),34,1)];
    imagesc( sinogramOut1);
    reconCT1 = backproj1( sinogramOut1,[],'linear',100);
    if (debugPlot == 1)
        figure(gcf+1);clf;reconCT1=interp2(reconCT1,1);% keep the same size with wavelet LCT
        imagesc([0:size(reconCT1,1)]*dX,[0:size(reconCT1,2)]*dX,abs(reconCT1));
        formatImage(2);
        title('Filtered Back Projection');
        ylabel('Y (mm)');
        xlabel('X (mm)');
```

```
    end
end

Nfft=length(H);
[loD,hiD,loR,hiR] = wfilters('bior2.2');
LoD = fft(loD',Nfft);
HiD = fft(hiD',Nfft);

% approximation subband
SrampA = pp;

theta = 0:nAngle-1;
theta_rad = theta*dAngle*pi/180;

for itheta = 1:nAngle
    SrampA(:,itheta) = pp(:,itheta).*FFT_scale(LoD,sin(theta_rad(itheta)),'Lin').*...
    FFT_scale(LoD,cos(theta_rad(itheta)),'Lin');
    %        SrampA(:,itheta) = boxfilt( SrampA(:,itheta),60);
end;

SrampA = real(ifft(SrampA));     % SrampA is the scaling ramp filtered projections
SrampA(len+1:end,:) = [];   % Truncate the filtered projections
figure(gcf+1);
imagesc(SrampA);
SrampA =[repmat(SrampA(36,1:end),36,1);SrampA(36:67,1:end); repmat(SrampA(67,1:end),34,1)];

figure(gcf+1);
imagesc(SrampA);grid on;

RA = backproj1(SrampA,[],'linear',100);
if (debugPlot == 1)
    figure(gcf+1);clf;
    imagesc([0:size(RA,1)]*dX,[0:size(RA,2)]*dX,abs(RA));
    formatImage(2);
    title('Approximate Subimage');
    ylabel('Y (mm)');
    xlabel('X (mm)');
end

SrampD1=p; % the projections being filtered along horizontal direction
for itheta = 1:nAngle
    SrampD1(:,itheta) = pp(:,itheta).*FFT_scale(LoD,sin(theta_rad(itheta)),'Lin').*...
      FFT_scale (HiD,cos(theta_rad(itheta)),'Lin');
    %      SrampD1(:,itheta) = boxfilt( SrampD1(:,itheta),60);
end;

SrampD1 = real(ifft( SrampD1));
% SrampD1 is the wavelet ramp filtered projections with horizontal orientations
SrampD1(len+1:end,:) = [];   % Truncate the filtered projections
SrampD1 =[repmat(SrampD1(36,1:end),35,1); SrampD1(36:67,1:end); repmat(SrampD1(67,1:end),34,1)];
% reconstructed horizontal detailed subimage
RD1 = backproj1( SrampD1,[],'linear',100);
```

```
for itheta = 1:nAngle % along vertical direction
    SrampD2(:,itheta) = pp(:,itheta).*FFT_scale(HiD,sin(theta_rad(itheta)),'Lin').*...
    FFT_scale(LoD,cos(theta_rad(itheta)),'Lin');
    %  SrampD2(:,itheta) = boxfilt( SrampD2(:,itheta),60);
end;

SrampD2 = real(ifft( SrampD2));   % wavelet ramp filtered projections  with vertical orientations
SrampD2(len+1:end,:) = [];   % Truncate the filtered projections
SrampD2 =[repmat(SrampD2(36,1:end),35,1); SrampD2(36:67,1:end); repmat(SrampD2(67,1:end),34,1)];

RD2 = backproj1( SrampD2,[],'linear',100); %vertical detail subimage

for itheta = 1:nAngle % along diagonal directions
    SrampD3(:,itheta) = pp(:,itheta).*FFT_scale(HiD,sin(theta_rad(itheta)),'Lin').*...
       FFT_scale(HiD,cos(theta_rad(itheta)),'Lin');
    %   SrampD3(:,itheta) = boxfilt( SrampD3(:,itheta),60);
end;

SrampD3 = real(ifft( SrampD3));     % wavelet ramp filtered projections with diagonal orientations
SrampD3(len+1:end,:) = [];   % Truncate the filtered projections
SrampD3 =[repmat(SrampD3(36,1:end),35,1); SrampD3(36:67,1:end); repmat(SrampD3(67,1:end),34,1)];

RD3 = backproj1( SrampD3,[],'linear',100); %diagonal detail subimage

figure(gcf+1);clf;
subplot(2,2,1);
imagesc(abs([RA]));
subplot(2,2,2);
imagesc(abs([RD1]));
subplot(2,2,3);
imagesc(abs([RD2]));
subplot(2,2,4);
imagesc(abs([RD3]));

frec = idwt2(RA(1:2:end,1:2:end), RD1(1:2:end,1:2:end), ...
    RD2(1:2:end,1:2:end), RD3(1:2:end,1:2:end),loR,hiR);
figure(gcf+1);
imagesc([0:size(frec,1)]*dX,[0:size(frec,2)]*dX,abs(frec));
formatImage(2);
title('Wavelet Based Tomography');
ylabel('Y (mm)');
xlabel('X (mm)');

frec = idwt2(RA(1:end,1:end), RD1(1:end,1:end), ...
    RD2(1:end,1:end), RD3(1:end,1:end),loR,hiR);
figure(gcf+1);
imagesc([0:size(frec,1)]*dX,[0:size(frec,2)]*dX,abs(frec));
formatImage(2);
title('Wavelet Based Tomography');
ylabel('Y (mm)');
xlabel('X (mm)');
figure(gcf+1);
imagesc([0:size(frec,1)]*dX,[0:size(frec,2)]*dX,interp2(abs(frec)));
```

```
formatImage(2);
reconN = frec *dTime/interpFactor/1e12/dY/1e-3 * 3e8;

S1=size(reconCT1);
S2=size(frec);
diff1 = -(reconCT1(20:180,20:180)-frec(20:180,20:180));
figure(gcf+1);clf;
imagesc([0:size(diff1,1)]*dX,[0:size(diff1,2)]*dX,abs(diff1));
formatImage(2);
title('difference');
ylabel('Y (mm)');
xlabel('X (mm)');
```

```
function Hsc = FFT_scale(H,a,interp)

% evaluates H(aw) given H(w)
% need a <= 1
% interp = 'NN'    use nearest neighbour interpolation (default)
%        = 'Lin'   use linear interpolation
%
%   Xiaoxia Yin
%   December 2006
%

len = length(H);
Hsc = zeros(size(H));
if (nargin < 3)
    interp = 'NN';
end;
if (a >= 0)
    if strcmp(interp, 'Lin')
        for ii = 1:len/2
            x = a*(ii-1)+1;
            if (mod(x,1) == 0)
                Hsc(ii) = H(x);
            else
                x1 = floor(x);
                Hsc(ii) = H(x1) + (H(x1+1)-H(x1))*(x-x1);
            end;
        end;
    elseif strcmp(interp, 'NN')
        idx = round(a*(0:(len/2-1)))+1;
        Hsc(1:len/2) = H(idx);
    end;
else
    if strcmp(interp, 'Lin')
        for ii = 1:len/2
            x = abs(a)*(ii-1)+1;
            if (mod(x,1) == 0)
                Hsc(ii) = H(x)';
```

```
            else
                x1 = floor(x);
                Hsc(ii) = (H(x1) + (H(x1+1)-H(x1))*(x-x1))';
            end;
        end;
    elseif strcmp(interp, 'NN')
        idx = round(abs(a)*(0:(len/2-1)))+1;
        Hsc(1:len/2) = H(idx)';
    end;
end;
Hsc((len/2+1):len) = Hsc(len/2:-1:1)';
```

```
function [img,tI,H] = Sepbackproj(varargin)

p = varargin{1};

theta = pi / size(p,2);
theta = (0:(size(p,2)-1))* theta;

string_args = {'nearest neighbor', 'linear', 'spline'};
arg = varargin{3};
idx = strmatch(lower(arg),string_args);
interp = string_args{idx};
N =varargin{4};
len=size(p,1);

img = zeros(N);        % Allocate memory for the image.

% Define the x & y axes for the reconstructed image so that the origin
% (center) is in the spot which RADON would choose.
xax = (1:N)-ceil(N/2);
x = repmat(xax, N, 1);    % x coordinates, the y coordinates are rot90(x)
y = rot90(x);

costheta = cos(theta);
sintheta = sin(theta);
ctrIdx = ceil(len/2);     % index of the center of the projections

% Zero pad the projections to size 1+2*ceil(N/sqrt(2)) if this
% quantity is greater than the length of the projections
imgDiag = 2*ceil(N/sqrt(2))+1;  % largest distance through image.
if size(p,1) < imgDiag
    rz = imgDiag - size(p,1);  % how many rows of zeros
    p = [zeros(ceil(rz/2),size(p,2)); p; zeros(floor(rz/2),size(p,2))];
    ctrIdx = ctrIdx+ceil(rz/2);
end

% Backprojection - vectorized in (x,y), looping over theta
if strcmp(interp, 'nearest neighbor')
    for i=1:length(theta)
```

```
        proj = p(:,i);
        t = round(x*costheta(i) + y*sintheta(i));
        img = img + proj(t+ctrIdx);
    end
elseif strcmp(interp, 'linear')
    for i=1:length(theta)
        proj = p(:,i);
        t = x.*costheta(i) + y.*sintheta(i);
        tI(:,:,i)=t;% record the intresting area
        a = floor(t);
        img = img + (t-a).*proj(a+1+ctrIdx) + (a+1-t).*proj(a+ctrIdx);
    end
elseif strcmp(interp, 'spline')
    for i=1:length(theta)
        proj = p(:,i);
        taxis = (1:size(p,1)) - ctrIdx;
        t = x.*costheta(i) + y.*sintheta(i);
        projContrib = interp1(taxis,proj,t(:),'*spline');
        img = img + reshape(projContrib,N,N);
    end
end

img = img*pi/(2*length(theta));
```

Local Reconstruction via THz QCL

THz_QCL_LT.m

```
close all;
clear;
clc;
%---------Read data
A = xlsread('2005May30sample291s2.xls', 2, 'C4:T292');
A1=max(A)/A;
Am=max(A1)
Nor=Am./A; dX=0.2;
figure(gcf+1);
imagesc(Nor)
sinogramOut1=log(Nor);
filtSinogram = wiener2(sinogramOut1,[2,2]);
figure(gcf+1)
imagesc(filtSinogram)
figure(gcf+1)
imagesc(sinogramOut1);

%------- global reconstruction via FBP
reconCT = iradon( filtSinogram,[],'nearest','Hann',250);

%----- Local reconstruction via FBP
if 1==0
```

```
size(A); %(289,18)
nAngle=size(A,2)
AA=zeros(50,nAngle);
BB=zeros(50,nAngle);
% sinogramOut2 =[AA;filtSinogram(81:180,1:end);BB];
sinogramOut2 =[AA;filtSinogram(51:239,1:end);BB];
%S3:sinogramOut2 =[AA;sinogramOut1(11:240,1:end);BB];
figure(gcf+1);
imagesc(sinogramOut2)
reconCT = iradon(sinogramOut2,[],'nearest','Hann',250);
figure(gcf+1)
imagesc(reconCT);
ylabel('Y (mm)');
xlabel('X (mm)');

p=sinogramOut2;
len=size(p,1);
order = max(64,2^nextpow2(2*len));

% First create a ramp filter - go up to the next highest
% power of 2.

filt = 2*( 0:(order/2) )./order;
w = 2*pi*(0:size(filt,2)-1)/order;   % frequency axis up to Nyquist

d=1;
filt(w>pi*d) = 0;                      % Crop the frequency response
filt = [filt' ; filt(end-1:-1:2)'];    % Symmetry of the filter

H=filt;Nfft=length(H);

p(length(H),1)=0;  % Zero pad projections

% In the code below, I continuously reuse the array p so as to
% save memory.  This makes it harder to read, but the comments
% explain what is going on.

pF = fft(p,Nfft);    % p holds fft of projections

for i = 1:size(pF,2)
    pp(:,i) = pF(:,i).*H; % frequency domain filtering
end

figure(gcf+1); clf;
plot(real(pp(:,2)));hold on;
plot(real(pF(:,2)),'r');

pt = real(ifft(pp));     % p is the filtered projections
pt(len+1:end,:) = [];   % Truncate the filtered projections
figure(gcf+1);clf;
plot(pt(:,i)); hold on;
plot(sinogramOut2(:,i),'r');
figure(gcf+1);clf;
```

```
imagesc( sinogramOut2);
figure(gcf+1);clf;
sinogramOut3 =[repmat(pt(81,1:end),80,1);pt(81:190,1:end); repmat(pt(190,1:end),99,1)];
% hole reconstruction
imagesc( sinogramOut3);
[reconCT1,tI] = backproj1( sinogramOut3,[],'linear',250);

figure(gcf+1);clf;
imagesc([0:size(reconCT1,2)]*dX,[0:size(reconCT1,1)]*dX,interp2(abs(reconCT1),2));
ylabel('Y (mm)');
xlabel('X (mm)');  formatImage(2);

figure(gcf+1);clf;% keep the same size with wavelet LCT
dX=0.2; % a small adjustment of the zoomed image based on the zoomed global data..
imagesc([0:size(reconCT1(80+2:229-35,78-4:166),2)]*dX,[0:size(reconCT1(80+2:229-35,78-4:166),1)]*dX,...
    interp2(abs(reconCT1(80+2:229-35,78-4:166)),2)); formatImage(2);
title('Filtered Back Projection');
ylabel('Y (mm)');
xlabel('X (mm)');

figure(gcf+1);clf;
SegTrac=reconCT1(80+2:229-35,78-4:166);
min(min(SegTrac))
max(max(SegTrac))

SegTrac1=ceil(SegTrac.*10000+109);
min(min(SegTrac1))
max(max(SegTrac1));
figure(gcf+1);clf;
imagesc([0:size(SegTrac1,2)]*dX,[0:size(SegTrac1,1)]*dX,interp2(abs(SegTrac1),2));
formatImage(2);
title('Filtered Back Projection');
ylabel('Y (mm)');
xlabel('X (mm)');
size(SegTrac1);
figure(gcf+1);clf;

for i=1:195
    ImageHis(i)=length(find(SegTrac1==i));
end
[a,b]=max(ImageHis);
sum(ImageHis);
figure(gcf+1);clf;
h1=ImageHis(1:195);
horz=1:195;
bar(horz,h1);axis on; grid on;
axis([0 195 0 158])
% h = findobj(gca,'Type','patch');
% set(h,'FaceColor','r','EdgeColor','w')

% (80-67)/5000=0.0026;
HoldInd=(SegTrac1<=100);
figure(gcf+1);clf;
```

```
imagesc(HoldInd);
axis on; grid on;
%chasing the edge
[imX,imY]=size(HoldInd);
coY=ceil(imY/2);% 47 pixel
coX=ceil(imX/2);% 57 pixel
if 1==1
    for Iy=1:coY-1
        for Ix=1: coX-1
            A1= HoldInd( coX-1+Ix-1,coY-1+Iy+1);% calculation start from (coX,coY)
            A2= HoldInd( coX-1+Ix,  coY-1+Iy+1);
            A3= HoldInd( coX-1+Ix+1,coY-1+Iy+1);
            A4= HoldInd( coX-1+Ix-1,coY-1+Iy);
            A5= HoldInd( coX-1+Ix+1,coY-1+Iy);
            A6= HoldInd( coX-1+Ix,  coY-1+Iy);
            A7= HoldInd( coX-1+Ix-1,coY-1-1+Iy);
            A8= HoldInd( coX-1+Ix,  coY-1-1+Iy);
            A9= HoldInd( coX-1+Ix+1,coY-1-1+Iy);

            A=[A1,A2,A3,A4,A5,A6,A7,A8,A9];
            if length(find(A==1))<=6
                HoldInd(coX-1+Ix,coY-1+Iy)=0;
            else
                HoldInd(coX-1+Ix,coY-1+Iy)=1;
            end
        end
    end
    figure(gcf+1);clf;
    imagesc(HoldInd);
    % the second quadrant of the coordinates
end

if 1==1
    for Iy=1:coY-2
        for Ix=1:coX-2
            A1= HoldInd( coX+Ix-1,coY-Iy+1);% calculation start from (coX,coY)
            A2= HoldInd( coX+Ix,coY-Iy+1);
            A3= HoldInd( coX+Ix+1,coY-Iy+1);
            A4= HoldInd( coX+Ix-1,coY-Iy);
            A5= HoldInd( coX+Ix+1,coY-Iy);
            A6= HoldInd( coX+Ix,coY-Iy);
            A7= HoldInd( coX+Ix-1,coY-1-Iy);
            %            A8= HoldInd( co+lx,coY-1-Iy);
            A8= HoldInd( coX+Ix,coY-1-Iy);
            A9= HoldInd( coX+Ix+1,coY-1-Iy);

            A=[A1,A2,A3,A4,A5,A6,A7,A8,A9];
            if length(find(A==1))<=6
                HoldInd(coX+Ix,coY-Iy)=0;
            else
                HoldInd(coX+Ix,coY-Iy)=1;
            end
        end
```

```
    end
    figure(gcf+1);clf;
    imagesc(HoldInd);
end

if 1==1
    % the third quadrant of the coordinates
    for Iy=1:coY-2
        for Ix=1:coX-2
            A1= HoldInd( coX-Ix-1,coY-Iy+1);% calculation start from (coX,coY)
            A2= HoldInd( coX-Ix,coY-Iy+1);
            A3= HoldInd( coX-Ix+1,coY-Iy+1);
            A4= HoldInd( coX-Ix-1,coY-Iy);
            A5= HoldInd( coX-Ix+1,coY-Iy);
            A6= HoldInd( coX-Ix,coY-Iy);
            A7= HoldInd( coX-Ix-1,coY-1-Iy);
            A8= HoldInd( coX-Ix,coY-1-Iy);
            A9= HoldInd( coX-Ix+1,coY-1-Iy);

            A=[A1,A2,A3,A4,A5,A6,A7,A8,A9];
            if length(find(A==1))<=6
                HoldInd(coX-Ix,coY-Iy)=0;
            else
                HoldInd(coX-Ix,coY-Iy)=1;
            end
        end
    end
    figure(gcf+1);clf;
    imagesc(HoldInd);
end

% the fourth quadrant of the coordinates
for Iy=1:coY-2
    for Ix=1:coX-2
        A1= HoldInd( coX-Ix-1,coY+Iy+1);% calculation start from (coX,coY)
        A2= HoldInd( coX-Ix,coY+Iy+1);
        A3= HoldInd( coX-Ix+1,coY+Iy+1);
        A4= HoldInd( coX-Ix-1,coY+Iy);
        A5= HoldInd( coX-Ix+1,coY+Iy);
        A6= HoldInd( coX-Ix,coY+Iy);
        A7= HoldInd( coX-Ix-1,coY-1+Iy);
        A8= HoldInd( coX-Ix,coY-1+Iy);
        A9= HoldInd( coX-Ix+1,coY-1+Iy);

        A=[A1,A2,A3,A4,A5,A6,A7,A8,A9];
        if length(find(A==1))<=6
            HoldInd(coX-Ix,coY+Iy)=0;
        else
            HoldInd(coX-Ix,coY+Iy)=1;
        end
    end
end
figure(gcf+1);clf;
```

```
    imagesc(HoldInd);
    %coX(fix) coY(mov)

    for Ey=1:coY
        if length(find(HoldInd(:,coY-1+Ey)==1))<=8
            [Eya,Eyb]=find(HoldInd(:,coY-1+Ey)==1);
            HoldInd(Eya,Eyb)=0;
            HoldInd(:,coY-1+Ey+1:end)=0;
        end
    end
    figure(gcf+1);clf;
    imagesc(HoldInd);

    for Ey=1:coY
        if length(find(HoldInd(:,coY-Ey)==1))<=8
            [Eya,Eyb]=find(HoldInd(:,coY-Ey)==1);
            HoldInd(Eya,Eyb)=0;
            HoldInd(:,1:coY-Ey-1)=0;
            break
        end
    end
    figure(gcf+1);clf;
    imagesc(HoldInd);

    for Ex=1:coX-1
        if length(find(HoldInd(coX-Ex,:)==1))<=8
            [Eya,Eyb]=find(HoldInd(coX-Ex,:)==1);
            HoldInd(Eya,Eyb)=0;
            HoldInd(1:coX-Ex,:)=0;
        end
    end
    figure(gcf+1);clf;
    imagesc(HoldInd);

    for Ex=1:coX-1
        if length(find(HoldInd(coX+Ex,:)==1))<=8
            [Eya,Eyb]=find(HoldInd(coX+Ex,:)==1);
            HoldInd(Eya,Eyb)=0;
            HoldInd(coX+Ex:end,:)=0;
            break
        end
    end
    figure(gcf+1);clf;
    imagesc(HoldInd);
    formatImage(2);
    figure(gcf+1);
    imagesc([0:size(HoldInd,1)]*dX,[0:size(HoldInd,2)]*dX,interp2(abs(HoldInd),2));
    formatImage(2);
    title('Traditional Back Projection');
    ylabel('Y (mm)');
    xlabel('X (mm)');
end
```

```
%-----------wavelet based local tomography

size(A); %(289,18)
nAngle=size(A,2)
AA=zeros(50,nAngle);
BB=zeros(50,nAngle);
% sinogramOut2 =[AA;filtSinogram(81:180,1:end);BB];
sinogramOut2 =[AA;filtSinogram(51:239,1:end);BB];%S3:sinogramOut2 =[AA;sinogramOut1(11:240,1:end);BB];
figure(gcf+1);
imagesc(sinogramOut2)
reconCT = iradon(sinogramOut2,[],'nearest','Hann',250);

p=sinogramOut2;
len=size(p,1);
order = max(64,2^nextpow2(2*len));

% First create a ramp filter - go up to the next highest
% power of 2.

filt = 2*( 0:(order/2) )./order;
w = 2*pi*(0:size(filt,2)-1)/order;   % frequency axis up to Nyquist

d=1;
filt(w>pi*d) = 0;                      % Crop the frequency response
filt = [filt' ; filt(end-1:-1:2)'];    % Symmetry of the filter


H=filt;Nfft=length(H);

p(length(H),1)=0;  % Zero pad projections

% In the code below, I continuously reuse the array p so as to
% save memory.  This makes it harder to read, but the comments
% explain what is going on.

pF = fft(p,Nfft);    % p holds fft of projections

for i = 1:size(pF,2)
    pp(:,i) = pF(:,i).*H; % frequency domain filtering
end

Nfft=length(H);
[loD,hiD,loR,hiR] = wfilters('bior2.2');

LoD = fft(loD',Nfft);
HiD = fft(hiD',Nfft);

dAngle=18;
% approximation subband
SrampA = pp;

theta = 0:nAngle-1;
theta_rad = theta*dAngle*pi/180;
```

```
for itheta = 1:nAngle
    SrampA(:,itheta) = pp(:,itheta).*FFT_scale(LoD,sin(theta_rad(itheta)),'Lin').*...
           FFT_scale(LoD,cos(theta_rad(itheta)),'Lin');
    % SrampA(:,itheta) = boxfilt( SrampA(:,itheta),60);
end;

SrampA = real(ifft(SrampA));     % SrampA is the approximated ramp filtered projections
SrampA(len+1:end,:) = []; cSrampA=SrampA;
% Truncate the filtered projections
figure(gcf+1);
imagesc(SrampA);
formatImage(2);grid off;
title('Wavelet ramp filtered sinogram');

SrampA =[repmat(SrampA (81,1:end),80,1);SrampA(81:190,1:end); repmat(SrampA (190,1:end),99,1)];
[RA,WtI] = backproj1(SrampA,[],'linear',250);%calculate the area of interest
figure(gcf+1);clf;
imagesc([0:size(RA(80:229-35,78-4:166),2)]*dX,[0:size(RA(80:229-35,78-4:166),1)]*dX,interp2(abs(RA...
       (80:229-35,78-4:166)),2));
grid on;
formatImage(2);
title('Approximate Subimage');
ylabel('Y (mm)');
xlabel('X (mm)');
if 1==1
    SrampD1=p;
    for itheta = 1:nAngle
        SrampD1(:,itheta) = pp(:,itheta).*FFT_scale(LoD,sin(theta_rad(itheta)),'Lin').*...
           FFT_scale(HiD,cos(theta_rad(itheta)),'Lin');
        %      SrampD1(:,itheta) = boxfilt( SrampD1(:,itheta),60);
    end;

    SrampD1 = real(ifft( SrampD1));
    SrampD1(len+1:end,:) = [];
    SrampD1 =[repmat(SrampD1(81,1:end),80,1); SrampD1(81:190,1:end); repmat(SrampD1(190,1:end),99,1)];
% maximum intensity 6.2718
    RD1 = backproj1( SrampD1,[],'linear',250);


    for itheta = 1:nAngle
        SrampD2(:,itheta) = pp(:,itheta).*FFT_scale(HiD,sin(theta_rad(itheta)),'Lin').*...
            FFT_scale(LoD,cos(theta_rad(itheta)),'Lin');
        %  SrampD2(:,itheta) = boxfilt( SrampD2(:,itheta),60);
    end;

    SrampD2 = real(ifft( SrampD2));
    SrampD2(len+1:end,:) = [];   % Truncate the filtered projections
    SrampD2 =[repmat(SrampD2(81,1:end),80,1); SrampD2(81:190,1:end); repmat(SrampD2(190,1:end),99,1)];
% maximum intensity 6.2718
    RD2 = backproj1( SrampD2,[],'linear',250);

    for itheta = 1:nAngle
```

```
        SrampD3(:,itheta) = pp(:,itheta).*FFT_scale(HiD,sin(theta_rad(itheta)),'Lin').*...
            FFT_scale(HiD,cos(theta_rad(iteta)),'Lin');
        %   SrampD3(:,itheta) = boxfilt( SrampD3(:,itheta),60);
    end;

    SrampD3 = real(ifft( SrampD3));
    SrampD3(len+1:end,:) = [];
    SrampD3 =[repmat(SrampD3(81,1:end),80,1); SrampD3(81:190,1:end); repmat(SrampD3(190,1:end),99,1)];
% maximum intensity 6.2718
    RD3 = backproj1( SrampD3,[],'linear',250);

    figure(gcf+1);clf;
    subplot(2,2,1);
    imagesc([0:size(RA,1)]*dX,[0:size(RA,2)]*dX,interp2(abs(RA),3));%imagesc(abs([RA]));
    ylabel('Y (mm)');
    xlabel('X (mm)');
    subplot(2,2,2);
    imagesc([0:size(RD1,1)]*dX,[0:size(RD1,2)]*dX,interp2(abs(RD1),3)); %imagesc(abs([RD1]));
    ylabel('Y (mm)');
    xlabel('X (mm)');
    subplot(2,2,3);
    imagesc([0:size(RD2,1)]*dX,[0:size(RD2,2)]*dX,interp2(abs(RD2),3)); %imagesc(abs([RD2]));
    ylabel('Y (mm)');
    xlabel('X (mm)');
    subplot(2,2,4);
    imagesc([0:size(RD3,1)]*dX,[0:size(RD3,2)]*dX,interp2(abs(RD3),3)); %imagesc(abs([RD3]));
    ylabel('Y (mm)');
    xlabel('X (mm)');

    frec1= idwt2(RA(1:end,1:end), RD1(1:end,1:end), ...
        RD2(1:end,1:end), RD3(1:end,1:end),loR,hiR);
    figure(gcf+1);
    imagesc([0:size(frec1,1)]*dX,[0:size(frec1,2)]*dX,interp2(abs(frec1),2));
    formatImage(2);
    title('Wavelet Based Tomography');
    ylabel('Y (mm)');
    xlabel('X (mm)');
end

figure(gcf+1);clf;
SegTrac=RA(80:229-35,78-4:166);
min(min(SegTrac))
max(max(SegTrac))

SegTrac1=ceil(SegTrac.*5000+110);
Ami=min(min(SegTrac1)); %
Amx=max(max(SegTrac1)); %239
figure(gcf+1);clf;
imagesc([0:size(SegTrac1,2)]*dX,[0:size(SegTrac1,1)]*dX,interp2(abs(SegTrac1),2));
size(SegTrac1)
figure(gcf+1);clf;

for i=1:Amx
```

```
    ImageHis(i)=length(find(SegTrac1==i));
end
[a,b]=max(ImageHis);
sum(ImageHis);
figure(gcf+1);clf;
h1=ImageHis(1:Amx);
horz=1:Amx;
bar(horz,h1);
axis([0 Amx 0 a])
% h = findobj(gca,'Type','patch');
% set(h,'FaceColor','r','EdgeColor','w')

% (80-67)/5000=0.0026;
HoldInd=(SegTrac1<=95);%83
figure(gcf+1);clf;
imagesc(HoldInd);
axis on; grid on;
%chasing the edge
[imX,imY]=size(HoldInd);
coY=ceil(imY/2);% 45 pixel
coX=ceil(imX/2);% 75 pixel
if 1==1
        % the first quadrant of the coordinates
    for Iy=1:coY-1
        for Ix=1:coX-1
            A1= HoldInd( coX-1+Ix-1,coY-1+Iy+1);% calculation start from (coX,coY)
            A2= HoldInd( coX-1+Ix,  coY-1+Iy+1);
            A3= HoldInd( coX-1+Ix+1,coY-1+Iy+1);
            A4= HoldInd( coX-1+Ix-1,coY-1+Iy);
            A5= HoldInd( coX-1+Ix+1,coY-1+Iy);
            A6= HoldInd( coX-1+Ix,  coY-1+Iy);
            A7= HoldInd( coX-1+Ix-1,coY-1-1+Iy);
            A8= HoldInd( coX-1+Ix,  coY-1-1+Iy);
            A9= HoldInd( coX-1+Ix+1,coY-1-1+Iy);

            A=[A1,A2,A3,A4,A5,A6,A7,A8,A9];
            if length(find(A==1))<=6
                HoldInd(coX-1+Ix,coY-1+Iy)=0;
            else
                HoldInd(coX-1+Ix,coY-1+Iy)=1;
            end
        end
    end
    figure(gcf+1);clf;
    imagesc(HoldInd);grid on;
    % the second quadrant of the coordinates
end

if 1==1
    for Iy=1:coY-2
        for Ix=1:coX-2
            A1= HoldInd( coX+Ix-1,coY-Iy+1);% calculation start from (coX,coY)
            A2= HoldInd( coX+Ix,coY-Iy+1);
```

```
            A3= HoldInd( coX+Ix+1,coY-Iy+1);
            A4= HoldInd( coX+Ix-1,coY-Iy);
            A5= HoldInd( coX+Ix+1,coY-Iy);
            A6= HoldInd( coX+Ix,coY-Iy);
            A7= HoldInd( coX+Ix-1,coY-1-Iy);
            A8= HoldInd( coX+Ix,coY-1-Iy);
            A9= HoldInd( coX+Ix+1,coY-1-Iy);

            A=[A1,A2,A3,A4,A5,A6,A7,A8,A9];
            if length(find(A==1))<=6
                HoldInd(coX+Ix,coY-Iy)=0;
            else
                HoldInd(coX+Ix,coY-Iy)=1;
            end
        end
    end
    figure(gcf+1);clf;
    imagesc(HoldInd);
end

if 1==1
    % the third quadrant of the coordinates
    for Iy=1:coY-2
        for Ix=1:coX-2
            A1= HoldInd( coX-Ix-1,coY-Iy+1);% calculation start from (coX,coY)
            A2= HoldInd( coX-Ix,coY-Iy+1);
            A3= HoldInd( coX-Ix+1,coY-Iy+1);
            A4= HoldInd( coX-Ix-1,coY-Iy);
            A5= HoldInd( coX-Ix+1,coY-Iy);
            A6= HoldInd( coX-Ix,coY-Iy);
            A7= HoldInd( coX-Ix-1,coY-1-Iy);
            A8= HoldInd( coX-Ix,coY-1-Iy);
            A9= HoldInd( coX-Ix+1,coY-1-Iy);

            A=[A1,A2,A3,A4,A5,A6,A7,A8,A9];
            if length(find(A==1))<=6
                HoldInd(coX-Ix,coY-Iy)=0;
            else
                HoldInd(coX-Ix,coY-Iy)=1;
            end
        end
    end
    figure(gcf+1);clf;
    imagesc(HoldInd);
end

% the fourth quadrant of the coordinates
for Iy=1:coY-2
    for Ix=1:coX-2
        A1= HoldInd( coX-Ix-1,coY+Iy+1);% calculation start from (coX,coY)
        A2= HoldInd( coX-Ix,coY+Iy+1);
        A3= HoldInd( coX-Ix+1,coY+Iy+1);
        A4= HoldInd( coX-Ix-1,coY+Iy);
```

```
        A5= HoldInd( coX-Ix+1,coY+Iy);
        A6= HoldInd( coX-Ix,coY+Iy);
        A7= HoldInd( coX-Ix-1,coY-1+Iy);
        A8= HoldInd( coX-Ix,coY-1+Iy);
        A9= HoldInd( coX-Ix+1,coY-1+Iy);

        A=[A1,A2,A3,A4,A5,A6,A7,A8,A9];
        if length(find(A==1))<=6
            HoldInd(coX-Ix,coY+Iy)=0;
        else
            HoldInd(coX-Ix,coY+Iy)=1;
        end
    end
end
figure(gcf+1);clf;
imagesc(HoldInd);
%coX(fix) coY(mov)

for Ey=1:coY
    if length(find(HoldInd(:,coY-1+Ey)==1))<=8
        [Eya,Eyb]=find(HoldInd(:,coY-1+Ey)==1);
        HoldInd(Eya,Eyb)=0;
        HoldInd(:,coY-1+Ey+1:end)=0;
    end
end
figure(gcf+1);clf;
imagesc(HoldInd);

for Ey=1:coY
    if length(find(HoldInd(:,coY-Ey)==1))<=8
        [Eya,Eyb]=find(HoldInd(:,coY-Ey)==1);
        HoldInd(Eya,Eyb)=0;
        HoldInd(:,1:coY-Ey-1)=0;
        break
    end
end
figure(gcf+1);clf;
imagesc(HoldInd);

for Ex=1:coX-1
    if length(find(HoldInd(coX-Ex,:)==1))<=8
        [Eya,Eyb]=find(HoldInd(coX-Ex,:)==1);
        HoldInd(Eya,Eyb)=0;
        HoldInd(1:coX-Ex,:)=0;
    end
end
figure(gcf+1);clf;
imagesc(HoldInd);

for Ex=1:coX-1
    if length(find(HoldInd(coX+Ex,:)==1))<=8
        [Eya,Eb]=find(HoldInd(coX+Ex,:)==1);
        HoldInd(Eya,Eyb)=0;
```

```
        HoldInd(coX+Ex:end,:)=0;
        break
    end
end

figure(gcf+1);clf;
imagesc(HoldInd);
figure(gcf+1);
imagesc([0:size(HoldInd,1)]*dX,[0:size(HoldInd,2)]*dX,interp2(abs(HoldInd),2));
formatImage(2);
title('Wavelet Based Tomography');
ylabel('Y (mm)');
xlabel('X (mm)');
```

DVD containing additional data is included with the print copy held in the University of Adelaide Library.

Bibliography

ABBOTT-D. (2000). Directions in terahertz technology, *Proceedings 22nd IEEE GaAs IC Symposium*, Seattle, WA, pp. 263–266.

ALIVISATOS-A. P. (1996). Semiconductor clusters, nanocrystals, and quantum dots, *Science*, **271**, pp. 933–937.

ALIVISATOS-A. P. (2004). The use of nanocrystals in biological detection, *Nature Biotechnology*, **22**, pp. 47–52.

ALTON-J. (2005). *Bound-to-Continuum THz Quantum Cascade Lasers (PhD Thesis)*, University of Cambridge, UK.

American Physical Society (2007). Web. http://flux.aps.org/meetings/YR99/CENT99/abs/S8060003.html Last Checked: December 18 2007.

ARNONE-D., CIESLA-C., AND PEPPER-M. (2000). Terahertz imaging comes into view, *Physics World*, **13**(4), pp. 35–40.

ASHLEY-A., AND PALKA-F. (1973). Transmission cavity and injection stabilization of an X-band transferred electron oscillator, *IEEE MTT-S International Microwave Symposium Digest*, **73**(1), pp. 181–182.

ATKESON-C., MOORE-A., AND SCHAAL-S. (1997). Locally weighted learning, *Artificial Intelligence Review*, **11**(1-5), pp. 11–73.

AUSTON-D. (1983). Impulse response of photoconductors in transmission lines, *IEEE Journal of Quantum Electronics*, **19**(4), pp. 639–648.

BARBIERI-S., ALTON-J., BEERE-H. E., FOWLER-J., FORD-J., LINFIELD-E. H., AND RITCHIE-D. A. (2004). 2.9 THz quantum cascade lasers operating up to 70 K in continuous wave, *Applied Physics Letters*, **85**(10), pp. 1674–1676.

BARTELS-A., CERNA-R., KISTNER-C., THOMA-A., HUDERT-F., JANKE-C., AND DEKORSY-T. (2007). Ultrafast time-domain spectroscopy based on high-speed asynchronous optical sampling, *Review of Scientific Instruments*, **78**(3), Art. No. 035107.

BEARD-M., TURNER-G., AND SCHMUTTENMAER-C. (2002). Terahertz spectroscopy, *Journal of Physical Chemistry*, **106**(29), pp. 7146–7159.

BENGIO-Y., AND GRANDVALET-Y. (2004). No unbiased estimator of the variance of k-fold cross-validation, *Journal of Machine Learning Research*, **5**, pp. 1089–1105.

BERENSTEIN-C., AND WALNUT-D. (1994). Local inversion of the radon transform in even dimensions using wavelets, *75 Years of Radon Transform*, pp. 38–58.

BERGER-V., AND SIRTORI-C. (2004). Multispectral classification techniques for terahertz pulsed imaging: an example in histopathology, *Semiconductor Science and Technology*, **19**(8), pp. 964–970.

BERRY-E., BOYLE-R., FITZGERALD-A., AND HANDLEY-J. (2005). Time frequency analysis in terahertz pulsed imaging, *Computer Vision Beyond the Visible Spectrum (Advances in Pattern Recognition)*, Springer Verlag, London, UK, pp. 290–329.

BERRY-E., HANDLEY-J., FITZGERALD-A., MERCHANT-W., BOYLE-R., ZINOV'EV-N., MILES-R., CHAMBERLAIN-J., AND SMITH-M. (2004). Nonlinear phase matching in THz semiconductor waveguides, *Medical Engineering & Physics*, **26**(5), pp. 423–430.

BERRYMAN-M. J., AND RAINSFORD-T. (2004). Classification of terahertz data as a tool for the detection of cancer, *Medical Engineering & Physics*, **6416**(12006), pp. 423–430.

BILGOT-A., PERRIER-V., AND DESBAT-L. (2004). Wavelets, local tomography and interventional x-ray imaging, *2004 IEEE on Nuclear Science Symposium Conference Record*, **6**, pp. 3505–3509.

BORN-M., AND WOLF-E. (2002). *Principles of Optics: Electromagnetic Theory of Propagation, Interference and Diffraction of Light*, Seventh Edition, Cambridge University Press, Cambridge, UK.

BOW-S. (2002). *Pattern Recognition and Image Preprocessing (Signal Processing and Communications Series)*, second edition edn, Marcel Dekker, Inc., NY, USA.

BRABEC-T., SPIELMANN-C., CURLEY-P. F., AND KRAUSZ-F. (1992). Kerr lens mode locking, *Optics Letters*, **17**(18), pp. 639–648.

BRINK-J., LIM-J., WANG-G., HEIKEN-J., DEYOE-L., AND VANNIER-M. (1995). Technical optimization of spiral CT for depiction of renal artery stenosis: in vitro analysis, *Radiology*, **194**, pp. 157–163.

BROMAGE-J., RADIC-S., AGRAWAL-G. P., STROUD-C. R., FAUCHET-P. M. J., AND SOBOLEVSKI-R. (1998). Spatiotemporal shaping of half-cycle terahertz pulses by diffraction through conductive apertures of finite thickness, *Journal of the Optical Society of America B-Optical Physics*, **15**(7), pp. 1953–1959.

BROWN-E. R., MCINTOSH-K. A., NICHOLS-K. B., AND DENNIS-C. L. (1995). Photomixing up to 3.8 THz in low-temperature-grown GaAs, *Review of Scientific Instruments*, **66**(3), pp. 285–287.

BROWN-E. R., SMITH-F. W., AND MCINTOSH-K. A. (1993). Coherent millimeterwave generation by heterodyne conversion in low-temperature-grown GaAs photoconductors, *Journal of Applied Physics*, **73**(3), pp. 1480–1484.

BROWN-L. G. (1992). A survey of image registration techniques, *Computing-Surveys*, **24**(4), pp. 325–376.

BROWN-M. S., FIECHTNER-G. J., RUDD-J. V., ZIMDARS-D. A., WARMUTH-M., AND GORD-J. R. (2006). Water-vapor detection using asynchronous THz sampling, *Applied Spectroscopy*, **60**(3), pp. 261–265.

BRUCHERSEIFER-M., NAGEL-M., BOLIVAR-H. P., KURZ-H., BOSSERHOFF-A., AND BUTTNER-R. (2000). Label-free probing of the binding state of DNA by time-domain terahertz sensing, *Applied Physics Letters*, **77**(24), pp. 4049–4051.

CAI-J., AND LI-Y. (2005). *Lecture Notes in Computer Science*, Springer, Berlin, Heidelberg.

CAI-Y., BRENER-I., LOPATA-J., WYNN-J., PFEIFFER-L., STARK-J. B., WU-Q., ZHANG-X. C., AND FEDERICI-J. F. (1998). Design and performance of a THz emission and detection setup based on a semi-insulating GaAs emitter, *Applied Physics Letters*, **73**(4), pp. 444–446.

CANDÈS-E. J., DEMANET-L., DONOHO-D., AND YING-L. (2006). Fast discrete curvelet transforms, *Multiscale Modeling & Simulation*, **5**, pp. 861–899.

CANTOR-A., CHEO-P., FOSTER-M., AND NEWMAN-L. (1981). Application of submillimeter wave lasers to high voltage cable inspection, *IEEE Journal of Quantum Electronics*, **17**(4), pp. 477–489.

CANU-S., GRANDVALET-Y., GUIGUE-V., AND RAKOTOMAMONJY-A. (2005). SVM and kernel methods matlab toolbox, *Perception Systèmes et Information, INSA de Rouen, Rouen, France*.

CARIN-L., FELSEN-L. B., KRALJ-D., OH-H. S., LEE-W. C., AND PILLAI-S. U. (1997). Wave-oriented signal processing of dispersive time-domain scattering data, *IEEE Transactions on Antennas and Propagation*, **45**(4), pp. 592–600.

CARRIG-T. J., RODRIGUEZ-G., CLEMENT-T. S., TAYLOR-A. J., AND STEWART-K. R. (1995). Scaling of terahertz radiation via optical rectification in electrooptic crystals, *Applied Physics Letters*, **66**(2), pp. 121–123.

CHANG-C.-C., AND LIN-C.-J. (2001). Libsvm: a library for support vector machines, *Software available at http: //www.csie.ntu.edu.tw/ cjlin/ libsvm*.

CHAN-W. L., DEIBEL-J., AND MITTLEMAN-D. M. (2007). Imaging with terahertz radiation, *Reports on Progress in Physics*, **70**(8), pp. 1325–1379.

CHEN-Q., AND ZHANG-X C. (2001). Semiconductor dynamic aperture for near-field terahertz wave imaging, *IEEE Journal of Selected Topics in Quantum Electronics*, **7**(4), pp. 608–614.

CHEN-Q., JIANG-Z., XU-G., AND ZHANG-X. C (2000). Near-field terahertz imaging with a dynamic aperture, *Optics Letters*, **25**(15), pp. 1122–1124.

CHEVILLE-R. A., AND GRISCHKOWSKY-D. (1995). Time domain terahertz impulse ranging studies, *Applied Physics Letters*, **67**(14), pp. 1960–1962.

CHEVILLE-R. A., MCGOWAN-R. W., AND GRISCHKOWSKY-D. (1997). Late-time target response measured with terahertz impulse ranging, *IEEE Transactions on Antennas and Propogation*, **45**, pp. 1518-1524.

CHOI-M. K., TAYLOR-K., BETTERMANN-A., AND VAN DERWEIDE-D. (2002). Broadband 10-300 GHz stimulus-response sensing for chemical and biological entities, *Physics in Medicine and Biology*, **47**(21), pp. 3777–3789.

CHUANG-K. S., TZENG-H. L., CHEN-S., WU-J., AND CHEN-T. (2006). Fuzzy c-means clustering with spatial information for image segmentation, *Computerized Medical Imaging and Graphics*, **30**, pp. 9–15.

COGDILL-R. P., FORCHT-R. N., SHEN-Y. C., TADAY-P. F., CREEKMORE-J. R., ANDERSON-C. A., AND III-J. K. D. (2007). Comparison of terahertz pulse imaging and near-infrared spectroscopy for rapid, non-destructive analysis of tablet coating thickness and uniformity, *Journal of Pharmaceutical Innovation*, **2**(1-2), pp. 29–36.

COIFMAN-R., AND WICKERHAUSER-M. (1992). Entropy-based algorithms for best basis selection, *IEEE Transactions on Information Theory*, **38**(2), p. 713–718.

COVER-T. M. (1965). Geometrical and statistical properties of systems of linear inequalities with applications in pattern recognition, *IEEE Transactions on Electronic Computers*, **14**, pp. 326–334.

CRAWLEY-D., WITHINGTON-S., AND OBRADOVIC-J. (2006). Area-scan camera for terahertz holography, *Review of Scientific Instruments*, **77**(5), Art. No. 053106.

CRISTIANINI-N., AND SHAWE-TAYLOR-J. (2000). *An Introduction to Support Vector Machines and Other Kernel Based Methods*, Cambridge University Press, Cambridge, UK.

CUBANSKI-D., AND CYGANSKI-D. (1995). Multivariate classification through adaptive Delaunay-based C spline approximation, *IEEE Transactions on Pattern Analysis and Machine Intelligence*, **17**(4), pp. 403–417.

DARMO-J., TAMOSIUNAS-V., FASCHING-G., KRÖLL-J., UNTERRAINER-K., BECK-M., GIOVANNINI-M., FAIST-J., KREMSER-C., AND DEBBAGE-P. (2004). Imaging with a terahertz quantum cascade laser, *Optics Express*, **12**(9), pp. 1879–1884.

DAUBECHIES-I. (1988). Orthonormal bases of compactly supported wavelets, *Communications on Pure & Applied Mathematics*, **41**(7), pp. 909–996.

DAUBECHIES-I. (1992). *Ten lectures on wavelets*, Society for Industrial and Applied Mathematics, Philadelphia, PA, USA.

DAVIES-A. G., LINFIELD-E. H., AND JOHNSTON-M. B. (2002). The development of terahertz sources and their applications, *Physics in Medicine and Biology*, **47**(21), pp. 3679–3689.

Defence Research & Development Organization (2008). Web. http://www.drdo.org/pub/techfocus/dec01/multispectral.htm Last Checked: January 14 2008.

DELANEY-A. H., AND BRESLER-Y. (1995). Multiresolution tomographic reconstruction using wavelets, *IEEE Transactions on Image Processing*, **4**(6), pp. 799–813.

DIVINE-D. V., AND GODTLIEBSEN-F. (2007). Bayesian modeling and significant features exploration in wavelet power spectra, *Nonlinear Processes in Geophysics*, **14**, pp. 79–88.

DOBRIN-M., AND SAVIT-C. (1988). *Introduction to Geophysical Prospecting, 4th ed.*, McGraw-Hill, New York.

DOMINGOS-P. (1999). The role of Occam's Razor in knowledge discovery, *Data Mining and Knowledge Discovery*, **3**, pp. 409–425.

DONOHO-D. L. (1995). De-noising by soft thresholding, *IEEE Transactions on Information Theory*, **41**(3), pp. 613–627.

DORNEY-T. D., SYMES-W. W., BARANIUK-R. G., AND MITTLEMAN-D. M. (2002). Terahertz multistatic reflection imaging, *Journal of the Optical Society of America A-Optics Image Science and Vision*, **19**(7), pp. 1432–1442.

DUDA-R., AND HART-P. (1973). *Pattern Classification and Scene Analysis*, 4th edn, John Wiley and Sons Inc, New York, USA.

DUDA-R., HART-P., AND STORK-D. (2001). *Pattern Classification*, 2nd edn, John Wiley and Sons Inc, New York, USA.

DUVILLARET-L., GARET-F., AND COUTAZ-L. (1996). A reliable method for extraction of material parameters in terahertz time-domain spectroscopy, *IEEE Journal of Selected Topics in Quantum Electronics*, **2**(3), pp. 739–746.

DUVILLARET-L., GARET-F., AND COUTAZ-L. (2000). Influence of noise on the characterization of materials by terahertz time-domain spectroscopy, *Journal of the Optical Society of America B: Optical Physics*, **17**(3), pp. 452–461.

FAIST-J., BECK-M., AELLEN-T., AND GINI-E. (2001). Quantum-cascade lasers based on a bound-to-continuum transition, *Applied Physics Letters*, **78**(2), pp. 147–149.

FAIST-J., CAPASSO-F., SIVCO-D. L., SIRTORI-C., HUTCHINSON-A. L., AND CHO-A. Y. (1994). Quantum cascade laser, *Science*, **264**(5158), pp. 1023–1025.

FAURE-P. (1976). Stochastic realization algorithms, *In System Identification: Advances and Case Studies*, Eds. R. K. Mehra and D. G. Larniotis, Academic Press, New York, USA.

FEDERICI-J. F., GARY-D., BARAT-R., AND MICHALOPOULOU-Z.-H. (2007). T-rays vs. terrorists, *IEEE Spectrum*, **44**, pp. 47–52.

FEDERICI-J. F., MITROFANOV-O., LEE-M., HSU-J. P., BRENER-I., HAREL-R., WYNN-J. D., PFEIFFER-L. N., AND WEST-K. W. (2002). Terahertz near-field imaging, *Physics in Medicine and Biology*, **47**(21), pp. 3727–3734.

FEDERICI-J. F., SCHULKIN-B., HUANG-F., GARY-D., BARAT-R., OLIVEIRA-F., AND ZIMDARS-D. (2005). THz imaging and sensing for security applications-explosives, weapons and drugs, *Semicond. Sci. Technol.*, **20**, pp. S266–S280.

FERGUSON-B. (2004). *Three Dimensional T-Ray Inspection Systems (PhD Thesis)*, University of Adelaide.

FERGUSON-B., AND ABBOTT-D. (2001a). De-noising techniques for terahertz responses of biological samples, *Microelectronics Journal (Elsevier)*, **32**(12), pp. 943–953.

FERGUSON-B., AND ABBOTT-D. (2001b). Wavelet de-noising of optical terahertz pulse imaging data, *Fluctuation and Noise Letters*, **1**(2), pp. L65–L70.

FERGUSON-B., AND ZHANG-X. C. (2002). Materials for terahertz science and technology, *Nature Materials*, **1**(1), pp. 26–33.

FERGUSON-B., LIU-H., HAY-S., FINLAY-D., ZHANG-X.-C., AND ABBOTT-D. (2004). In vitro osteosacoma biosensing using THz time domain spectroscopy, *in* J. Neev., and M. Reed. (eds.), *Proc. of SPIE BioMEMS and Nanotechnology*, Vol. 5275, Bellingham, Australia, pp. 304–316.

FERGUSON-B., WANG-S., GRAY-D., ABBOTT-D., AND ZHANG-X. C. (2002a). T-ray computed tomography, *Optics Letters*, **27**(15), pp. 1312–1314.

FERGUSON-B., WANG-S., GRAY-D., ABBOTT-D., AND ZHANG-X. C. (2002b). Toward functional 3D T-ray imaging, *Physics in Medicine and Biology (IOP)*, **47**, pp. 3735–3742.

FERGUSON-B., WANG-S., GRAY-D., ABBOTT-D., AND ZHANG-X. C. (2002c). Identification of biological tissue using chirped probe THz imaging, *Microelectronics Journal (Elsevier)*, **33**(12), pp. 1043–1051.

FERGUSON-B., WANG-S., ZHONG-H., ABBOTT-D., AND ZHANG-X.-C. (2003). Powder retection with T-ray imaging, *Proceeding of SPIE Terahertz for Military and Security Applications*, Vol. 5070, pp. 7–16.

FISCHER-B., HOFFMANN-M., H. HELM-G. M., AND JEPSEN-P. U. (2005a). Chemical recognition in terahertz time-domain spectroscopy and imaging, *Semiconductor Science and Technology*, **20**(7), pp. S246–S253.

FISCHER-B., HOFFMANN-M., H. HELM-R. W., RUTZ-F., KLEINE-OSTMANN-T., KOCH-M., AND JEPSEN-P. U. (2005b). Terahertz time-domain spectroscopy and imaging of artificial RNA, *Optics Express*, **13**(14), pp. 5205–5215.

FITZGERALD-A. J., BERRY-E., ZINOVEV-N. N., WALKER-G. C., SMITH-M. A., AND CHAMBERLAIN-J. M. (2002). An introduction to medical imaging with coherent terahertz frequency radiation, *Physics in Medicine and Biology*, **47**(7), pp. R67–R84.

FITZGERALD-A. J., WALLACE-V. P., JIMENEZ-LINAN-M., BOBROW-L., PYE-R. J., PURUSHOTHAM-A. D., AND ARNONE-D. D. (2006). Terahertz pulsed imaging of human breast tumors, *Radiology*, **239**(2), pp. 533–540.

FITZGERALD-A., PICKWELL-E., WALLACE-V., PURUSHOTHAM-A., PINDER-S., LINAN-M., PYE-R., AND HA-T. (2005). Medical applications of broadband terahertz pulsed radiation, *The 18th Annual Meeting of the IEEE Lasers and Electro-Optics Society*, pp. 120–121.

FLEMING-J. (1974). High resolution submillimeter-wave Fourier-transform spectrometry of gases, *IEEE Transactions on Microwave Theory and Techniques*, **MT-22**(12), pp. 1023–1025.

FLEMING-J. (2001). An adaptive version of the boost by majority algorithm, *Machine Learning*, **43**(3), pp. 293–318.

Florida State University (2005). Web. http://micro.magnet.fsu.edu/index.html Last Checked: August 19 2005.

FRÖHLICH-H. (1980). The biological effects of microwaves and related questions, *Adv. Electronics and Electron Physics*, **53**, pp. 85–152.

FUKUNAGA-K., AND HUMMELS-D. M. (1989). Leave-one-out procedures for nonparametric error estimates, *IEEE Transactions on Pattern Analysis and Machine Intelligence*, **II**(4), pp. 421–423.

FUKUNAGA-K., AND KESSELL-D. L. (1973). Nonparametric Bayes error estimation using unclassified samples, *IEEE Transactions on Information Theory*, **IT-19**(4), pp. 434–440.

GALVÃO-R., HADJILOUCAS-S., BECERRA-V. M., AND BOWEN-J. (2005). Subspace system identification framework for the analysis of multimoded propagation of THz-transient signals, *Measurement Science and Technology*, **16**(5), pp. 1037–1053.

GALVÃO-R., HADJILOUCAS-S., BOWEN-J., AND COELHO-C. (2003). Optimal discrimination and classification of THz spectra in the wavelet domain, *Optics Express*, **11**(12), pp. 1462–1473.

GALVÃO-R., HADJILOUCAS-S., ZAFIROPOULOS-A., WALKER-G. C., BOWEN-J. W., AND DUDLEY-R. (2007). Optimization of apodization functions in terahertz transient spectrometry, *Optics Letters*, **32**(20), pp. 3008–3010.

GIRAUD-G., AND WYNNE-K. (2003). A comparison of the low-frequency vibrational spectra of liquids obtained through infrared and Raman spectroscopies, *Journal of Chemical Physics*, **119**(22), pp. 11753–11764.

GLADKOVA-N., PETROVA-G., NIKULIN-N., LOPOVOK-S., SNOPOVA-L., CHUMAKOV-Y., NASONOVA-V., GELIKONOV-V., GELIKONOV-G., KURANOV-R., SERGEEV-A., AND FELDCHTEIN-F. (2000). In vivo optical cohetence tomography imaging of human skin: norm and pathology, *Skin Research and Technology*, **6**(1), pp. 6–16.

GLOBUS-T., WOOLARD-D., AND SAMUELS-A. (2002). Submillimeter-wave fourier transform spectroscopy of biological macromolecules, *Journal of Applied Physics*, **91**(9), pp. 6105–6113.

GMACHL-C., CAPASSO-F., SIVCO-D. L., AND CHO-A. Y. (2001). Recent progress in quantum cascade lasers and applications, *Report on Progress in Physics*, **64**, pp. 1533–1601.

GONZALEZ-R. C., AND WOODS-R. E. (2002). *Digital Image Processing*, Prentice-Hall, Inc., New Jersey.

GRAVES-E., WEISSLEDER-R., AND NTZIACHRISTOS-V. (2004). Fluorescence molecular imaging of small animal tumour models, *Current Molecular Medicine*, **4**, pp. 419–430.

GREGORY-I., TRIBE-W., COLE-B., BAKER-C., EVANS-M., BRADLEY-I., LINFIELD-E., DAVIES-A., AND MISSOUS-M. (2004). Phase sensitive continuous-wave THz imaging using diode lasers, *Electronics Letters*, **40**(2), pp. 143–145.

GROSSE-E. (2002). THz radiation from free electron lasers and its potential for cell and tissue studies, *Physics in Medicine and Biology*, **47**(21), pp. 3755–3760.

GRUNDLER-W., AND KAISER-F. (1992). Experimental evidence for coherent excitations correlated with cell growth nanobiology, *Nanobiology*, **1**, pp. 163–176.

GUEST-M., BUSH-I., VAN DAM-H., SHERWOOD-P., THOMAS-J., VAN LENTHE-J., HAVENITH-R., AND KENDRICK-J. (2005). The GAMESS-UK electronic structure package: algorithms, developments and applications, *Molecular Physics*, **103**(6-8), pp. 719–747.

GUO-Y., ZHANG-H., WANG-X., AND CAVALLARO-R. (2001). VLSI implementation of Mallat fast discrete wavelet transform algorithm with reduced complexity, *IEEE Global Telecommunications Conference*, **1**, pp. 25–29.

GU-P., CHANG-F., TANI-M., SAKAI-K., AND PAN-C. (1999). Generation of coherent cw-terahertz radiation using a tunable dual-wavelength external cavity laser diode, *Japanese Journal of Applied Physics. Part 2. Letters*, **38**(11A), pp. L1246–L1248.

GU-P., TANI-M., KONO-S., SAKAI-K., AND ZHANG-X.-C. (2002). Study of terahertz radiation from InAs and InSb, *Applied Physics Letters*, **91**(9), pp. 5533–5537.

GUYON-I., WESTON-J., AND BARNHILL-S. (2002). Gene selection for cancer classification using support vector machines, *Machine Learning*, **46**, pp. 389–422.

HADJILOUCAS-S., AND BOWEN-J. (1999). Precision of quasioptical null-balanced bridge techniques for transmission and reflection coefficient measurements, *Review of Scientific Instruments*, **70**(1), pp. 213–219.

HADJILOUCAS-S., GALVÃO-R., AND BOWEN-J. (2002). Analysis of spectroscopic measurements of leaf water content at THz frequencies using linear transforms, *Journal of the Optical Society of America A*, **19**(12), pp. 2495–2509.

HADJILOUCAS-S., GALVÕ-R. K. H., BECERRA-V. M., BOWEN-J. W., MARTINI-R., BRUCHERSEIFER-M., PELLEMANS-H. P. M., HARING BOLÍVAR-P., KURZ-H., AND CHAMBERLAIN-J. M. (2004). Comparison of state space and ARX models of a waveguide's THz transient response after optimal wavelet filtering, *IEEE Transactions on Microwave Theory and Techniques MTT*, **52**(10), pp. 2409–2419.

HADJILOUCAS-S., KARATZAS-L. S., AND BOWEN-J. (1999). Measurements of leaf water content using terahertz radiation, *IEEE Transactions on Microwave Theory and Techniques*, **47**(2), pp. 142–149.

HANDLEY-J. W., FITZGERALD-A. J., BERRY-E., AND BOYLE-R. D. (2002). Wavelet compression in medical terahertz pulsed imaging, *Physics in Medicine and Biology*, **47**(21), pp. 3885–3892.

HANGYO-M., NAGASHIMA-T., AND NASHIMA-S. (2002). Spectroscopy by pulsed terahertz radiation, *Semiconductor Science and Technology*, **13**, pp. 1727–1738.

HAN-P., AND ZHANG-X. C. (2001). Free-space coherent broadband terahertz time-domain spectroscopy, *Measurement Science and Technology*, **12**(11), pp. 1747–1756.

HAN-P., CHO-G., AND ZHANG-X. C. (2000). Time-domain transillumination of biological tissues with terahertz pulses, *Optics Letters*, **25**(4), pp. 242–244.

HANSON-K. M., AND WECKSUNG-G. W. (1983). Bayesian approach to limited-angle reconstruction in computed tomography, *Journal of Optical Society of America*, **73**(11), pp. 1501–1509.

HARALICK-R., AND SHAPIRO-L. (1985). Image segmentation techniques, *Computer Vision, Graphics, and Image Processing*, **29**, pp. 100–132.

HARAN-G., SUN-W. D., WYNNE-K., AND HOCHSTRASSER-R. M. (1997). Femtosecond far-infrared pump-probe spectroscopy: a new tool for studying low-frequency vibrational dynamics in molecular condensed phases, *Chemical Physics Letters*, **274**(4), pp. 365–371.

HASTIE-T., TIBSHIRANI-R., AND FRIEDMAN-J. H. (2003). *The Elements of Statistical Learning: Data Mining, Inference, and Prediction*, Springer, New York.

HAUS-H., AND MECOZZI-A. (1993). Noise of mode-locked lasers, *IEEE Journal of Quantum Electronics*, **29**(3), pp. 983–996.

HEARST-M. A. (1998). Trends controversies: Support vector machines, *IEEE Intelligent Systems*, **13**(4), pp. 18–28.

HERMAN-G. T. (1980). *Image Reconstruction from Projections: The Fundamentals of Computerized Tomography*, Academic Press, New York, USA.

HERRMANN-M., TABATA-H., AND KAWAI-T. (2005). Terahertz time-domain spectroscopy and imaging of DNA, *International Quantum Electronics Conference*, pp. 1240–1241.

HERRMANN-M., TANI-M., AND SAKAI-K. (2000). Display modes in time-resolved terahertz imaging, *Japanese Journal of Applied Physics Part 1-Regular Papers Short Notes & Review Papers*, **39**(11), pp. 6254–6258.

HOLSCHNEIDER-M. (1991). Inverse radon transforms through inverse wavelet transforms, *Inverse Problems*, **7**(6), pp. 853–861.

HUANG-D., SWANSON-E. A., LIN-C. P., SCHUMAN-J. S., STINSON-W. G., CHANG-W., HEE-M. R., FLOTTE-T., GREGORY-K., PULIAFITO-C. A., AND FUJIMOTO-J. G. (1991). Optical coherence tomography, *Science*, **254**(5035), pp. 1178–1181.

HU-B., AND NUSS-M. (2001). Imaging with terahertz waves, *Optics Letters*, **20**(16), pp. R101–R112.

HUBBARD-B. (1998). *The world according to wavelets*, 2nd edn, A.K.Peters, Wellesley, Massachusetts.

IZUMIDA-S., ONO-S., LIU-Z., OHTAKE-H., AND SARUKURA-N. (1999). Spectrum control of THz radiation from InAs in a magnetic field by duration and frequency chirp of the excitation pulses, *Applied Physics Letters*, **75**(4), pp. 451–453.

JAIN-S., AND DESHPANDE-G. (2004). Parametric modeling of brain signals, *The Proceeding of IEEE: Technology for Life: North Carolina Symposium on Biotechnology and Bioinformatics*, pp. 85–91.

JAN-J. S. (2006). *Medical Image Processing, Reconstruction and Restoration: Concepts and Methods*, Marcel Dekker Inc, New York, USA.

JANKE-C., FÖRST-M., NAGEL-M., KURZ-H., AND BARTELS-A. (2005). Asynchronous optical sampling for high-speed characterization of integrated resonant terahertz sensors, *Optics Letters*, **30**(11), pp. 1405–1407.

JENSEN-A., AND LA COUR-HARBO-A. (2001). *Ripples in Mathematics: The Discrete Wavelet Transform*, Springer Verlag, Berlin.

JEON-T. I., AND GRISCHKOWSKY-D. (1998). Characterization of optically dense, doped semiconductors by reflection THz time domain spectroscopy, *Applied Physics Letters*, **72**(23), pp. 3032–3034.

JIANG-Z., AND ZHANG-X.-C. (1998a). Electro-optic measurement of THz field pulses with a chirped optical beam, *Applied Physics Letters*, **72**(16), pp. 1945–1947.

JIANG-Z., AND ZHANG-X.-C. (1998b). Electro-optic measurement of thz field pulses with a chirped optical beam, *Applied Physics Letters*, **72**(16), pp. 1945–1947.

JIANG-Z., AND ZHANG-X.-C. (1998c). Single-shot spatiotemporal terahertz field imaging, *Optics Letters*, **23**(14), pp. 1114–1116.

JOHNSON-J. L., DORNEY-T. D., AND MITTLEMANA-D. M. (2001). Enhanced depth resolution in terahertz imaging using phase-shift interferometry, *Applied Physics Letters*, **78**(6), pp. 835–837.

JOHNSTONE-M., AND DONOHO-L. (1995). Adapting to unknown smoothness via wavelet shrinkage, *Journal of the Statistical Association*, **90**(432), pp. 1220–1224.

JOHNSTON-M. B. (2007). Superfocusing of terahertz waves, *Nature Photonics*, **1**(1), pp. 14–15.

JOLLIFFE-I. (2002). *Principal Component Analysis*, 2nd edn, Springer-Verlag, New York, Berlin, Heidelberg.

JONES-I., RAINSFORD-T., FISCHER-B., AND ABBOTT-D. (2006). Far-infrared vibrational spectra of all-trans, 9-cis and 13-cis retinal measured by THz time-domain spectroscopy, *Vibrational Spectroscopy*, **41**(2), pp. 144–154.

KAFKA-J. D., AND BAER-T. (1987). Prism-pair dispersive delay lines in optical pulse compression, *Optics Letters*, **12**, pp. 401–403.

KAISER-G. (1994). *A Friendly Guide to Wavelets*, Birkhäuser Boston, Cambridge, Mass.

KAK-A. C., AND SLANEY-M. (1988). *Principles of Computerized Tomographic Imaging*, IEEE Press, New York, USA.

KALENDER-W., SEISSLER-W., KLOTZ-E., AND VOCK-P. (1990). Spiral volumetric CT with single-breath-hold technique, continuous transport, and continuous scanner rotation, *Radiology*, **176**, pp. 181–183.

KALOUPTSIDIS-N., AND THEODORIDIS-S. (1993). *Adaptive System Identification and Signal Processing Algorithms*, Prentice-Hall, Inc, NJ, USA.

KARPOWICZ-N., ZHONG-H., LIN-K.-I., HWANG-J.-S., AND ZHANG-X.-C. (2005a). Comparison between pulsed terahertz time-domain imaging and continuous wave terahertz imaging, *Semiconductor Science and Technology*, **20**(7), pp. S293–S299.

KARPOWICZ-N., ZHONG-H., ZHANG-C., LIN-K.-I., HWANG-J.-S., XU-J., AND ZHANG-X.-C. (2005b). Compact continuous-wave subterahertz system for inspection applications, *Applied Physics Letters*, **86**(5), Art. No. 054105.

KATO-R., KONDO-S., IGO-T., OKITA-T., KONISHI-T., SUEMINE-S., OKUDA-S., AND ISOYAMA-G. (2000). Lasing at 150 μm wavelength and measurement of the characteristics of the free-electron laser at ISIR, Osaka University, *Nuclear Instruments and Methods in Physics Research Section A: Accelerators, Spectrometers, Detectors and Associated Equipment*, **445**(1-3), pp. 169–172.

KAWASE-K., OGAWA-Y., WATANABE-Y., AND INOUE-H. (2003). Non-destructive terahertz imaging of illicit drugs using spectral fingerprints, *Optics Express*, **11**(20), pp. 2549–2554.

KAWASE-K., SATO-M., TANIUCHI-T., AND ITO-H. (1996). Coherent tunable thz-wave generation from LiNbO3 with monolithic grating coupler, *Physics Letters*, **68**(18), pp. 2483–2485.

KEARNS-M. (1997). A bound on the error of cross validation using the approximation and estimation rates, with consequences for the training-test split, *Journal of the American Statistical Association*, **9**(5), pp. 1143–1161.

KERECMAN-A. (1973). The tungsten-P type silicon point contact diode, *IEEE MTT-S International Microwave Symposium Digest*, **73**(1), pp. 30–34.

KIM-K. I., JUNG-K., PARK-S. H., AND KIM-H. J. (2002). Support vector machines for texture classification, *IEEE Transactions on Pattern Analysis and Machine Intelligence*, **24**(11), pp. 1542–1550.

KIM-S. M., HATAMI-F., HARRIS-J. S., KURIAN-A. W., FORD-J., KING-D., SCALARI-G., GIOVANNINI-M., HOYLER-N., AND HARRIS-J. F. G. (2006). Biomedical terahertz imaging with a quantum cascade laser, *Applied Physics Letters*, **88**(15), Art. No. 153903.

KIM-S. M., HATAMI-F., HARRIS-J. S., KURIAN-A. W., FORD-J., KING-D., SCALARI-G., GIOVANNINI-M., HOYLER-N., FAIST-J., AND HARRIS-G. (2004). Biomedical terahertz imaging with a quantum cascade laser, *Applied Physics Letters*, **88**, Art. No. 153903.

KINDT-J. T., AND SCHMUTTENMAER-C. A. (1999). Theory for determination of the low-frequency time-dependent response function in liquids using time-resolved terahertz pulse spectroscopy, *Journal of Chemical Physics*, **110**(17), pp. 8589–8596.

KISTNER-C., ANDRÉ-A., FISCHER-T., THOMA-A., JANKE-C., BARTELS-A., GISLER-T., MARET-G., AND DEKORSY-T. (2007). Hydration dynamics of oriented DNA films investigated by time-domain terahertz spectroscopy, *Applied Physics Letters*, **90**(23), Art. No. 233902.

KÖHLER-R., IOTTI-R. C., TREDICUCCI-A., AND ROSSI-F. (2001). Design and simulation of terahertz quantum cascade lasers, *Applied Physics Letters*, **79**, pp. 3920–3922.

KÖHLER-R., TREDICUCCI-A., BELTRAM-F., BEERE-H. E., LINFIELD-E. H., DAVIES-A. G., AND RITCHIE-D. A. (2002a). High-intensity interminiband terahertz emission from chirped superlattices, *Applied Physics Letters*, **80**(11), pp. 156–159.

KÖHLER-R., TREDICUCCI-A., BELTRAM-F., BEERE-H. E., LINFIELD-E. H., DAVIES-A. G., RITCHIE-D. A., IOTTI-R. C., AND ROSSI-F. (2002b). Terahertz semiconductor-heterostructure laser, *Nature*, **417**(6885), pp. 156–159.

KÖHLER-R., TREDICUCCI-A., MAURO-C., BELTRAM-F., BEERE-H. E., LINFIELD-E. H., DAVIES-A. G., AND RITCHIE-D. A. (2004). Terahertz quantum-cascade lasers based on an interlaced photon-phonon cascade, *Applied Physics Letters*, **84**(8), pp. 1266–1268.

KOLEHMAINEN-V., SILTANEN-S., JÄRVENPÄÄ-S., J.P.-K., KOISTINEN-P., LASSAS-M., PIRTTILÄ-J., AND SOMERSALO-E. (2003). Statistical inversion for medical x-ray tomography with few radiographs: II. application to dental radiology, *Physics in Medicine and Biology*, **48**, pp. 1465–1490.

KRISHNAGOPAL-S., KUMAR-V., MAITI-S., PRABHU-S. S., AND SARKAR-S. K. (2004). Free-electron lasers, *Current Science*, **87**(8), pp. 1066–1078.

KUBLER-C., HUBER-R., AND LEITENSTORFER-A. (2005). Ultrabroadband terahertz pulses: generation and field-resolved detection, *Semiconductor Science and Technology*, **20**, pp. S128–S133.

LAHTINEN-T., NUUTINEN-J., ALANEN-E., TURUNEN-M., NUORTIO-L., USENIUS-T., AND HOPEWELL-J. (1999). Quantitative assessment of protein content in irradiated human skin, *International Journal of Radiation Oncology Biology Physics*, **43**(3), pp. 635–638.

LASCH-P., AND NAUMANN-D. (1998). FT-IR microspectroscopic imaging of human carcinoma thin sections based on pattern recognition techniques, *Cellular and Molecular Biology*, **44**(1), pp. 189–202.

L. DAKOVSKI, L.G. ANDKUBERA-B., AND SHAN-J. (2005). Localized terahertz generation via optical rectification in ZnTe, *Optical Society of America*, **22**(8), pp. 1667–1670.

LEE-A. W. M., QIN-Q., KUMAR-S., WILLIAMS-B. S., AND HU-Q. (2006). Real-time terahertz imaging over a standoff distance (>25 meters), *Applied Physics Letters*, **89**(24), Art. No. 141125.

LEE-H., LEE-J., AND KIM-J. (2001). A micromachined photoconductive near-field probe for picosecond pulse propagation measurement on coplanar transmission lines, *IEEE Journal of Selected Topics in Quantum Electronics*, **7**(4), pp. 674–682.

LEITENSTORFER-A., HUNSCHE-S., SHAH-J., NUSS-M. C., AND KNOX-W. H. (1999). Femtosecond charge transport in polar semiconductors, *Physical Review Letters*, **82**(25), pp. 5140–5143.

LEVINE-M. D. (1985). *Vision in Man and Machines*, McGraw-Hill, Inc., New York.

LIANG-G., WILKES-D. M., AND CADZOW-J. A. (1993). ARMA model order estimation based on the eigenvalues of the covariance matrix, *IEEE Transactions on Signal Processing*, **41**(10), pp. 3003–3009.

LJUNG-L. (1999). *System Identification: Theory for the User*, 2nd edn, Prentice Hall PTR, New Jersey, USA.

LÖFFLER-T., BAUER-T., SIEBERT-K., ROSKOS-H., FITZGERALD-A., AND CZASCH-S. (2001). Terahertz dark-field imaging of biomedical tissue, *Optics Express*, **4434**(245), pp. 25–36.

LÖFFLER-T., SIEBERT-K., CZASCH-S., AND BAUER, T.AND ROSKOS-H. (2002). Visualization and classification in biomedical terahertz pulsed imaging, *Physics in Medicine and Biology*, **47**(2002), pp. 3847–3852.

LUO-H., LIU-H. C., SONG-C. Y., AND WASILEWSKI-Z. R. (2005). Background-limited terahertz quantum-well photodetector, *Applied Physics letters*, **86**(23), Art. No. 231103.

MACQUEEN-J. B. (1967). Some methods for classification and analysis of multivariate observations, *Proceedings of 5-th Berkeley Symposium on Mathematical Statistics and Probability*, Vol. 1, University of California Press, Berkeley, pp. 281–297.

MADYCH-W. R. (1999). Tomography, approximate reconstruction, and continuous wavelet transforms, *Applied and Computational Harmonic Analysis*, **7**(1), pp. 54–100.

MALLAT-S. (1989). A theory for multiresolution signal decomposition: The wavelet representation, *IEEE Transactions on Pattern Analysis and Machine Intelligence*, **14**(7), pp. 674–693.

MALLAT-S. G. (1999). *A Wavelet Tour of Signal Processing*, San Diego : Academic Press, CA.

MARKELZ-A., ROITBERG-A., AND HEILWEIL-E. (2000). Pulsed terahertz spectroscopy of DNA, bovine serum albumin and collagen between 0.1 and 2.0 THz, *Chemical Physics Letters*, **320**(1-2), pp. 42–48.

MARTEL-P., CALMETTES-P., AND HENNION-B. (1991). Vibrational modes of hemoglobin in red blood cells, *Biophysical Journal*, **59**(2), pp. 363–377.

MA-X. F., AND ZHANG-X. C. (1993). Determination of ratios between nonlinear-optical coefficients by using subpicosecond optical rectification, *Journal of the Optical Society of America B: Optical Physics (JOSA B)*, **10**(7), pp. 1175–1179.

McElroy-R., and Wynne-K. (1997). Ultrafast dipole solvation measured in the far infrared, *Physical Review Letters*, **79**(16), pp. 3078–3081.

McLachlan-G. J. (1992). *Discriminant Analysis and Statisical Pattern Recognition*, Wiley, New York, USA

McLachlan-G. J. (2005). *Discriminant Analysis and Statistical Pattern Recognition*, Wiley-Interscience, NY, USA.

McLaughlin-R., Corchia-A., Johnston-M. B., Chen-Q., Ciesla-C. M., Arnone-D. D., Jones-G. A. C., Linfield-E. H., Davies-A. G., and Pepper-M. (2000). Enhanced coherent terahertz emission from indium arsenide in the presence of a magnetic field, *Applied Physics Letters*, **76**(15), pp. 2038–2040.

McManus-J. B., Nelson-D. D., Shorter-J. H., Jimenez-R., Herndon-S., Saleska-S., and Zahniser-M. (2005). A high precision pulsed quantum cascade laser spectrometer for measurements of stable isotopes of carbon dioxide, *Journal of Modern Optics*, **52**(16), pp. 2309–2321.

Menikh-A., MacColl-R., Mannella-C. A., and Zhang-X.-C. (2002). Terahertz biosensing technology: Frontiers and progress, *ChemPhysChem*, **3**(8), pp. 655–658.

Menikh-A., Mickana-S. P., Liu-H.-B., MacCollb-R., and Zhang-X. C. (2004). Label-free amplified bioaffinity detection using terahertz wave technology, *Biosensors and Bioelectronics*, **20**(3), pp. 658–662.

Meyer-Base-A. (2003). *Pattern Recognition for Medical Imaging*, Elsevier, Inc, California, USA.

Meyer-Y. (1990). *Ondelettes et Operateurs*, Tome 1, Herrmann, Paris.

Mickan-S., Abbott-D., Munchb-J., Zhang-X. C., and van Doorn-T. (2000). Analysis of system trade-offs for terahertz imaging, *Microelectronics Journal*, **31**(7), pp. 503–514.

Mickan-S. P. (2003). *T-ray Biosensing (PhD Thesis)*, University of Adelaide.

Mitchell-T. M. (1997). *Machine Learning*, International Edition, McGraw-Hill Book Co., Singapore.

Mitrofanov-O., Brener-I., Harel-R., Wynn-J. D., Pfeiffer-L. N., West-K. W., and Federici-J. (1998). THz near-field imaging, *Optics Communications*, **150**(1-6), pp. 22–26.

Mitrofanov-O., Brener-I., Harel-R., Wynn-J. D., Pfeiffer-L. N., West-K. W., and Federici-J. (2000). Terahertz near-field microscopy based on a collection mode detector, *Applied Physics Letters*, **77**(22), pp. 3496–3498.

Mitrofanov-O., Harel-R., Lee-M., Pfeiffer-L. N., West-K., Wynn-J. D., and Federici-J. (2001a). Study of single-cycle pulse propagation inside a thz near-field probe, *Applied Physics Letters*, **78**(2), pp. 252–254.

Mitrofanov-O., Lee-M., Hsu-J. W. P., Brener-I., Harel-R., Federici-J., Wynn-J. D., Pfeiffer-L. N., and West-K. W. (2001b). Collection mode near-field imaging with 0.5 THz pulses, *IEEE Journal of Selected Topics in Quantum Electronics*, **7**(4), pp. 600–607.

Mittleman-D., Jacobsen-R., and Nuss-M. (1996). T-ray imaging, *IEEE Journal of Selected Topics in Quantum Electronics*, **2**(3), pp. 679–692.

MITTLEMAN-D. M., HUNSCHE-S., BOIVIN-L., AND NUSS-M. C. (1997). T-ray tomography, *Optics Letters*, **22**(12), pp. 904–906.

MITTLEMAN-D., NEELAMANI-R., RUDD-R. B. J., AND KOCH-M. (1999). Recent advances in terahertz imaging, *Applied Physics B - Lasers and Optics*, **68**(6), pp. 1085–1094.

MUKHERJEE-D., PAL-P., AND DAS-J. (1996). Sodar image segmentation by fuzzy *c*-means, *Signal Processing*, **54**, pp. 295–301.

MULLEN-K., AND ENNIS-D. (1987). Mathematical formulation of multivariate Euclidean models for discrimination methods, *Psychometrika*, **52**(2), pp. 235–249.

MULLER-K.-R., MIKA-S., RATSCH-G., TSUDA-K., AND SCHÖLKOPF-B. (2001). An introduction to kernel-based learning algorithms, *IEEE Transactions on Neural Networks*, **12**(2), pp. 181–201.

NAGASHIMA-T., AND HANGYO-M. (2001). Measurement of complex optical constants of a highly doped Si wafer using terahertz ellipsometry, *Applied Physics Letters*, **79**(24), pp. 3917–3919.

NASHIMA-S., TAKATA-K., AND HANGYO-M. (2001). Measurement of optical properties of highly doped silicon by terahertz time domain reflection spectroscopy, *Applied Physics Letters*, **79**(24), pp. 3923–3925.

NG-B. W.-H. (2003). *Wavelet Based Image Texture Segmentation using a Modified K-means Algorithm (PhD Thesis)*, University of Adelaide.

NGUYEN-K. L., MICHAEL-L. J., GLADDEN-L., WORRALL-C. H., ALEXANDER, P. BEERE-H. E., PEPPER-M., RITCHIE-D. A., ALTON-J., BARBIERI-S., AND LINFIELD-E. H. (2006). Three-dimensional imaging with a terahertz quantum cascade laser, *Optics Express*, **14**(6), pp. 2123–2129.

NISHIZAWA-J., SASAKI-T., SUTO-K., TANABE-T., SAITO-K., YAMADA-T., AND KIMURA-T. (2005). THz transmittance measurements of nucleobases and related molecules in the 0.4- to 5.8-THz region using a GaP THz wave generator, *Optics Communications*, **246**(1-3), pp. 229–239.

NTZIACHRISTOS-V., RIPOLL-J., WANG-L. V., AND WEISSLEDER-R. (2005). Looking and listening to light: the evolution of whole-body photonic imaging, *Nature Biotechnology*, **23**(3), pp. 313–320.

OLSON-T., AND DESTEFANO-J. (1994). Wavelet localization of the Radon transform, *IEEE Transactions on Signal Processing*, **42**(8), pp. 2055–067.

OZYUZER-L., KOSHELEV-A. E., KURTER-C., GOPALSAMI-N., LI-Q., TACHIKI-M., KADOWAKI-K., YAMAMOTO-T., MINAMI-H., YAMAGUCHI-H., TACHIKI-T., GRAY-K. E., KWOK-W.-K., AND WELP-U. (2007). Emission of coherent THz radiation from superconductors, *Science*, **318**(5854), pp. 1291–1293.

PAIVA-H., AND GALVÃO-R. (2006). Wavelet-packet identification of dynamic systems in frequency subbands, *Signal Processing*, **86**(8), pp. 2001–2008.

PEARCE-J., AND MITTLEMAN-D. M. (2001). Propagation of single-cycle terahertz pulses in random media, *Optics Letters*, **26**, pp. 2002–2004.

PEARCE-J., AND MITTLEMAN-D. M. (2003). Using terahertz pulses to study light scattering, *Proceedings of the Sixth International Conference on Electrical Transport and Optical Properties of Inhomogeneous Media*, Vol. 338, pp. 92–96.

PEARCE-J., CHOI-H., MITTLEMAN-D. M., WHITE-J., AND ZIMDARS-D. (2005). Terahertz wide aperture reflection tomography, *Optics Letters*, **30**(13), pp. 1653–1655.

PERCIVAL-D., AND WALDEN-A. (2000). *Wavelet Methods for Time Series Analysis*, Cambridge University Press, Cambridge, England.

PICKWELL-E., AND WALLACE-V. (2006). Biomedical applications of terahertz technology, *Journal of Physics D: Applied Physics*, **39**(17), pp. R301–R310.

PICKWELL-E., COLE-B. E., FITZGERALD-A. J., WALLACE-V., AND PEPPER-M. (2004). Simulation of terahertz pulse propagation in biological systems, *Applied Physics Letters*, **84**(12), pp. 2190–2192.

PITTNER-S., AND KAMARTHI-S. V. (1999). Feature extraction from wavelet coefficients for pattern recognition tasks, *IEEE Transactions on Pattern Analysis and Machine Intelligence*, **21**(1), pp. 83–88.

POPPE-A., XU-L., KRAUSZ-F., AND SPIELMANN-C. (1998). Noise characterisation of sub-10-fs Ti:sapphire oscillators, *IEEE Journal of Selected Topics in Quantum Electronics*, **4**(2), pp. 179–184.

PRADARUTTI-B., MATTHÄUS-G., RIEHEMANN-S., NOTNI-G., NOLTE-S., AND TÜNNERMANN-A. (2007). Advanced analysis concepts for terahertz time domain imaging, *Optics Communications - Elsevier*, **279**(2), pp. 248–254.

PROAKIS-J., AND MANOLAKIS-D. (1996). *Digital Signal Processing: Principles, Algorithms, and Applications*, Prentice-Hall, Inc., NJ, USA.

QIAN-S. (2002). *Time-Frequency and Wavelet Transforms*, 1st edn, Prentice Hall, Inc., New Jersey, USA

RANTALA-M., VANSKA-S., JARVENPAA-S., KALKE-M., LASSAS-M., MOBERG-J., AND SILTANEN-S. (2006). Wavelet-based reconstruction for limited-angle X-Ray tomography, *IEEE Transactions on Medical Imaging*, **25**, pp. 210–217.

RASHID-FARROKHI-F., LIU-K., BERENSTEIN-C., AND WALNUT-D. (1997). Wavelet-based multiresolution local tomography, *IEEE Transactions on Image Processing*, **6**(10), pp. 1412–1430.

RAUDYS-S. (2001). *Statistical and Neural Classifiers: An Integrated Approach to Design*, 1st edn, Springer-Verlag London Ltd, London, U.K.

REID-M., AND FEDOSEJEVS-R. (2005). Quantitative comparison of terahertz emission from <100> InAs surfaces and a GaAs large-aperture photoconductive switch at high fluences, *Applied Optics*, **44**(1), pp. 149–153.

RICE-A., JIN-Y., MA-X. F., AND ZHANG-X.-C. (1994). Terahertz optical rectification from <110> zinc-blende crystals, *Applied Physics Letters*, **64**(11), pp. 1324–1326.

ROCHAT-M., SCALARI-G., HOFSTETTER-D., BECK-M., FAIST-J., BEERE-H. E., DAVIES-A. G., LINFIELD-E. H., AND RITCHIE-D. A. (2002). Continuous-wave operation of far-infrared quantum cascade lasers, *Electronics Letters*, **38**(25), pp. 1675–1676.

RØNNE-C., ASTRAND-P., AND KEIDING-S. (1999). THz spectroscopy of liquid H_2O and D_2O, *Physical Review Letters*, **82**(14), pp. 2888–2891.

RUDD-J. V., ZIMDARS-D. A., AND WARMUTH-M. W. (2000). Compact fiber-pigtailed terahertz imaging system, *Proceedings of SPIE:Commercial and Biomedical Applications of Ultrafast Lasers II*, Vol. 1, pp. 27–35.

RUFFIN-A. B., DECKER-J., SANCHEZ-PALENCIA-L., LE HORS, L-., F.-W. J., NORRIS-T. B., AND RUDD-J. V. (2000). Time reversal and object reconstruction with single-cycle pulses, *Optics Letters*, **26**(10), pp. 681–683.

RUFFIN-A. B., RUDD-J. V., DECKER-J., SANCHEZ-PALENCIA-L., LE HORS, L-., F.-W. J., AND NORRIS-T. B. (2002). Time reversal terahertz imaging, *IEEE Journal of Quantum Electronics*, **38**(8), pp. 1110–1119.

SAETA-P. N., GREENE-B. I., AND CHUANG-S. L. (1993). Short terahertz pulses from semiconductor surfaces: The importance of bulk difference-frequency mixing, *Applied Physics Letters*, **63**(25), pp. 3482–3484.

SALEH-B. E. A., AND TEICH-M. C. (1991). *Fundamentals of Photonics*, John Wiley & Sons, Inc., NewYork.

SCALARI-G., WALTHER-C., FAIST-J., BEERE-H., AND RITCHIE-D. (2006). Electrically switchable, two-color quantum cascade laser emitting at 1.39 and 2.3 THz, *Applied Physics Letters*, **88**(14), Art. No. 141102.

SCALES-J. (1995). *Theory of Seismic Imaging*, Springer-Verlag, Berlin.

SCHADE-U., HOLLDACK-K., KUSKE-P., WÜSTEFELD-G., AND HÜBERS-H.-W. (2004). THz near-field imaging employing synchrotron radiation, *Applied Physics Letters*, **84**(8), pp. 1422–1424.

SCHAFTENAAR-G., AND NOORDIK-J. (2000). Molden: a pre- and post-processing program for molecular and electronic structures, *Journal of Computer-Aided Molecular Design*, **14**(2), pp. 123–134.

SCHALKOFF-R. (1992). *Pattern Classification: Statistical, Structural and Neural Approaches*, John Wiley and Sons, Inc., New York, USA.

SCHMIDT-LANGHORST-C., AND WEBER-H. G. (2005). Optical sampling techniques, *Journal of Optical and Fiber Communications Reports*, **2**(1), pp. 86–114.

SCHMUTTENMAER-C. (2004). Exploring dynamics in the far-infrared with terahertz spectroscopy, *Chemical Reviews*, **104**(4), pp. 1759–1779.

SCHÖLKOPF-B., AND SMOLA-A. (2002). *Learning with Kernels Support Vector Machines, Regularization, Optimization, and Beyond*, MIT Press, Cambridge, MA.

SCHÖLKOPF-B., BURGES-C. J. C., AND SMOLA-A. J. (1998). *Advances in Kernel Methods: Support Vector Learning*, The MIT Press, Cambridge, MA, USA.

SCHÜRMANN-J. (1996). *Pattern Classification: A Unified View of Statistical and Neural Approaches*, John Wiley and Sons, Inc., New York.

SHAN-J., WEISS-C., WALLENSTEIN-R., BEIGANG-R., AND HEINZ-T. F. (2001). Origin of magnetic field enhancement in the generation of terahertz radiation from semiconductor surfaces, *Optics Letters*, **26**(11), pp. 849–851.

SHAO-J. (1993). Linear model selection by cross-validation, *Journal of the American Statistical Association*, **88**(422), pp. 486–494.

SHAWE-TAYLOR-J., AND CRISTIANINI-N. (2004). *Kernel Methods for Pattern Analysis*, Cambridge University Press, Cambridge, UK.

SHEN-Y., TADAY-P., NEWNHAM-D., AND PEPPER-M. (2005). Chemical mapping using reflection terahertz pulsed imaging, *Semiconductor Science and Technology*, **20**, pp. S254–S257.

SHERLOCK-B. G., AND MONRO-D. M. (1998). On the space of orthonormal wavelets, *IEEE Transactions on Signal Processing*, **46**(6), pp. 1716–1720.

SHIKATA-J., KAWASE-K., TANIUCHI-T., AND ITO-H. (2002). Fourier-transform spectrometer with a terahertz-wave parametric generator, *Japanese Journal of Applied Physics Part 1-Regular Papers Short Notes & Review Papers*, **41**(1), pp. 134–138.

SIEBE-F., SIEBERT-K., LEONHARDT-R., AND ROSKOS-H. G. (1999). A fully tunable dual-color CW Ti:AL_2O_3 laser, *IEEE Journal of Quantum Electronics*, **35**(11), pp. 1731–1736.

SIEBERT-K. J., LÖFFLER-T., QUAST-H., THOMSON-M., BAUER-T., LEONHARDT-R., CZASCH-S., AND ROSKOS-H. G. (2002). All-optoelectronic continuous wave THz imaging for biomedical applications, *Physics in Medicine and Biology*, **47**(21), pp. 3743–3748.

SIEGEL-P. H. (2002). Terahertz technology, *IEEE Transactions on Microwave Theory and Techniques*, **50**(3), pp. 910–928.

SIEGEL-P. H. (2004). Terahertz technology in biology and medicine, *IEEE Transactions on Microwave Theory and Techniques*, **52**(10), pp. 2438–2447.

SIRTORI-C., GMACHL-C., CAPASSO-F., FAIST-J., SIVCO-D. L., HUTCHINSON-A. L., AND CHO-A. Y. (1998a). Long-wavelength ($\lambda \approx$ 8-11.5 μm) semiconductor lasers with waveguides based on surface plasmons, *Optics Letters*, **23**(17), pp. 1366–1368.

SIRTORI-C., TREDICUCCI-A., CAPASSO-F., FAIST-J., SIVCO-D. L., HUTCHINSON-A. L., AND CHO-A. Y. (1998b). Dual-wavelength emission from optically cascaded intersubband transitions, *Optics Letters*, **23**(6), pp. 463–465.

SJÖBERG-J., ZHANG-Q., LJUNG-L., BENVENISTE-A., DEYLON-B., GLORENNEC-P.-Y., HJALMARSSON-H., AND JUDITSKY-A. (1995). Nonlinear black-box modeling in system identification: a unified overview, *Automatica*, **31**(12), pp. 1691–1724.

SMITH-B. J., AND ADHAMI-R. R. (2000). Enhanced localized computerized tomography employing the discrete wavelet transform, *Circuits, Systems, and Signal Processing*, **19**(5), pp. 399–409.

SMITH-P., AUSTON-D., AND NUSS-M. (1988). Subpicosecond photoconducting dipole antennas, *IEEE Journal of Quantum Electronics*, **24**(2), pp. 255–260.

SMYE-S. W., CHAMBERLAIN-J. M., FITZGERALD-A. J., AND BERRY-E. (2001). The interaction between terahertz radiation and biological tissue, *Physics in Medicine and Biology*, **46**(9), pp. R101–R112.

SPARROW-C. (1916). On spectroscopic resolving power, *Astrophysics Journal*, **44**(2), pp. 76–86.

STARCK-J.-L., CANDÈ-E. J., AND DONOHO-D. L. (2002). The curvelet transform for image denoising, *IEEE Transactions on Image Processing*, **11**, pp. 670–683.

STRACHAN-C. J., TADAY-P. F., NEWNHAM-D. A., GORDON-K. C., ZEITLER-J. A., PEPPER-M., AND RADES-T. (2004). Using terahertz pulsed spectroscopy to study crystallinity of pharmaceutical materials, *Chemical Physics Letters*, **390**(1-3), pp. 20–24.

STRACHAN-C. J., TADAY-P. F., NEWNHAM-D. A., GORDON-K. C., ZEITLER-J. A., PEPPER-M., AND RADES-T. (2005). Using terahertz pulsed spectroscopy to quantify pharmaceutical polymorphism and crystallinity, *Journal of Pharmaceutical Sciences*, **94**(4), pp. 837–846.

STRANG-G., AND NGUYEN-T. (1996). *Wavelets and Filter Banks*, 1st edn, Wellesley-Cambridge Press, Wellesley, USA.

SUN-B., YAO-J.-Q., ZHANG-B.-G., T.-L.-Z., AND WANG-P. (2007). Theoretical study of phase-matching properties for tunable terahertz-wave generation in isotropic nonlinear crystals, *Journal Optoelectronics Letters*, **3**(2), pp. 152–156.

SUN-F., JI-W., AND ZHANG-X.-C. (2000). Two-photon absorption induced saturation of THz radiation in ZnTe, *Conference on Lasers and Electro-Optics'2000*, Vol. 39, pp. 479–480.

TADAY-P., BRADLEY-I., ARNONE-D., AND PEPPER-M. (2003). Using terahertz pulse spectroscopy to study the crystalline structure of a drug: A case study of the polymorphs of ranitidine hydrochloride, *Journal of Pharmaceutical Sciences*, **92**(4), pp. 831–838.

TAFLOVE-A., AND HAGNESS-S. (2001). *The Finite-Difference Time-Domain Method*, Artech House Publishers, Boston, MA.

TEARNEY-G. J., BREZINSKI-M. E., SOUTHERN-J. F., BOUMA-B. E., HEE-M. R., AND FUJIMOTO-J. G. (1995). Determination of the refractive index of highly scattering human tissue by optical coherence tomography, *Optics Letters*, **20**(21), pp. 2258–2260.

THERRIEN-C., AND OPPENHEIM-A. (1992). *Discrete Random Signals and Statistical Signal Processing*, Prentice Hall, New Jersey, USA.

TONOUCHI-M. (2007). Cutting-edge terahertz technology, *Nature Photonics*, **1**(2), pp. 97–105.

TREACY-E. B. (1969). Optical pulse compression with diffraction gratings, *IEEE Journal of Quantum Electronics*, **5**(9), pp. 454–458.

TREDICUCCI-A., CAPASSO-F., GMACHL-C., SIVCO-D. L., HUTCHINSON-A. L., AND CHO-A. Y. (1998). High performance interminiband quantum cascade lasers with graded superlattices, *Applied Physics Letters*, **73**(15), pp. 2101–2103.

TREDICUCCI-A., KÖHLER-R., MAHLER-L., BEERE-H. E., LINFIELD-E. H., AND RITCHIE-D. A. (2005). Quantum cascade laser, *Semiconductor Science and Technology*, **20**(7), pp. S222–S227.

TRIER-Ø. D., AND JAIN, A. K. TAXT-T. M. (1996). Feature extraction methods for character recognition – a survey, *Pattern Recognition*, **29**(4), pp. 641–662.

TUQUN-J., AND VAIDYANATHAN-P. P. (2000). A state-space approach to the design of globally optimal FIR energy compaction filters, *IEEE Transaction Signal Processing*, **48**(10), pp. 2822–2838.

University of California (2008). Web. http://www.cstars.ucdavis.edu/classes/mexusenvi/tut2.htm Last Checked: January 14 2008.

VAIDYANATHAN-P. P. (1993). *Multirate Systems and Filter Banks*, Prentice Hall, New Jersey, USA.

VAINBERG-É. I., KAZAK-I. A., AND KUROZAEV-V. P. (1981). Reconstruction of the internal three-dimentsional structure of objects based on real-time internal projection, *Soviet J. Nondestructive Testing*, **17**, pp. 415–423.

VAN EXTER-M., AND GRISCHKOWSKY-D. R. (1990). Characterization of an optoelectronic terahertz beam system, *IEEE Transactions on Microwave Theory and Techniques*, **38**(11), pp. 1684–1691.

VAN EXTER-M., FATTINGAR-C. L., AND GRISCHKOWSKY-D. (1989). High-brightness terahertz characterised with an ultrafast detector, *Applied Physics Letters*, **55**, pp. 337–339.

VAN OVERSCHEE-P., AND DE MOOR-B. (1994). N4SID: Subspace algorithms for the identification of combined deterministic-stochastic systems, *Automatica, Special Issue on Statistical Signal Processing and Control*, **30**(1), pp. 75–93.

VAN OVERSCHEE-P., AND DE MOOR-B. (1995). Choice of state-space basis in combined deterministic-stochastic subspace identification, *Automatica, Special Issue on Trends in System Identification*, **31**(12), pp. 1877–1883.

VAPNIK-V. N. (1995). *The Nature of Statistical Learning Theory*, Springer-Verlag, New York.

VAPNIK-V. N. (1998). *Statistical Learning Theory*, John Wiley & Sons, Inc., Wiley, New York.

VERGHESE-S., MCINTOSH-K. A., S. CALAWA-W. F. D., DUERR-E. K., AND MOLVAR-K. A. (1998). Generation and detection of coherent terahertz waves using two photomixers, *Applied Physics Letters*, **73**(26), pp. 3743–3748.

VETTERLI-M., AND KOVACEVIC-J. (1995). *Wavelets and Subband Coding*, Prentice-Hall PTR, New Jersey.

VITIELLO-M. S., SCAMARCIO-G., SPAGNOLO-V., LOSCO-T., GREEN-R. P., TREDICUCCI-A., BEERE-H. E., AND RITCHIE-D. A. (2006). Electron-lattice coupling in bound-to-continuum THz quantum-cascade lasers, *Physical Review Letters*, **88**(24), Art. No. 241109.

VOHLAND-M., STOFFELS-J., HAU-C., AND SCHULER-G. (2007). Remote sensing techniques for forest parameter assessment: Multispectral classification and linear spectral mixture analysis, *Silva Fennica*, **41**(3), pp. 441–456.

VOLKOV-V., BUSHUEV-A., KENDJEBULATOV-E., MITYANINA-N., MYAKISHEV-D., PETROV-V., SEDLYAROV-I., AND TRIBENDIS-A. (2000). VEPP-2000 single mode cavity, *Proceedings of EPAC 2000, Vienna, Austria*, pp. 2008–2010.

WALLACE-V., FITZGERALD-A., SHANKAR-S., FLANAGAN-N., PYE-R., CLUFF-J., AND ARNONE-D. D. (2004a). Terahertz pulsed imaging of basal cell carcinoma ex vivo and in vivo, *Journal of Investigative Dermatology*, **151**(2), pp. 424–432.

WALLACE-V. P., TADAY-P. F., FITZGERALD-A. J., WOODWARD-R. M., CLUFF-J., PYE-R. J., AND ARNONE-D. D. (2004b). Terahertz pulsed imaging and spectroscopy for biomedical and pharmaceutical applications, *Faraday Discussions*, **126**, pp. 255–263.

WALNUT-D. F. (2001). *An Introduction to Wavelet Analysis*, 1st edn, Birkhäuser, Boston, USA.

WALTHER-M. (2003). *Modern Spectroscopy on Biological Molecules-Structure and Bonding investigated by THz time-domain and transient phase-grating spectroscopy (PhD Thesis)*, the University of Freiburg, Germany.

WALTHER-M., FISCHER-B., SCHALL-M., HELM-H., AND JEPSEN-P. U. (2000). Far-infrared vibrational spectra of all-trans, 9-cis and 13-cis retinal measured by THz time-domain spectroscopy, *Chemical Physics Letters*, **332**(3-4), pp. 389–395.

WANG-S., FERGUSON., ABBOTT-D., AND X.-C.-Z. (2003). T-ray imaging and tomography, *Journal of Biological Physics*, **29**(2-3), pp. 247–256.

WANG-S., FERGUSON-B., AND ZHANG-X.-C. (2004a). Pulsed terahertz tomography, *Journal of Physics D Applied Physics*, **37**(4), pp. R1–R36.

WANG-S., FERGUSON-B., AND ZHANG-X.-C. (2004b). Pulsed terahertz tomography, *Journal of Physics D Applied Physics*, **37**(6), p. 964.

WATANABE-Y., KAWASE-K., IKARI-T., ITO-H., ISHIKAWA-Y., AND MINAMIDE-H. (2003). Spatial pattern separation of chemicals and frequency-independent components using terahertz spectroscopic imaging, *Applied Optics*, **42**(28), pp. 5744–5748.

WEISS-C., WALLENSTEIN-R., AND BEIGANG-R. (2000). Magnetic-field-enhanced generation of terahertz radiation in semiconductor surfaces, *Applied Physics Letters*, **77**(25), pp. 4160–4162.

WEISS-S., AND KULIKOWSKI-C. (1991). *Computer Systems that Learn*, Morgan Kaufmann Publishers Inc., San Francisco, CA, USA.

WESTON-J., GRETTON-A., AND ELISSEEFF-A. (2003). SVM practical session (how to get good results without cheating), *Machine Learning Summer School*.

WILLIAMS-B. (2007). Terahertz quantum-cascade lasers, *Nature Photonics*, **1**(9), pp. 517–525.

WILLIAMS-B., KUMAR-S., HU-Q., AND RENO-J. (2004). Resonant-phonon terahertz quantum-cascade laser operating at 2.1 THz ($\lambda \simeq 141\mu$m), *Electronics Letters*, **40**(7), pp. 431–433.

WILLIAMS-B. S., CALLEBAUT-H., KUMAR-S., HU-Q., AND RENO-J. L. (2003). 3.4-THz quantum cascade laser based on longitudinal-optical-phonon scattering for depopulation, *Applied Physics Letters*, **82**(7), pp. 1015–1017.

WITHAYACHUMNANKUL-W., FERGUSON-B., RAINSFORD-T., FINDLAY-D., MICKAN-S. P., AND ABBOTT-D. (2006). T-ray relevant frequencies for osteosarcoma classification, *Proceedings of SPIE Photonics: Microelectronics, MEMS and Nanotechnology*, **6038**, Art. No. 60381H.

WITHAYACHUMNANKUL-W., FERGUSON-B., RAINSFORD-T., MICKAN-S., AND ABBOTT-D. (2005). Simple material parameter estimation via terahertz time-domain spectroscopy, *IEE Electron Letters*, **41**(14), pp. 801–802.

WITHAYACHUMNANKUL-W., PNG-G., YIN-X.-X., ATAKARAMIANS-S., JONES-I., LIN-H.-Y., UNG-S. Y., BALAKRISHNAN-J., NG-B.-H., FERGUSON-B., MICKAN-S., FISCHER-B., AND ABBOTT-D. (2007). T-ray sensing and imaging, *Proceedings of the IEEE*, **95**(8), pp. 1528–1558.

WOODWARD-R. M., COLE-B., WALACE-V. P., ARNONE-D. D., PYE-R., LINFIELD-E. H., PEPPER-M., AND DAVIES-A. G. (2002). Terahertz pulse imaging in reflection geometry of human skin cancer and skin tissue, *Physics in Medicine and Biology*, **47**(21), pp. 3853–3863.

WOODWARD-R. M., WALLACE-V. P., PYE-R. J., COLE-B. E., ARNONE-D. D., LINFIELD-E. H., AND PEPPER-M. (2003). Terahertz pulse imaging of ex vivo basal cell carcinoma, *Journal of Investigative Dermatology*, **120**(1), pp. 72–78.

WOODWARD-R., WALLACE-V., ARNONE-D., LINFIELD-E., AND PEPPER-M. (2004). Terahertz pulsed imaging of skin cancer in the time and frequency domain, *Journal of Biological Physics*, **29**(2-3), pp. 257–259.

WOOLARD-D. L., BROWN-E. R., PEPPER-M., AND KEMP-M. (2005). Terahertz frequency sensing and imaging: A time of reckoning future applications?, *Proceedings of the IEEE*, **93**(10), pp. 1722–1743.

WU-Q., HEWITT-T. D., AND ZHANG-X. (1996). Two-dimensional electrooptic imaging of THz beams, *Applied Physics Letters*, **69**(8), pp. 1026–1028.

XIE-A., VAN DER MEER-A., AND AUSTIN-R. (2002). Excited-state lifetimes of far-infrared collective modes in proteins, *Physical Review Letters*, **88**(1), Art. No. 018102.

Yale University (2008). Web. http://www.yale.edu/ceo/Projects/swap/land-cover/Unsupervised+classification.htm Last Checked: January 14 2008.

YARIV-A. (1991). *Optical Electronics, 4th edn*, Oxford University Press, Oxford.

YASUI-T., SANEYOSHI-E., AND ARAKI-T. (2005). Asynchronous optical sampling terahertz time-domain spectroscopy for ultrahigh spectral resolution and rapid data acquisition, *Optics Letters*, **87**(6), Art. No. 061101.

YIN-X.-X., NG-W.-H. B., FERGUSON-B., AND ABBOTT-D. (2007a). Application of auto-regressive models and wavelet sub-bands for classifying terahertz pulse measurements, *Journal of Biological Systems*, **15**, pp. 551–571.

YIN-X.-X., KONG-K. M., LIM-J. W., NG-B. W.-H., FERGUSON-B., MICKAN-S. P., AND ABBOTT-D. (2007b). Enhanced T-ray signal classification using wavelet preprocessing, *Medical & Biological Engineering & Computing (Springer)*, **45**(6), pp. 611–616.

YIN-X.-X., NG-W.-H. B., FERGUSON-B., AND ABBOTT-D. (2007c). Terahertz local tomography using wavelets, *Joint 32nd International Conference on Infrared and Millimeter Waves and 15th International Conference on Terahertz Electronics (IRMMW-THz 2007)*, Cardiff, UK.

YIN-X.-X., NG-W.-H. B., FERGUSON-B., AND ABBOTT-D. (2007d). Terahertz local tomography using wavelets, *in* W. G. Kropatsch., M. Kampel., and A. Hanbury. (eds.), *Computer Analysis of Images and Patterns of Lecture Notes in Computer Science*, Vol. 4673, Vienna, Austria, pp. 878–885.

YIN-X.-X., NG-W.-H. B., FERGUSON-B., AND ABBOTT-D. (2008a). Wavelet based local tomographic image using terahertz techniques, *Digital Signal Processing*, p. DOI:10.1016/j.dsp.2008.06.009.

YIN-X.-X., NG-W.-H. B., FERGUSON-B., MICKAN-P. S., AND ABBOTT-D. (2007e). 2-D wavelet segmentation in 3-D T-ray tomography, *IEEE Sensors Journal*, **7**(3), pp. 342–343.

YIN-X.-X., NG-W.-H. B., FERGUSON-B., MICKAN-P. S., AND ABBOTT-D. (2007f). 2D wavelet-based segmentation by fusion in 3D terahertz tomography, *IEEE International Symposium on Industrial Electronics (ISIE)*, Vigo, Spain, pp. 3409–3414.

YIN-X.-X., NG-W.-H. B., FISCHER-B. M., FERGUSON-B., MICKAN-P. S., AND ABBOTT-D. (2006). Feature extraction from terahertz pulses for classification of RNA data via support vector machines, *in* J.-C. Chiao., A. S. Dzurak., C. Jagadish., and D. V. Thiel. (eds.), *Proceeding of SPIE Micro and Nanotechnology: Materials, Processes, Packaging, and Systems III*, Vol. 6415, Adelaide, Australia, Art. No. 641516.

YIN-X.-X., NG-B. W.-H., FISCHER-B., FERGUSON-B., AND ABBOTT-D. (2007g). Application of autoregressive models and wavelet sub-bands for classifying terahertz pulse measurements, *Journal of Biological Systems*, **15**(4), pp. 551–571.

YIN-X.-X., NG-B. W.-H., FISCHER-B. M., FERGUSON-B., AND ABBOTT-D. (2007h). Support vector machine applications in terahertz pulsed signals feature sets, *IEEE Sensors Journal*, **7**(11-12), pp. 1597–1608.

YIN-X.-X., NG-B. W.-H., ZEITLER-J. A., NGUYEN-K. L., GLADDEN-L., AND ABBOTT-D. (2008b). Local reconstruction for three dimensional terahertz imaging using a CW quantum cascade laser, *in* H. Arabnia. (ed.), *The 2008 International Conference on Image Processing, Computer Vision, and Pattern Recognition (IPCV'08)*, Vol. I, Las Vegas Nevada, USA, pp. 252–258.

ZEITLER-J. A., SHEN-Y., BAKER-C., TADAY-P. F., PEPPER-M., AND RADES-T. (2007a). Analysis of coating structures and interfaces in solid oral dosage forms by three dimensional terahertz pulsed imaging, *Journal of Pharmaceutical Sciences*, **96**(2), pp. 330–340.

ZEITLER-J. A., TADAY-P. F., NEWNHAM-D. A., PEPPER-M., GORDON-K. C., AND RADES-T. (2007b). Terahertz pulsed spectroscopy and imaging in the pharmaceutical setting - a review, *Journal of Pharmacy and Pharmacology*, **59**(2), pp. 209–223.

ZHANG-X.-C., AND AUSTON-D. H. (1992). Optoelectronic measurement of semiconductor surfaces and interfaces with femtosecond optics, *Journal of Applied Physics*, **71**(1), pp. 326–338.

ZHANG-X.-C., HU-B. B., DARROW-J. T., AND AUSTON-D. H. (1990). Generation of femtosecond electromagnetic pulses from semiconductor surfaces, *Physical Review Letters*, **56**(11), pp. 1011–1013.

ZHANG-X.-C., MA-X. F., JIN-Y., LU-T.-M., BODEN-E. P., PHELPS-P. D., STEWART-K. R., AND YAKYMYSHYN-C. P. (1992). Terahertz optical rectification from a nonlinear organic crystal, *Applied Physics Letters*, **61**(26), pp. 3080–3082.

ZHANG-Y., WANG-R., AND MONROE-K. (1997). Using wavelet network in nonparametric estimation, *IEEE Transaction Neural Networks*, **8**(2), pp. 227–236.

ZHANG-Y., WANG-R., AND MONROE-K. (2004). Multi-resolution and multi-spectral image fusion for urban object extraction, *Proceedings of XXth ISPRS Congress, Commission III*, Istanbul, Turkey, pp. 960–966.

ZHAO-G., SCHOUTEN-N., VAN DER VALK-N., WENCKEBACH-W., AND PLANKEN-P. (2002). Design and performance of a THz emission and detection setup based on a semi-insulating GaAs emitter, *Review of Scientific Instruments*, **73**(4), pp. 1715–1719.

ZHAO-S. (1999). Wavelet filtering for filtered backprojection in computed tomography, *Applied and Computational Harmonic Analysis*, **6**(3), pp. 346–373.

Glossary

AR	auto regressive, 78
ARMA	auto regressive moving average, 81
ASOPS	asynchronous optical sampling, 30
BCC	basal cell carcinoma, 57
BTC	bound-to-continuum, 18
CCD	charge-coupled device, 43
CIL	complex insertion loss, 126
CSL	chirped superlattice, 18
CSR	coherent synchrotron radiation, 51
CT	computed tomography, 6
CV	cross-validation, 148
CW	continuous wave, 5
DWPTs	discrete wavelet packet transforms, 97
DWT	discrete wavelet transform, 83
EM	electromagnetic, 55
EO	electrooptic, 23
EOS	electrooptic sampling, 27
FBP	filtered back projection, 9
FCM	fuzzy *c*-means, 9
FELs	free-electron lasers, 16
FFTs	fast Fourier transforms, 153
FIR	far-infrared, 77
FIR	finite impulse response, 173
FWT	fast wavelet transform, 90
FWHM	full-width-half-maximum, 315
GCT	global computed tomography, 251
GCV	generalized cross-validation, 279
GPIB	General Purpose Interface Bus, 317
GVD	group velocity dispersion, 209
HBO	human bone osteoblasts, 170
HOS	human osteosarcoma, 170

IDWPT	discrete wavelet packet transform, 173
IDWT	inverse discrete wavelet transform, 173
IRT	inverse Radon transform, 217
ITO	indium tin oxide, 207
IWT	inverse wavelet transform, 219
LDA	linear discriminant analysis, 71
LCT	local computed tomography, 253
LIA	lock in amplifier, 252
LOO	leave-one-out, 148
MA	moving average, 113
MQW	multiple-quantum-well, 250
MRI	magnetic resonance imaging, 4
MRA	multiresolution analysis, 83
MSA	multiscale approximation, 84
MSE	mean-square error, 130
NF	near-field, 50
NHB	normal human bone, 171
OAP	off-axis paraboloid, 48
OR	optical rectification, 23
PET	positron emission tomography, 4
PC	photoconductive, 12
PC	Pockel's cell, 17
PCA	principal components analysis, 71
PCA	photoconductive antenna, 28
PE	polyethylene, 161
PEV	prediction error variance, 114
poly-A	polyadenylic acid, 557
poly-C	polycytidylic acid, 55
QCL	quantum cascade laser, 5
QWP	quarter-wave plate, 28
RCS	radar cross-section, 44
RNA	ribonucleic acid, 201
ROA	region of artifacts, 234
ROC	receiver operating characteristic, 147

ROE	region of exposure, 232
ROI	region of interest, 9, 225
RP	resonant-phonon, 19
SCT	spiral computed tomography, 285
SL	superlattice, 18
S/N	signal-to-noise ratio, 36
SNR	signal-to-noise ratio, 250
SNIM	scanning near-field imaging, 52
SURE	Stein's unbiased risk estimate, 105
SVD	singular value decomposition, 121
SVM	support vector machine, 141
TDS	time domain spectrometry, 12
TE	transverse-electric, 25
TFP	thin-film polarizing, 17
THz	terahertz, 3
T-ray	THz, 3
TM	transverse-magnetic, 25
TPI	terahertz pulsed imaging, 13
TPO	THz-wave parametric oscillator, 71
VC	Vapnik-Chervonenkis, 141
WART	wide aperture reflection tomography, 43
WT	wavelet transform, 61
ZnTe	Zinc Telluride, 22

Index

Résumé

Xiaoxia (Sunny) Yin was born in Dalian, China. She received the BEng Degree in Industrial Electronics from Dalian University, Liaoning, P. R. China, and is currently working toward the PhD degree on three dimensional terahertz computed tomography under Derek Abbott and Brian Ng. Her research interests include multiresolution analysis, segmentation, image reconstruction & classification, and their applications to T-ray imaging. In 2007, she was a visiting scholar at the University of Reading, UK, under Dr. Silas Hadjiloucas and at the University of Cambridge, UK, under Prof. Lynn F. Gladden as well as at Rensselaer Polytechnic Institue in Troy, NY, USA, under Prof. X.-C. Zhang. She has authored and co-authored more than 18 peer-reviewed publications.

Ms Yin received a series of awards, including the PhD Scholarship of The University of Adelaide (2005), WavE Travel Fellowship from Switzerland (2006), The International Association for Pattern Recognition (IAPR) travel stipend from Hong Kong (2006), Research Abroad Scholarship from The University of Adelaide (2006), the Roger Pysden Memorial Fellowship from Australia Business, ABL State Chamber (2006), a student scholarship from the 2007 IEEE International Symposium on Industrial Electronics in Vigo, Spain (2007), a Mutual Community Postgraduate Travel Grant from the University of Adelaide (2007), an Overseas Travel Fellowship from The Australian Research Council Nanotechnology Network (ARCNN) (2007), a D. R. Stranks Traveling Fellowship from the University of Adelaide (2007), and an Australian Postdoctoral (APD) Fellowship from the Australian Research Council (2008).

Scientific Genealogy

My scientific genealogy via my primary supervisor, Derek Abbott

Xiaoxia (Sunny) Yin's Scientific Genealogy			
1774	MA	University of Cambridge	John Cranke
1782	MA	University of Cambridge	Thomas Jones
1811	MA	University of Cambridge	Adam Sedgwick
1830	MA	University of Cambridge	William Hopkins
1857	MA	University of Cambridge	Edward John Routh
1868	MA	University of Cambridge	John William Strutt (Lord Rayleigh)
1883	MA	University of Cambridge	Joseph John Thomson
1903	MA	University of Cambridge	John Sealy Townsend
1923	DPhil	University of Oxford	Victor Albert Bailey
1948	MSc	University of Sydney	Ronald Ernest Aitchison
1964	PhD	University of Sydney	Peter Harold Cole
1980	PhD	University of Adelaide	Kamran Eshraghian
1995	PhD	University of Adelaide	Derek Abbott
2008	PhD submitted	University of Adelaide	Xiaoxia (Sunny) Yin

My scientific genealogy via my co-supervisor, Brian Wai-Him Ng

Xiaoxia (Sunny) Yin's Scientific Genealogy			
1865	PhD	University of Jena	Johannes Conrad
1875	PhD	University of Halle	Hermann Paasche
1892	PhD	University of Marburg	Karl Eugen Guthe
1912	PhD	University of Michigan	Neal Hooker Williams
1928	PhD	University of Michigan	Walter Scott Huxford
1941	MS	Northwestern University	Richard Ward Jones
1964	PhD	Northwestern University	Robert Bartholomew Pinter
1991	PhD	University of Washington	Abdesselam (Salim) Bouzerdoum
2003	PhD	University of Adelaide	Brian Wai-Him Ng
2008	PhD submitted	University of Adelaide	Xiaoxia (Sunny) Yin